National Library of Canada
Acquisitions and Bibliographic Services Branch
395 Wellington Street
Ottawa, Ontario
K1A 0N4

Bibliothèque nationale du Canada
Direction des acquisitions et des services bibliographiques
395, rue Wellington
Ottawa (Ontario)
K1A 0N4

Your file Votre référence

Our file Notre référence

NOTICE

The quality of this microform is heavily dependent upon the quality of the original thesis submitted for microfilming. Every effort has been made to ensure the highest quality of reproduction possible.

If pages are missing, contact the university which granted the degree.

Some pages may have indistinct print especially if the original pages were typed with a poor typewriter ribbon or if the university sent us an inferior photocopy.

AVIS

La qualité de cette microforme dépend grandement de la qualité de la thèse soumise au microfilmage. Nous avons tout fait pour assurer une qualité supérieure de reproduction.

S'il manque des pages, veuillez communiquer avec l'université qui a conféré le grade.

La qualité d'impression de certaines pages peut laisser à désirer, surtout si les pages originales ont été dactylographiées à l'aide d'un ruban usé ou si l'université nous a fait parvenir une photocopie de qualité inférieure.

Canada

FROST-HEAVE INDUCED INTERACTION BETWEEN BURIED PIPELINES AND SOILS

by

Jun Hu

A THESIS SUBMITTED IN PARTIAL FULFILLMENT

OF THE REQUIREMENTS FOR THE DEGREE OF

DOCTOR OF PHILOSOPHY

in the Department of Civil Engineering & Applied Mechanics

McGill University

January 1996

ISBN 0-612-12387-1

Abstract

This thesis investigates the interaction between frozen soil and a pipeline embedded in a discontinuous frost heave zone. The computational modelling procedures proposed in the thesis include the modelling of frost heave generation, the constitutive modelling of the frozen soil, the structural behaviour of the pipeline and the constitutive modelling of the soil-pipeline interface. The interactive thermo-hydro-mechanical processes encountered in the problem are generally time-dependent and non-linear.

The frost heave modelling utilizes the three-dimensional form of a *modified hydrodynamic frost heave model.* A finite element implementation of the model is used to estimate the frost heave in a one-dimensional element. The comparison of the numerical results with an experimental result indicates that the prediction by computational modelling can reasonably simulate observations of one-dimensional experiments. Two-dimensional and three-dimensional simulations also indicate that the numerical modelling can predict trends of frost heave development which are consistent with the localized cooling at the base of a cuboidal element.

In the development of the interaction effects, the mechanical behaviour of the frozen soil is represented by a complete creep model. The proposed complete creep model can take into consideration all three creep processes associated with frozen soils. Computations have also been conducted to calibrate the predictions of the creep model with observed experimental data. Extensive computations have been performed to investigate the general creep responses of a variety of geotechnical structures.

To examine frozen soil-pipeline interaction problems, the pipeline is modelled either as a Bernoulli-Euler beam or as a cylindrical shell which accommodates both flexural and shear stiffness effects. The numerical procedures are applied to examine the pipeline freezing experiment conducted at the large scale facility in Caen, France. The temperature profiles, soil heave, pipeline deformation and flexural moments developed in the pipeline due to the generation of frost heave in the discontinuous frost heave region are documented.

Résumé:

L'objectif de la présente étude porte sur les interactions existant entre un sol à l'état de gel et un pipeline souterrain localisé dans une zône discontinue de soulèvement dû au gel. Les méthodes de modélisation suggérées à l'intérieur de ce document comprennent la modélisation de l'engendrement du soulèvement du sol causé par le gel, la modélisation constitutive du sol à l'état de gel, le comportement mécanique du pipeline de même que la modélisation constitutive de l'interface sol-pipeline. Les divers phénomènes thermo-hydro-mécaniques interactifs observés au sein de cette étude furent, de façon générale, non linéaires et s'exprimaient en fonction du temps.

La modélisation du phénomène de soulèvement dû au gel utilisée consiste en une version tridimensionnelle d'un modèle hydrodynamique de soulèvement dû au gel. L'utilisation du modèle, cette fois basé sur les principes d'analyse d'éléments finis, fût mis de l'avant afin d'obtenir une estimation du phénomène de soulèvement dû au gel dans un élément uni-dimensionnel. La comparaison des résultats numériques avec les données expérimentales indique qu'une prédiction par le biais d'une modélisation informatisée simule, de façon raisonnable, les résultats observés lors d'expériences uni-dimensionnelles. Des simulations à deux et trois dimensions indiquent également qu'une modélisation numérique peut prédire les tendences de de soulèvement dû au gel, ces dernières étant conformes avec le refroidissement localisé à la base d'un élément cuboïde.

Lors du développement d'effets interactifs, le comportement mécanique du sol à l'état de gel est représenté par un modèle portant sur le comportement du sol au fluage. Ce modèle peut inclure les trois procédés de fluage associés au sol à l'état de gel. Divers calculs ont également été effectués afin de calibrer les prédictions du modèle de comportement au fluage avec les données expérimentales. Ces calculs furent exécutés dans le but d'étudier le comportement réactionnel de diverses structures géotechniques face à la propriété de fluage à long temps du sol.

Afin d'examiner divers scénarios interactifs sol-pipeline, ce dernier est modélisé soit comme une poutre de type Bernoulli-Euler ou comme un membre cylindrique répondant à la fois aux effets de flexion et de rigidité au cisaillement. L'application des procédés numériques fût orientée dans le but d'examiner les expériences de gel de sections de pipeline réalisées au laboratoire à grande échelle de Caen, France. Finalement, ce document inclue l'interprétation complète des variations de température, soulèvement du sol dû au gel, déformation de pipeline, de même que l'engendrement de moments de flexion dans le pipeline causé par la formation de zônes de soulèvement.

Acknowledgements

I wish to express my deep gratitude to my supervisor, Professor A.P.S. Selvadurai for his excellent guidance, constant encouragement, continuous support and invaluable help without which this thesis would not be completed.

I would like to acknowledge Professor K. T. Law, Carleton University for his encouragement.

I would like to thank Dr. M.C. Au, Dr. Z.Q. Yue, Mr. D.Y. Wang, Dr. K. Sepehr and Dr. Q. Lan for useful discussions during the course of the research.

I would like to thank Mr. S. Paradis for the translation of the thesis abstract to French.

Thanks are also due to National Energy Board, Canada for providing the experimental data of the France-Canada joint pipeline test in Caen, France.

The financial support provided by Carleton University and McGill University is also acknowledged.

Dedication

To my dear parents

List of publications resulting from the work performed for this thesis

Selvadurai, A. P. S. and Hu, J. 1995. The axial loading of foundations embedded in frozen soils. *International Journal of Offshore and Polar Engineering and Proceedings of the 5th ISOPE Conference*, J. S. Chung, B. M. Das, B. J. Natvig and M. Olagnon (Eds.), The Hague, The Netherlands, Vol. 1, pp. 488 - 495.

Hu, J. and Selvadurai, A. P. S. 1995. Influence of tertiary creep on the uplift behaviour of a pipe embedded in a frozen soil. *Proceedings of the 2nd International Conference on Advances in Underground Pipeline Engineering*, J. K. Jeyapalan and M. Jeyapalan (Eds.), ASCE, Seattle, U.S.A., pp 345-358.

Hu, J. and Selvadurai, A. P. S. 1995. Computational modelling of frost heave. *Proceedings of 5th International Symposium on Numerical Models in Geomechanics*, G. N. Pande and S. Pietruszczak (Eds.), Davos, Switzerland, A. A. Balkema, pp. 293-300.

Selvadurai, A. P. S. and Hu, J. 1996. Mechanics of buried chilled gas pipelines, Proceedings of International Pipeline Conference, Calgary , Alberta (Under review).

Contents

List of Figures

Chapter 1

Introduction

1.1 General

In North America, the first documented use of an oil pipeline is that constructed in Pennsylvania in 1861 (Wolbert, 1979). This pipeline measured 10 cm in diameter and 10 km in length. Since then, pipelines have been increasingly utilized as efficient means for the transportation of many resources. At present, pipelines are used to transport energy resources and other fluidized materials, such as oil, natural gas, refined hydrocarbons, coal slurries, mine tailings, municipal and industrial waste and water (Selvadurai and Lee, 1981, 1982; Pickell, 1983; Jeyapalan, 1985; Selvadurai, et al., 1983). The common sizes of pipeline range from 35.56 cm (14 inches) to 76.2 cm (30 inches) in diameter. Large diameter pipelines, up to 121.92 cm (48 inches) in diameter, are gaining popularity as increased demands and are placed on the transportation of the above commodities. The wall thicknesses of pipelines can range from 0.32 cm (0.125 inch) to 1.27 cm (0.50 inch). Pipelines are a favoured mode for the transportation of the above various materials. The primary reasons are as follows: (i) long distance pipelines are less expensive compared to other forms of transportation such as trucks and rail. Pipeline rate for transportation of oil, for example, is about $\frac{1}{5}$ of the rail rate, $\frac{1}{20}$ of the highway rate and less than that for marine transportation; (ii) because of its stationary nature, pipelines are not as sensitive to malfunction or damage. Its continuous, reliable, efficient and safe operation is ideal for operations involving energy resource transportation; (iii) pipelines are able to

operate in adverse environment, for instance, in remote unexplored areas, offshore regions and permafrost arctic regions; (iv) buried pipelines can keep the environmental disturbances to a minimum.

There are of course disadvantages associated with the utilization of pipelines. These include the followings: (i) the initial capital cost is often large; (ii) leakage or blockage during operation cannot be easily located and rectified; (iii) with buried pipelines, the interaction with surrounding soils can introduce unfavourable operating conditions.

Pipelines have been extended to cover almost all populated areas in North America. In the early 1970s, two large pipeline projects were proposed to recover and transport the abundant resources of petroleum and natural gas discovered in northern arctic sedimentary basins. Due to great distances to southern consumers and the large volume of products to be transported, pipelines were considered to be ideally suited and feasible. The details of these proposed pipelines were as follows:

Alyeska warm oil pipeline (see Figure 1.1) is 1300 km in length and 121.92 cm (48 inches) in diameter, with 60 ^0C – 70 ^0C operating temperature . The construction commenced with an above ground pipeline in 1975 and the project was completed in 1977. Basically it has been regarded as a successful pipeline.

Alcan chilled gas pipeline was proposed from Prudhoe Bay field within the Arctic Circle, down the Mackenzie Valley to the United States (see Figure 1.2). A consideration of environmental factors, native rights and economical aspects suggested that buried pipelines were more acceptable. The 121.92 cm (48-inch) diameter and 6440 km (4000 mile) long pipeline would deliver 90.6 million m^3 (3.2 billion cubic feet) per day and 5% of total US consumption of natural gas. The pipeline would have been the most expensive non-military project ever undertaken at that time (1977). Public inquiries into variors aspects of the project, however, lead to its abandonment.

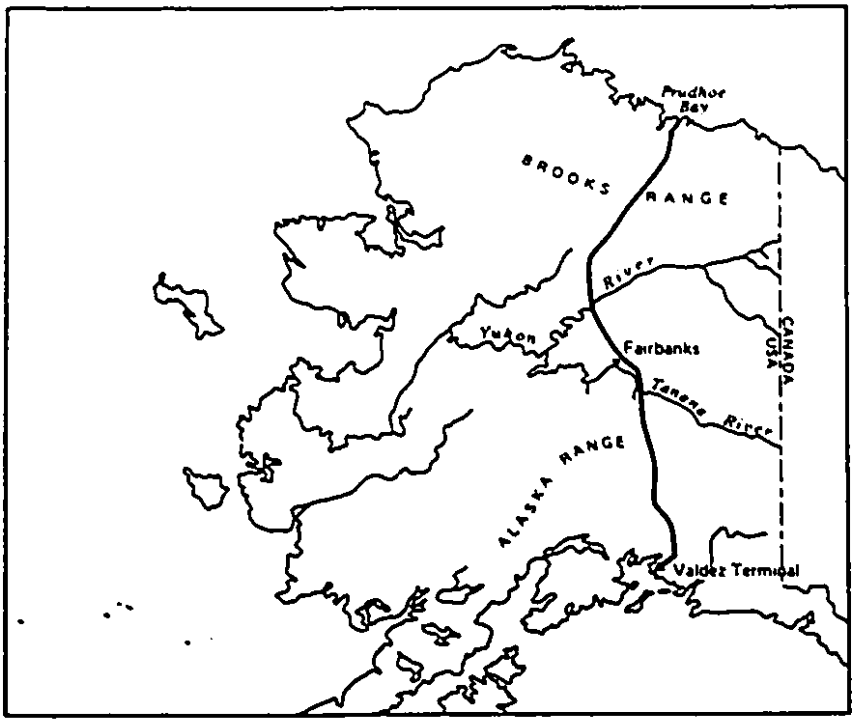

Figure 1.1: Route location of Alyeska oil pipeline (after Williams, 1986)

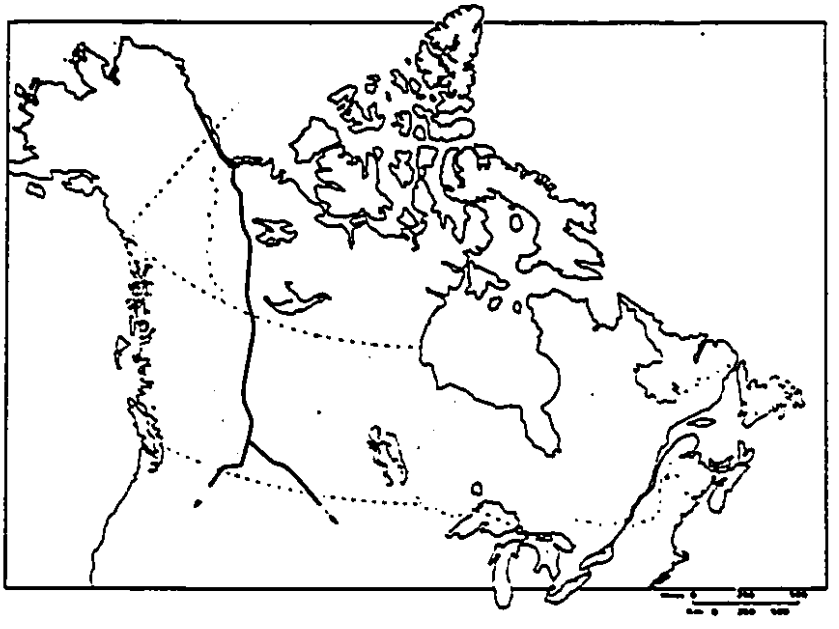

Figure 1.2: Route location of proposed Alcan chilled gas pipeline (after Williams, 1986)

1.2 Geotechnical Problems Associated with Buried Pipelines

Unlike above ground pipelines which can be subjected to the detrimental influences of corrosion, wind loads, earthquakes and interaction with human activities, buried pipeline behaviour is strongly influenced by considerations of geotechnical nature. The structural analysis and design of buried pipelines should take into consideration the mutual interaction between the pipeline and surrounding soil. Such interactions can result from the following (Selvadurai et al., 1983): (i) *movement of the surrounding soil*: fault displacement, frost heave, thawing settlement, soil consolidation, soil creep, ground subsidence due to underground mining, tunnelling, excavation or dewatering, ground movement due to landslides; (ii) *deformation and movement of pipeline*: these could include expansion or contraction due to temperature changes, flotation of a gas pipeline due to buoyancy caused by soil inundation, shape change due to internal pressure; and (iii) *external loadings*: including earthquakes, weight of earth embankments and berms, traffic loads and overburden. Variability of soil properties, environmental conditions and external loads along the length of pipeline can initiate differential movement of ground. Such differential ground movements can induce large stresses and strains in a pipeline located at transition zones and threaten its integrity.

The Alyeska oil pipeline and the Alcan gas pipeline were planned to pass through several thousand kilometres of continuous and discontinuous permafrost terrain under adverse climate condition. At the time of planning of these facilities, very few long distance pipelines had been built in northern region. Consequently little experience and information were available. The problems encountered by oil pipelines are substantially different from those encountered by gas pipelines because of the differenences in operating temperatures of the conveyed materials. The preferable operating

temperature for oil is about 60^0C to 70^0C. Transportation of oil at lower temperature becomes unfeasible since viscosity forces will inhibit their efficient transport. The primary problem associated with transportation of warm oil is that of the melting of permafrost and the resulting thaw-induced settlement around pipeline. In contrast to the warm operating temperature of oil, pressurized gas can be transported in a chilled state, usually a few degrees below 0^0C and slightly colder than the ambient temperature within the near surface region of permafrost. Gas in a chilled state will not induce thawing of the permafrost, which minimizes the risk of thaw settlement and environmental damage and a hazard to the pipeline in terms of flotation. It can, however, present alternative problems. The presence of a chilled gas pipeline in a frost susceptible zone can result in the gradual evolution of a zone of frozen soil around the pipeline. The uniform development of frost heave along a buried pipeline is not expected to have an adverse effect on the pipeline. However, when the frost susceptibility of the soil varies along the pipeline, and particularly if a pipeline located at the transition zone of frozen to unfrozen ground, freezing causes discontinuous or non-uniform heave which can create uplift of the pipeline particularly at zones where the heave processes are markedly different (see Figure 1.3).

Under these conditions, the dominant creep characteristics are a special feature of frozen soil. When uplift forces are large enough, significant movement of pipeline and failure of soils may occur. Bending and uplift forces on a pipeline also develop large strains and stresses in the pipe and can influence the performance of pipelines during their service life. An understanding of the frost heave processes and their accurate modelling are therefore important to the design of a buried pipeline.

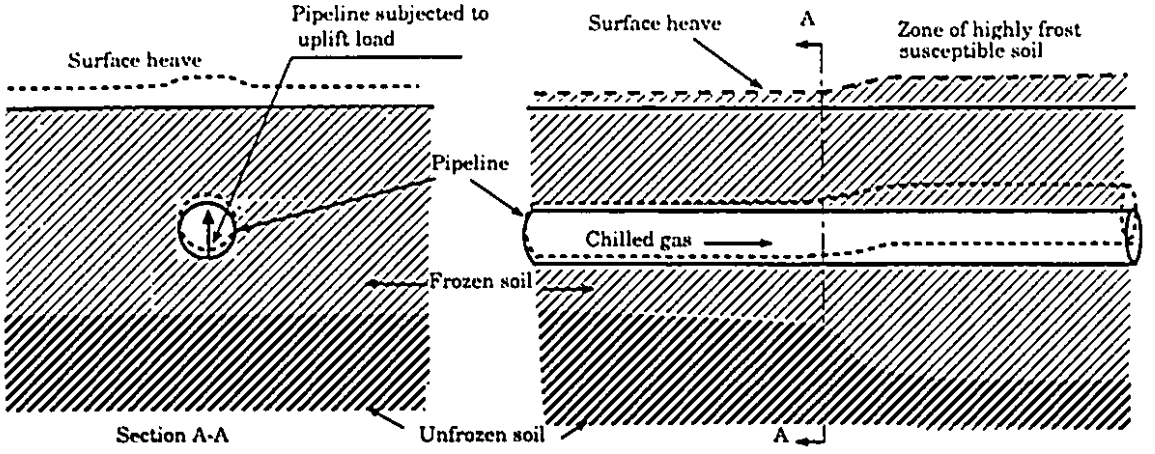

Figure 1.3: Uplift force on pipeline induced by discontinuous frost heave

1.3 Methodologies for Analysis and Design

A successful design can be enhanced by the development of satisfactory procedures for the modelling and analysis of soil-pipeline interaction. A modelling of interaction in a buried pipeline should include the following three aspects: (i) the mechanical behaviour of the soil (ii) the structural response of the pipeline, and (iii) the soil-pipeline interface which achieves the interaction between the pipeline and soil. In general, soils are non-homogeneous and can exhibit complicated non-linear, anisotropic and time-dependent constitutive properties. Pipelines exhibit resistance to axial, flexural and torsional stiffness as well as in plane flexural and membrane stiffness of the shell. The interface between the pipe wall and the soil can also exhibit complicated constitutive characteristics (Selvadurai and Boulon, 1995)

Analytical and computational techniques of varying complexity can be developed for the analysis of a soil-pipeline interaction problem. The rigorous modelling of the interaction problem involving 3-D responses of the pipeline and the soil mass is a complex exercise in computation modelling. Such solutions are computing intensive,

particularly in situations where non-linear and time-dependent effects are involved. An alternative approach to the three dimensional modelling utilizes simplified representations of the soil-pipeline interaction problem.

1.3.1 Winkler type models and other simplified models

The one dimensional Winkler model (Winkler, 1867; Hetenyi, 1946; Selvadurai, 1979) is the most basic and simplified model and has been extensively studied. In the linear elastic Winkler model, the soils surrounding the buried pipeline are treated as a series of unconnected linear elastic spring elements and the deflection δ at any point is thus directly proportional to the load (or stress) at that point and independent of loads (or stresses) applied at other points. The proportionality constant k is referred to the modulus of subgrade reaction. Reviews of the analysis of finite or infinite beam resting on linearly elastic deformable media are given in the treatises by Hetenyi (1946) and Selvadurai (1979).

Selvadurai (1985a) examined the soil-pipeline interaction induced by differential ground movement in the vertical direction. Soil was represented by linear elastic Winkler model and pipeline was modelled by Bernoulli-Euler beam. The flexural moments in the pipeline were obtained by the solution of the differential equation governing the Winkler type model. The paper also presented approximate expressions for estimating the elastic stiffness k under different depths of embedment. Also, the induced maximum flexural moments of pipeline embedded in stiff clay and in soft clay under ground displacement indicated that the latter case had smaller flexural moments.

Elastic idealization of soil cannot predict the complete deformation of soil since

naturally occurring soil media exhibit non-linear and time-dependent effects. However, it can be considered as a first approximation for the solution of a soil-pipeline interaction problem. Also the elastic modelling can be used for verification of numerical techniques which can be better adapted for the solution of complex practical situations. To represent the non-linearity of soils, following high order Winkler models, such as elastic-plastic, hyperbolic, bilinear Winkler models have also been developed (see e.g. Selvadurai et al., 1983).

Selvadurai et al. (1983) summarized the relationships that have been developed to describe the lateral load displacement behaviour of buried pipe. These relationships were of the hyperbolic (Audibert and Nyman, 1977), elastic-perfectly plastic type (Peng, 1978), which were based on experimental results and empirical estimations. Linear elastic parameters and shear strength parameters were utilized to characterize the above models.

Soldatos and Selvadurai (1985b) examined the problem of a linearly elastic beam resting on a nonlinear Winkler-type medium. The nonlinear elasticity of a soil medium was described by a hyperbolic function. A perturbation-Galerkin technique was used to reduce the initially nonlinear equation to a system of linearized equations. Analytical solutions were presented for the problem involving flexure of a beam of finite length which was subjected to a concentrated line load and the flexure of a finite beam having free edges subjected to an initial displacement at its middle point.

The advantage of the Winkler-type models is that the governing equations can be easily solved by finite difference methods, finite element methods and boundary element methods. The primary disadvantage of this model is specification of the subgrade modulus parameter k. A single parameter k cannot accurately represent the complex constitutive behaviour of soil. Furthermore it is not easy to obtain a value for k by experiment and the value of k varies with the change of supporting

conditions and the relative stiffness of the soil-pipeline system (Selvadurai, 1985a). Also the assumption that deflections occur only under the loading point is not realistic because of the strength of soil which allows load transmissibility within it (Selvadurai, 1979).

Instead of using the single parameter k for the Winkler model, two-parameter elastic models which possess some features of continuity were proposed by Filonenko-Borodich (1940), Hetenyi (1946), Pasternak (1954), Reissner (1958), Kerr (1964) and Vlazov and Leontiev (1966). A complete discussion of these models is given by Selvadurai (1979).

The interaction between pipeline and soil was examined by Selvadurai et al. (1990) and Selvadurai (1991) using the Pasternak two-parameter soil model which assumed the existence of shear interaction between the spring elements to represent the load transmissibility or continuity of soils. The pipeline of infinite length was assumed to rest on the surface of a soil overlain by a soft backfill which acted only as a flexible surcharge load. The interactions were induced by prescribing displacements which vary in a random fashion (Selvadurai et al., 1990) and random ground movements (Selvadurai, 1991). The Galerkin finite element scheme was used to solve the basic differential equations. A comparison was made between the Winkler model and the two-parameter Pasternak model to examine the influence of shear continuity and relative stiffness of the soil-pipeline system on the distribution of flexural moments. The results of these studies indicated that as the relative stiffness of the soil-pipeline system increased, the flexural moments by the two models were close. As the relative stiffness of the soil-pipeline system decreased, the flexural moments derived from the two models were largely different.

1.3.2 Numerical analysis using continuum models

Finite element methods have been used quite extensively for the analysis of soil-structure interaction problems. In numerical analysis, the soil masses are treated as continuous media and their mechanical behaviour can be represented by a variety of constitutive models corresponding to their properties, such as the elastic model, the plastic model, the visco-plastic model, etc. Similar considerations apply to the modelling of the structural response of the pipeline. In elementary treatments, the pipeline is modelled as a flexible beam that possesses flexural, axial, shear and torsional stiffness. In more advanced treatments, the shell action of the pipeline and non-linear stress-strain-time behaviour of the shell material are taken into consideration (Selvadurai and Pang, 1988).

A coupled boundary element and finite element scheme was used to simulate numerically the soil-pipeline interaction in a ground subsidence zone (Selvadurai, 1985b), and induced by surface load, ground movement or frost heave (Selvadurai, 1988). Here the surrounding soil was treated as an elastic medium and was represented by boundary elements. The pipeline was modelled as a series of finite elements which experiences only flexural behaviour consistent with the conventional Bernoulli-Euler beam theory. The effect of interface between soil and pipeline was assumed to be perfectly continuous. These results illustrated that the relative rigidity of the soil-pipeline system and location of the pipeline can influence the deflections and flexural moments.

Selvadurai and Pang (1988) carried out a 3-D non-linear finite element analysis of interaction which was induced by discontinuous ground displacement. Soil was modelled as an ideal elastic-plastic continuum which obeyed the Drucker-Prager yield criterion which in turn obeyed an associative flow rule. Soil was modelled by solid

brick elements and the pipeline was modelled by cylindrical shell elements. Complete continuous coupling between the shell elements and brick elements was considered. Distribution of bending moment along the pipeline and hoop stresses of the pipe induced by ground subsidence were given. The results indicated the relative stiffness of the soil-pipeline system and the yielding of the surrounding soils influence the magnitude of induced flexural stresses in pipelines.

In the modelling of soil-pipeline interaction induced by frost heave, adequate considerations should be given to the various time-dependent thermo-mechanical phenomena. The frost heave generation around a chilled gas pipeline and the resulting interaction between the pipeline and the frozen soil have been investigated by Nixon et al. (1983), Konrad and Morgenstern (1984), Ladanyi and Lemaire (1984), Dallimore and Williams (1984), Nixon (1987), Shen and Ladanyi (1991) and Selvadurai and Shinde (1993).

Nixon, Morgenstern and Reesor (1983) implemented a 2-D finite element analysis to examine the problem of a pipeline which crosses the transition zone from unfrozen to frozen ground. Soil was described by both a linear elastic model and a non-linear viscous power law model. Frost heave was predicted by the segregation potential model proposed by Konrad and Morgenstern (1982) and the effect of frost heave on the pipeline was simulated by non-linear applied pressure. The analysis ignored the influence of the stiffness of the pipeline and in the computation it was treated as a passive structural member. Soil strain at the pipe elevation was used to represent the strain in the pipeline. The results which used the power law creep model indicated that the maximum curvature at the pipe elevation was strongly dependent on the thickness of permafrost.

Konrad and Morgenstern (1984) calculated the amount of frost heave under a chilled gas pipeline using the segregation potential model. Radial heat flow and

circular symmetry along the centreline were assumed. The effect of pipe temperature, pipe insulation and ground temperature on frost heave were also discussed.

A model for the coupled analysis of heat, moisture and the stress field was proposed by Shen and Ladanyi (1991) to examine a soil-pipeline interaction problem. The prediction of frost heave was based on the hydrodynamic model. The stress-strain relationships were expressed by the incremental forms, and included a creep strain increment and a volume expansion strain increment. A two-dimensional coupled analysis of the heat transfer and moisture transfer equations were solved by a finite difference method. The mechanical equations were solved by the finite element method. At two extreme pipe-confinement conditions, i.e. one in which the pipeline was either rigidly fixed or free floating, a stress field, temperature field and moisture field at a given time were presented. It was considered that the true conditions would be located between these two limiting cases. The results of the analysis showed that the temperature field agreed well with the experimental value and stress fields around pipeline were close to the measurements.

The most comprehensive computational continuum modelling to date on the problem of frost heave induced soil-pipeline interaction was presented by Selvadurai and Shinde (1993). In their analysis, frost heave was simulated using a simple evolving two-dimensional rectangular frost bulb obtained via an empirical *geothermal simulator* (Nixon, 1987). The pipeline was modelled as a flexible beam with a circular cross section. The mechanical behaviour of the frozen soil was represented by a primary creep model and the unfrozen soil was modelled as an elastic medium. The influences of the heave process and creep behaviour in the primary stage of the frozen soils on the displacement and stress in the buried pipeline were presented. A fundamental observation was that the influences of creep deformation on flexural stresses in the pipeline were at variance with the conventional interpretations, where creep processes have the

general effect of relieving the stresses in embedded structural elements. The results of Selvadurai and Shinde (1993) pointed out that creep deformations of the frozen soils increased the relative displacements in the pipeline and in turn contributed to the development of increased flexural moments in the embedded pipeline.

1.3.3 Experimental modelling

A limited number of experiments which are related to the scope of this research dealing with soil-pipeline interaction have been reported in the literature. Experimental research related to pipelines embedded in unfrozen media are given by Selvadurai and Lee (1981, 1982), Pickell (1973) and Jeyapalan (1985). In this section, some results of interest to the soil-pipeline interaction problem will be presented.

Dallimore (1985) summarized the result of the Canada-France co-operative pipeline freezing test which was carried out at *Station de Gel* at the *Centre de Geomorphologie* at Caen, France. In a controlled environment hall, a steel pipeline measuring 18 m in length and 273 mm in diameter and containing an independent refrigeration system was buried at a transition boundary between a non-frost susceptible sandy soil and a highly frost susceptible silt. The experiment was a multi-disciplinary investigation which examined the evolution of frost heave, the deformation of pipeline and the induced stresses in the pipeline and the surrounding soils.

Slusarchuk et al. (1978) presented the results of a field test which studied the behaviour of a chilled, large-diameter gas pipeline buried in unfrozen frost susceptible ground. Four separate sections of pipe measuring 1.22 m in diameter and 12.2 m in length were buried under different conditions. These conditions were represented by the control, deep burial, restrained and gravel sections. The temperature in all sections was maintained at about $-10^{0}C$ by circulating chilled air through the pipes.

Frost penetration, frost heave and pore water pressure were monitored in the test. The results showed that small changes in the clay fraction appear to cause significant differences in the heave behaviour. The results also indicated that the increased overburden pressure had an effect on the rate of frost heave.

Trautmann et al. (1985) conducted a series of tests which examined the uplift force-displacement response of a pipe buried in granular soil defining under plane strain conditions. Force-displacement curves presented in these tests particularly emphasized the influence of the burial depth and soil density. The results showed that the finite element method which uses either hyperbolic or bilinear relationships can closely predict pipe uplift force in medium and dense sands. This study also indicated that maximum soil forces develop at displacements ranging from $0.005H$ to $0.015H$, where H is the depth of embedment to the centre of the pipe section.

Selvadurai (1993) summarized the results of a series of experiments which examined the enhancement of uplift capacity of buried pipeline embedded in compacted, moist, fine-grained and coarse-grained granular soils, by the arching action of strata-grid reinforcement. The strata-grid was placed immediately above the buried pipeline in an inclined configuration. It was observed the uplift capacity can be substantially increased by the use of this configuration of the reinforcement. It indicated that the increased uplift capacity can be maintained with increasing uplift displacements of the pipe section. This is in contrast to the result for unreinforced soil where the uplift capacity continues to deteriorate with progressive uplift displacements.

1.4 Scope of the Research

The general objective of this thesis research was to investigate the interaction between a buried chilled gas pipeline and surrounding soils using numerical methods which utilize the continuum approach for modelling of soil media. The interaction was induced by differential frost heave. The specific objectives of the research were as follows:

1. Based on the extensive review of available frost heave models in the literature, select a continuum frost heave model which can be utilized to simulate three-dimensional effects of frost heave generation.

2. Develop a constitutive model for frozen soil which accommodates frost heave induced deformations, elastic deformations and creep phenomena. Attention was focused on the development of a complete constitutive model which can describe the entire range of creep behaviour of frozen soils.

3. Implement the frost heave generation models and the constitutive models in a finite element code which can examine the frost heave induced interaction at the transition zone involving a frost susceptible soil. The pipeline was to be modelled either as a Bernoulli-Euler beam or a shell element which accommodates flexural and shear stiffness effects.

4. Identify through a review of the literature the plausible range of parameters governing the frost heave and constitutive responses of specific frost susceptible and frozen soils. Calibrate the model by available data from either laboratory studies or large scale experiments.

5. Conduct a numerical modelling of results of the Canada-France co-operative pipeline project, obtained at different stages of the test, by examining the temperature profiles, soil heave, pipeline deformations, bending moments and stresses in the

pipeline. The pipeline is located in a discontinuous frost heave region at the boundary between a frozen sand and a frost susceptible soil.

1.5 Summaries of Chapters

Chapter 2 deals with the three-dimensional frost heave modelling which is based on a modified hydrodynamic frost heave model. The basic processes in the model involves both heat transfer and moisture flow due to cryogenic effects. Then the model is implemented in a finite element code and such a code is used to examine frost heave generation under three-dimensional conditions. The results of the computational modelling of one-dimensional problems are compared with results of time-dependent frost heave generation in frost susceptible soils tested under one-dimensional conditions.

Chapter 3 focusses on the modelling of mechanical behaviour of frozen soils susceptible to creep. The chapter reviews the varying creep models available in the literature. The chapter also presents the development of a complete creep model. The proposed complete creep model takes into consideration all three creep processes associated with frozen soils. Computations are also conducted to calibrate the predictions of the creep model with observed experimental data.

Chapter 4 develops the numerical modelling of the pipeline. The formulations of a Bernoulli-Euler beam element and a shell element which accommodates flexural and shear stiffness effects are documented. The chapter also contains a verification of shell element modelling by comparison with a known analytical solution.

Chapter 5 deals with the computational analysis of the general creep responses of a variety of geotechnical structures. The structures used in the simulations include a cylindrical footing embedded in a frozen soil and a circular flexible footing placed on

the surface of frozen soil. The loadings can take the forms of either time-independent axial and lateral loads, a multi-step load or a quasi-cyclic load. Other problems examined include a pipe section subjected to uplift loads and an embedded footing which has an interface effect.

Chapter 6 focusses on the computational modelling of the Canada-France co-operative pipeline freezing test. This freezing experiment consists of two major freezing stages. The numerical modelling of the first freezing stage is to examine a buried chilled pipeline intersecting the boundary between the two initially unfrozen soils with significantly different frost susceptibility criteria. The modelling of second freezing stage investigates the problem of a buried chilled pipeline intersecting a transition zone between prefrozen and unfrozen, frost-susceptible soils. Numerical modelling for frost heave when cooling is provided only from an embedded pipeline is also presented.

Chapter 7 presents the conclusions drawn from the thesis research programme and recommendations for future research.

Chapter 2

Three-dimensional Modelling of Frost Heave

2.1 General

Frost heave is volumetric expansion by freezing in situ porewater and mainly migration water during the soil freezing process. The conditions which are required for frost heaving to occur include (i) freezing temperature; (ii) availability of water and (iii) frost-susceptible soil. Penner and Ueda (1977) showed that the overburden pressure also influences the magnitude of frost heave. Non-uniform distribution of any above conditions as well as restriction of frost heaving can induce considerable magnitude of force acting on structures.

The freezing of fine-grained soils often results in the generation of segregated ice, known as ice-lenses. Experimental observations indicate that the ice lenses grow at the isotherm of segregation temperature T_s which is normal to the direction of water flow (Hoekstra, 1969). The zone from the T_s isotherm, which is termed the freezing front, to the frost front (0^0 C isotherm) is referred to as freezing fringe (Miller, 1970). Further experimental evidence of the existence of a freezing fringe were obtained by Loch and Kay (1978).

2.2 Review of Frost Heave Models

Numerous frost heave models have been documented in the literature in geotechnical engineering and soil science. These models will be briefly discussed in this section.

Capillary model

The primary driving force which induces water movement to the warmest ice lenses is classified as capillary suction. In this model, the concept of ice intrusion is used and the advance of the freezing front can be determined by the comparison of radius of pore size r_p in the soil and the radius of interfacial curvature r_{iw} which is dependent on temperature. If $r_p > r_{iw}$, ice can penetrate into the rigid soil, otherwise the freezing front ceases to advance. Thereafter, water can migrate toward the freezing front due to suction until the ice starts to penetrate. As mentioned above, ice lenses usually form at some distance behind the freezing front for clay and silt, which is not identical with what is predicted by this model (Miller, 1978; Gilpin, 1979).

Hydrodynamic model

The coupling heat and moisture transport in a frozen soil was first proposed by Harlan (1973) in a hydrodynamic model. Frost heave generation and influence of overburden pressure were taken into consideration by Guymon and Luthin (1974), Taylor and Luthin (1978), Hopke (1980), Sheppard, Kay and Loch (1978), Jame and Norum (1980), Outcalt(1980), Berg et al. (1980) and Shen and Ladanyi (1987). The driving force of flow takes different forms including the concept of diffusivity and the water potential which is determined by the Clausius - Clapeyron equation.

Segregation potential model

Konrad and Morgenstern (1980, 1981, 1982) introduced a concept of *Segregation*

Potential. In their series of papers, segregation potential is regarded as an engineering parameter which can be used to couple the transfer of mass flow to heat flow. Based on the assumptions that (1) the Clausius-Clapeyron equation is valid at the base of the ice lens; (2) water flow is continuous across the frozen fringe, and water accumulates at the base of the warmest ice-lens; (3) the fringe is characterized by an overall permeability and (4) the temperature varies linearly in the fringe, when a soil sample freezes under different cold-side step temperatures but the same warm side temperature, the water intake flux is proportional to the temperature gradient in the fringe. The expression is given in the form

$$\mathbf{V} = SP \ \ \Delta T \tag{2.1}$$

where

$\mathbf{V}$ is water intake velocity vector;

SP is the segregation potential parameter;

ΔT is temperature gradient in the freezing fringe.

Using the ***segregation potential*** approach, Nixon (1987) and Selvadurai and Shinde (1993) approximated the evolving frost bulb by a rectangular cross section which is defined by a time-dependent width $B(t)$ and a time dependent depth $X(t)$ below the base of the pipeline (see Figure 2.1) in the empirical forms

$$\begin{aligned} X(t) &= X_0 t^{\eta_X} \\ B(t) &= B_0 t^{\eta_B} \end{aligned} \tag{2.2}$$

where X_0, B_0, η_X and η_B are constants which depend on the thermal and frost susceptibility characteristics of the soil.

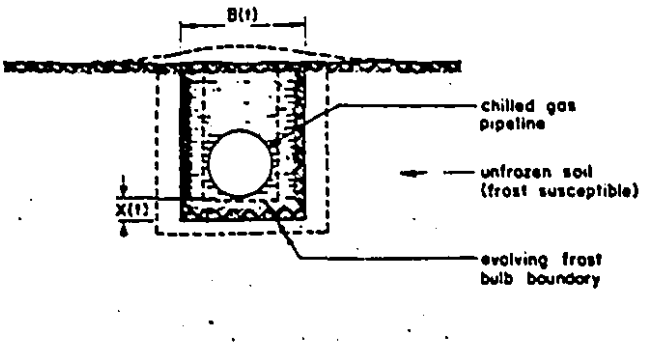

Figure 2.1: Evolving frost bulb by a rectangular region (after Selvadurai and Shinde, 1993)

Rigid ice model

Miller (1978, 1980) assumed that the pore ice and segregated ice in the freezing fringe are inter-connected and form an intricate and continuous rigid body of ice. Ice moves around the soil grains in a freezing fringe under temperature and pressure gradients, which refers to regelation. Ice lenses form by filling the gap which is caused by the relative movement of soil particles under ice pressure.

The above models primarily focus on one-dimensional treatments of frost heave generation. However, one-dimensional uniform deformations of frost heave are of limited interest to practical problems associated with frozen ground engineering. Frost heave mostly occurs in a non-uniform, discontinuous three-dimensional fashion. Recently, two- and three-dimensional frost heave models have been presented by Shen and Ladanyi (1991) and Fremond and Mikkola (1991).

A comprehensive continuum model of frost heave mechanics should take into consideration a variety of complex hydro-thermo-mechanical processes. These could include: (1) heat transfer and moisture migration within both unfrozen and frozen

regions; (2) ice lens formation due to segregation phase change and moving freezing front; (3) stress state and mechanical behaviour of frozen soil, especially creep phenomena. An accurate frost heave model should simultaneously take into consideration the above processes and the model should also: (1) be defined in terms of parameters which can be determined either from laboratory tests or field studies, and (2) be amenable to implementation in a computational code. At present a model which can meet all above requirements in three-dimensional form does not exist in the literature and coupling of all of the above processes in a mathematical model is a difficult task (Selvadurai and Shinde, 1993).

2.3 Modified Hydrodynamic Frost Heave Model

Shen and Ladanyi (1987, 1991) suggested a *modified hydrodynamic model* which couples the process of heat conduction, moisture migration and mechanical effects. The model can be extended to include generalized three-dimensional effects. The frost heave modelling in this thesis utilizes the methodology proposed by Shen and Ladanyi (1987, 1991) and calibrates a *modified hydrodynamic model* for frost action in soils with available experimental data.

It is assumed that the main mode of heat transfer in the frozen soil is by conduction and that the medium is thermally and hydraulically isotropic. In the ensuing sections, the governing equations are summarized. The equation governing heat conduction is given by (Shen and Ladanyi, 1987)

$$C\frac{\partial T}{\partial t} = \lambda \nabla^2 T + L\rho_{(i)}\frac{\partial \theta_{(i)}}{\partial t} \tag{2.3}$$

where

$$\nabla^2 = \frac{\partial^2}{\partial x^2} + \frac{\partial^2}{\partial y^2} + \frac{\partial^2}{\partial z^2} \tag{2.4}$$

is Laplace's operator referred to the three dimensional rectangular Cartesian coordinates (x, y, z). Also,

T is the temperature at a point within the continuum (units ^0C);

$\theta_{(i)}$ is the volume fraction of the ice (units m^3/m^3) which is related to the gravimetric ice content by $\theta = \rho_d w/\rho_{(w)}$.

The thermal and physical parameters of soil are as follows:

λ - thermal conductivity of soil $[Wm^{-1}(^0C^{-1})]$;

L- latent heat of fusion $[J/kg]$;

C- heat capacity of soil $[Jm^{-3}(^0C^{-1})]$;

$\rho_{(i)}$, $\rho_{(w)}$- density of ice and water $[kg/m^3]$;

ρ_d - dry density of soil $[kg/m^3]$;

w - water content by weight (kg/kg).

In a fine-grained soil, not all the water within the soil pores freezes at 0^0C. In some clays up to 50 % of the moisture may exist in a liquid state even at -2^0C (Konrad, 1984). This unfrozen water is mobile and can migrate under the action of a suction gradient. Again, assuming isotropy in relation to the moisture flow processes, the equation governing moisture flow can be obtained as

$$\frac{\partial}{\partial t}[\theta_{(w)} + \frac{\rho_{(i)}}{\rho_{(w)}}\theta_{(i)}] = \frac{k}{\rho_{(w)}g}\nabla^2 P_{(w)} \tag{2.5}$$

where

$P_{(w)}$ is the cryogenic suction pressure in the unfrozen water (Pa);

$\theta_{(w)}$ is the volume fraction of water;

g is gravitational acceleration $[m/sec^2]$.

$\rho_{(w)}$ is density of water $[kg/m^3]$;

k is permeability of soil [m/sec].

Pressure developed in the freezing processes consists of water pressure ($P_{(w)}$) and the ice pressure ($P_{(i)}$). The water pressure and the ice pressure are related by the Clausius - Clapeyron equation. By assuming that (i) the ice pressure reduces to zero at the frost front (0^0C isotherm), (ii) is equal to the local mean stress at or below the segregation temperature (T_s isotherm), and (iii) has a linear variation between the 0^0C and T_s isotherm (Shen and Ladanyi, 1987), the water pressure can be obtained from the relationship:

$$\frac{P_{(w)}}{\rho_{(w)}} - \frac{P_{(i)}}{\rho_{(i)}} = L \ln(\frac{T_k}{T_0}) \tag{2.6}$$

where T_k is the absolute temperature in the soil. Assuming that $\theta_{(w)} = f(T)$, and using Equations (2.3), (2.5) and (2.6), we obtain the equation governing coupled heat and moisture flow as

$$\overline{C}\frac{\partial T}{\partial t} = \overline{\lambda}\nabla^2 T + L\rho_{(w)}k\nabla^2 P_{(i)} \tag{2.7}$$

where

$$\overline{C} = C + L\rho_{(w)}\frac{\partial \theta_{(w)}}{\partial T} \tag{2.8}$$

$$\overline{\lambda} = \lambda + \frac{k\rho_{(w)}^2 L^2}{T_k} \tag{2.9}$$

If the effect of ice pressure on the heat conduction can be neglected, Equation (2.7) can be reduced to the form

$$\overline{C}\frac{\partial T}{\partial t} = \overline{\lambda}\nabla^2 T \tag{2.10}$$

Equations (2.5), (2.6) and (2.10) serve as the governing equations for coupled heat conduction and moisture flow. In these equations, the relationship between the liquid water content in frozen soil and the temperature $\theta_{(w)} = f(T)$ must be determined experimentally.

The boundary conditions governing the field equations are related to T, $P_{(w)}$ and $\theta_{(w)}$. Considering a region Ω with boundary S, the essential boundary conditions for the temperature field can be written as

$$T = T^* \quad on \ (x, y, z) \in S_1 \tag{2.11}$$

where S_1 is a subset of S. For a boundary S_2 through which there is heat loss

$$\lambda \frac{\partial T}{\partial n} + a_T T + b_T = 0 \quad on \ (x, y, z) \in S_2 \tag{2.12}$$

where a_T and b_T are constants chosen to fit a particular boundary and n is the unit normal to S_2.

Similarly on a boundary with prescribed $P_{(w)}$ we have

$$P_{(w)} = P^*_{(w)} \quad on \ (x, y, z) \in S_3 \tag{2.13}$$

The boundary condition governing restricted water flow across a boundary can be written as

$$k \frac{\partial P_{(w)}}{\partial n} + c_{(w)} P_{(w)} + d_{(w)} = 0 \quad on \ (x, y, z) \in S_4 \tag{2.14}$$

where $c_{(w)}$ and $d_{(w)}$ are constants chosen to fit the particular boundary. The formulation of the problem will be complete when suitable, initial conditions are prescribed for T and $P_{(w)}$, i.e.

$$T = \overline{T}^0; \quad P_{(w)} = \overline{P}^0_{(w)} \quad on \ (x, y, z) \in \Omega \tag{2.15}$$

It must be remarked that in the Clausius-Clapeyron Equation (2.6), both the pore water pressure and ice pressure are treated as scalar variables. While the pore water pressure can be treated as a scalar variable, the pressures in the ice will not be a scalar quantity. Due to the rigidity of the ice, the stresses in the ice will have a tensorial structure. This aspect is a limitation in the modelling but a useful and universally accepted result. The Clausius-Clapeyron equation can be generalized to include three dimensional effects (see e.g. Fremond and Mikkola, 1991). The adaptation of these results is however beyond the scope of this thesis.

The heat capacity and thermal conductivity in Equation (2.3) can be defined as follows (see e.g. Kay et al., (1977))

$$C = C_s\theta_s + C_w\theta_w + C_i\theta_i \tag{2.16}$$

where C_s, C_w and C_i are the heat capacities of the soil grains, water and ice and θ_s, θ_w and θ_i are the respective volume fractions. Also following Kay et al. (1977), we note that

$$\lambda = \lambda_s^{\theta_s}\lambda_w^{\theta_w}\lambda_i^{\theta_i} \tag{2.17}$$

where λ_s, λ_w and λ_i are, respectively, the thermal conductivities of the solid particles, water and ice.

The freezing of pore water induces a volumetric strain. By virtue of ice lens formation, the volumetric expansion is generally anisotropic. In the current study, however, the frost heave is assumed to be isotropic and associated incremental strains are given by

$$d\epsilon_{ij}^{(h)} = d\epsilon^{(h)}\delta_{ij} \tag{2.18}$$

where $d\epsilon^{(h)}$ is the volumetric expansion strain due to frost heave for a time interval dt, i.e.

$$d\epsilon^{(h)} = 0.09 d\theta_{(i)} + d\theta_{(w)} \tag{2.19}$$

where $d\theta_{(i)}$ and $d\theta_{(w)}$ are respectively the incremental changes in the pore ice content and pore water at time dt.

2.4 Finite Element Modelling

2.4.1 General

In the finite element scheme, the domain of the soil region which includes frozen and unfrozen soils is modelled by 8-noded three dimensional solid isoparametric elements. The continuous displacement vector $\{\underset{\sim}{u}\}$ within the material domain can be represented by the discretized nodal displacement vector $\{\underset{\sim}{u}_i\}$.

$$\{\underset{\sim}{u}\} = [\mathbf{N}]\{\underset{\sim}{u}_i\} \tag{2.20}$$

where [N] is the shape function matrix for the element. The strain vector can be written in the matrix form as

$$\{\underset{\sim}{\epsilon}\} = [\nabla]\{\underset{\sim}{u}\} \tag{2.21}$$

where $[\nabla]$ is a differential operator matrix relating displacements to strains. It follows that

$$\{\underset{\sim}{\varepsilon}\} = [\nabla][\mathbf{N}]\{\underset{\sim}{u}_i\} = [\mathbf{B}]\{\underset{\sim}{u}_i\} \tag{2.22}$$

where [**B**] is a matrix of strain-displacement relationship. A typical sub-matrix $[\mathbf{B}]_i$ is given as

$$[\mathbf{B}]_i = \begin{bmatrix} \frac{\partial N_i}{\partial x} & 0 & 0 \\ 0 & \frac{\partial N_i}{\partial y} & 0 \\ 0 & 0 & \frac{\partial N_i}{\partial z} \\ \frac{\partial N_i}{\partial y} & \frac{\partial N_i}{\partial x} & 0 \\ 0 & \frac{\partial N_i}{\partial z} & \frac{\partial N_i}{\partial y} \\ \frac{\partial N_i}{\partial z} & 0 & \frac{\partial N_i}{\partial x} \end{bmatrix} \tag{2.23}$$

The incremental form of the stress-strain relationship can be expressed as

$$\{d\underset{\sim}{\sigma}\} = [\mathbf{D}]\{d\underset{\sim}{\varepsilon}\} \tag{2.24}$$

where the stress increment vector $\{d\underset{\sim}{\sigma}\}$ and the strain increment vector $\{d\underset{\sim}{\varepsilon}\}$ are defined, respectively, as

$$\{d\underset{\sim}{\sigma}\}^T = \{\, d\sigma_{xx} \quad d\sigma_{yy} \quad d\sigma_{zz} \quad d\sigma_{xy} \quad d\sigma_{yz} \quad d\sigma_{xz} \,\} \tag{2.25}$$

$$\{d\underset{\sim}{\varepsilon}\}^T = \{\, d\epsilon_{xx} \quad d\epsilon_{yy} \quad d\epsilon_{zz} \quad d\epsilon_{xy} \quad d\epsilon_{yz} \quad d\epsilon_{xz} \,\} \tag{2.26}$$

For an isotropic linear-elastic material, [**D**] can be expressed in the form

$$[\mathbf{D}] = \frac{E(1-\nu)}{(1+\nu)(1-2\nu)} \begin{bmatrix} 1 & \frac{\nu}{1-\nu} & \frac{\nu}{1-\nu} & 0 & 0 & 0 \\ & 1 & \frac{\nu}{1-\nu} & 0 & 0 & 0 \\ & & 1 & 0 & 0 & 0 \\ & & & \frac{1-2\nu}{1-\nu} & 0 & 0 \\ & sym. & & & \frac{1-2\nu}{1-\nu} & 0 \\ & & & & & \frac{1-2\nu}{1-\nu} \end{bmatrix} \tag{2.27}$$

where E is Young's modulus and ν is Poisson's ratio.

The element stiffness matrix can be written as

$$[\mathbf{K}] = \int_{\Omega} [\mathbf{B}]^{T^*} [\mathbf{D}][\mathbf{B}] d\Omega \tag{2.28}$$

2.4.2 Finite element representation of heat transfer

In the finite element treatment of heat transfer, the Galerkin technique can be used to obtain the integral or weak form of the governing differential equation (2.10). By introducing an arbitrary weighting function δT for the temperature field, in general, we have

$$\int_{\Omega} \{\overline{\lambda} \nabla \delta T (\nabla T) - \overline{C} \delta T \frac{\partial T}{\partial t}\} d\Omega + \int_{S} \delta T \{a_T T + b_T\} dS = 0 \tag{2.29}$$

where a_T and b_T are constants which are chosen to fit the boundary S.

Introducing the shape function [N], it can be shown that (see Equation (2.10))

$$\int_{\Omega} [\mathbf{N}][\overline{\lambda} \nabla^2 T] d\Omega = \int_{\Omega} [\mathbf{N}] \overline{C} \frac{\partial T}{\partial t} d\Omega \tag{2.30}$$

Considering the natural boundary condition

$$\frac{\partial T}{\partial n} = 0 \tag{2.31}$$

and using the result

$$\{\mathbf{T}\} = [\mathbf{N}]\{\mathbf{T_i}\} \tag{2.32}$$

Equation (2.30) can be rewritten as

$$[\mathbf{K}]\{\mathbf{T}\} - [\mathbf{K_c}]\frac{\partial\{\mathbf{T}\}}{\partial t} = \{\mathbf{F}\} \tag{2.33}$$

where

$$[\mathbf{K}] = \int_\Omega \overline{\lambda}[\mathbf{B}]^{T^*}[\mathbf{B}]d\Omega \tag{2.34}$$

$$[\mathbf{K_c}] = \int_\Omega \overline{C}[\mathbf{N}]^{T^*}[\mathbf{N}]d\Omega \tag{2.35}$$

$$[\mathbf{B}] = \nabla[\mathbf{N}] \tag{2.36}$$

$[\mathbf{B}]^{T^*}$ denotes the transpose of $[\mathbf{B}]$ and $\{\mathbf{F}\}$ is a column matrix which is determined by the internal heat source and boundary conditions.

The time integration in Equation (2.33) is performed by employing a Crank-Nicholson method (Crank and Nicholson, 1947; Eranti, 1986). For the j^{th} and $(j+1)^{th}$ time increment

$$[[\mathbf{K}] + \frac{2}{\Delta t}[\mathbf{K_c}]]\{\mathbf{T}\}^{j+1} = [\frac{2}{\Delta t}[\mathbf{K_c}] - [\mathbf{K}]]\{\mathbf{T}\}^j + 2\{\mathbf{F}\} \tag{2.37}$$

The temperature field at any time t can be computed by summation of all temperatures computed by Equation (2.37) for each time step. It should be noted that the Crank-Nicholson method is stable for all values of time intervals. When the temperatures at some points are below the freezing temperature, the cryogenic suction or

pore water pressure, $P_{(w)}$, at these locations can be calculated by using the Clausius-Clapeyron equation (2.6). The moisture movement can be defined by the coupling between the volumetric moisture content $\theta_{(w)}$ and pore water pressure $P_{(w)}$.

2.4.3 Finite difference representation of water movement

The governing equation (2.5) can be solved by using an explicit finite difference scheme. We have

$$\begin{aligned}(\theta_{(i)})_{lmn}^{j+1} &= (\theta_{(i)})_{lmn}^{j} + \frac{\rho_{(w)}}{\rho_{(i)}}[a_l\overline{\lambda}_{l-\frac{1}{2}}^{j+1}(P_{(w)})_{l-1mn}^{j+1} \\ &-(a_l\overline{\lambda}_{l-\frac{1}{2}}^{j+1} + b_l\overline{\lambda}_{l+\frac{1}{2}}^{j+1})(P_{(w)})_{lmn}^{j+1} + b_l\overline{\lambda}_{l+\frac{1}{2}}^{j+1}(P_{(w)})_{l+1mn}^{j+1}] \\ &+\frac{\rho_{(w)}}{\rho_{(i)}}[a_m\overline{\lambda}_{m-\frac{1}{2}}^{j+1}(P_{(w)})_{lm-1n}^{j+1} - (a_m\overline{\lambda}_{m-\frac{1}{2}}^{j+1} \\ &+b_m\overline{\lambda}_{m+\frac{1}{2}}^{j+1})(P_{(w)})_{lmn}^{j+1} + b_m\overline{\lambda}_{m+\frac{1}{2}}^{j+1}(P_{(w)})_{lm+1n}^{j+1}] + \frac{\rho_{(w)}}{\rho_{(i)}}[a_n\overline{\lambda}_{n-\frac{1}{2}}^{j+1}(P_{(w)})_{lmn-1}^{j+1} \\ &-(a_n\overline{\lambda}_{n-\frac{1}{2}}^{j+1} + b_n\overline{\lambda}_{n+\frac{1}{2}}^{j+1})(P_{(w)})_{lmn}^{j+1} + b_n\overline{\lambda}_{n+\frac{1}{2}}^{j+1}(P_{(w)})_{lmn+1}^{j+1}] \\ &-\frac{\rho_{(w)}}{\rho_{(i)}}[(\theta_{(w)lmn})^{j+1} - (\theta_{(w)lmn})^{j}]\end{aligned} \tag{2.38}$$

with

$$a_l = \frac{\Delta t}{\Delta x_l(\Delta x_l + \Delta x_{l+1})} \tag{2.39}$$

$$b_l = \frac{\Delta t}{\Delta x_{l+1}(\Delta x_l + \Delta x_{l+1})} \tag{2.40}$$

l, m and n are the spatial nodes along x, y and z directions respectively.

2.4.4 Equivalent nodal force

The ultimate objective of the coupled heat-moisture flow algorithm is to utilize the procedures to compute the time-dependent evolution of frost heave strains within

the medium. Using the incremental initial strain method, the equivalent nodal force increment vector $d\{\mathbf{R}\}$ due to volumetric expansion in soil can be written as

$$d\{\mathbf{R}\} = \int_{\Omega} [\mathbf{B}]^T [\mathbf{D}] (d\epsilon_{ij}^{(h)} + d\epsilon_{ij}^{(c)} + d\epsilon_{ij}^{(th)}) d\Omega \tag{2.41}$$

where

$d\epsilon_{ij}^{(h)}$ is heave strain increment given in Equation (2.19);

$d\epsilon_{ij}^{(c)}$ is creep strain increment;

$d\epsilon_{ij}^{(th)}$ is thermal strain increment.

The thermal strain increment can be expressed in the form

$$d\epsilon_{ij}^{(th)} = \alpha \, dT \delta_{ij} \tag{2.42}$$

where

α is coefficient of linear expansion;

dT is the increment of temperature;

δ_{ij} is Kronecker delta function.

2.5 Numerical Simulation

A three-dimensional finite element code was developed following the procedures in the preceding sections. Using this code it is possible to model one-dimensional, two-dimensional and three-dimensional problems by applying the relevant initial conditions and boundary conditions. The results of the following frost heave experiments are used for the purpose of comparison with computational models.

2.5.1 The one-dimensional problem of frost heave development

(1) Penner's test

In the test carried out by Penner (1986), a cylindrical sample of saturated soil measuring 10 cm in diameter and 10 cm in length was used (see Figure 2.2). The freezing was conducted in an open system by ramping the temperature at the two ends of the cylindrical sample at 0.02 ^0C /day. The initial temperature at the top of the sample was 0.55 ^0C and the temperature at the base of the sample was specified at -0.35 ^0C. The resulting time-dependent frost heave and the frost penetration were recorded. The finite element procedure was used to examine this one dimensional problem. Figure 2.3 shows the three-dimensional finite element configuration used to model the one dimensional frost heave problem. Although the configuration of the finite element discretization is three dimensional, the boundary conditions applicable to heat flow, moisture transfer and deformations are organized in such a way that the hydro-thermo-mechanical processes result in a *one-dimensional problem* referred to a cuboidal region. The analysis is therefore applicable to the one-dimensional experimental configuration discussed by Penner (1986).

The paper by Penner (1986) recorded the development of frost heave in an experiment which lasted approximately 250 hours. Unfortunately, there was no record of the hydro-thermo-mechanical parameters applicable to the particular soil. The thermal conductivity and heat capacity parameters for soil grains, water and ice used in the numerical computation are the same as those cited by Harlan and Nixon (1978):

$$C_s = 2.20 \times 10^6 \quad C_w = 4.18 \times 10^6 \quad C_i = 1.93 \times 10^6 \quad (Jm^{-3}\,{}^oC^{-1}) \qquad (2.43)$$

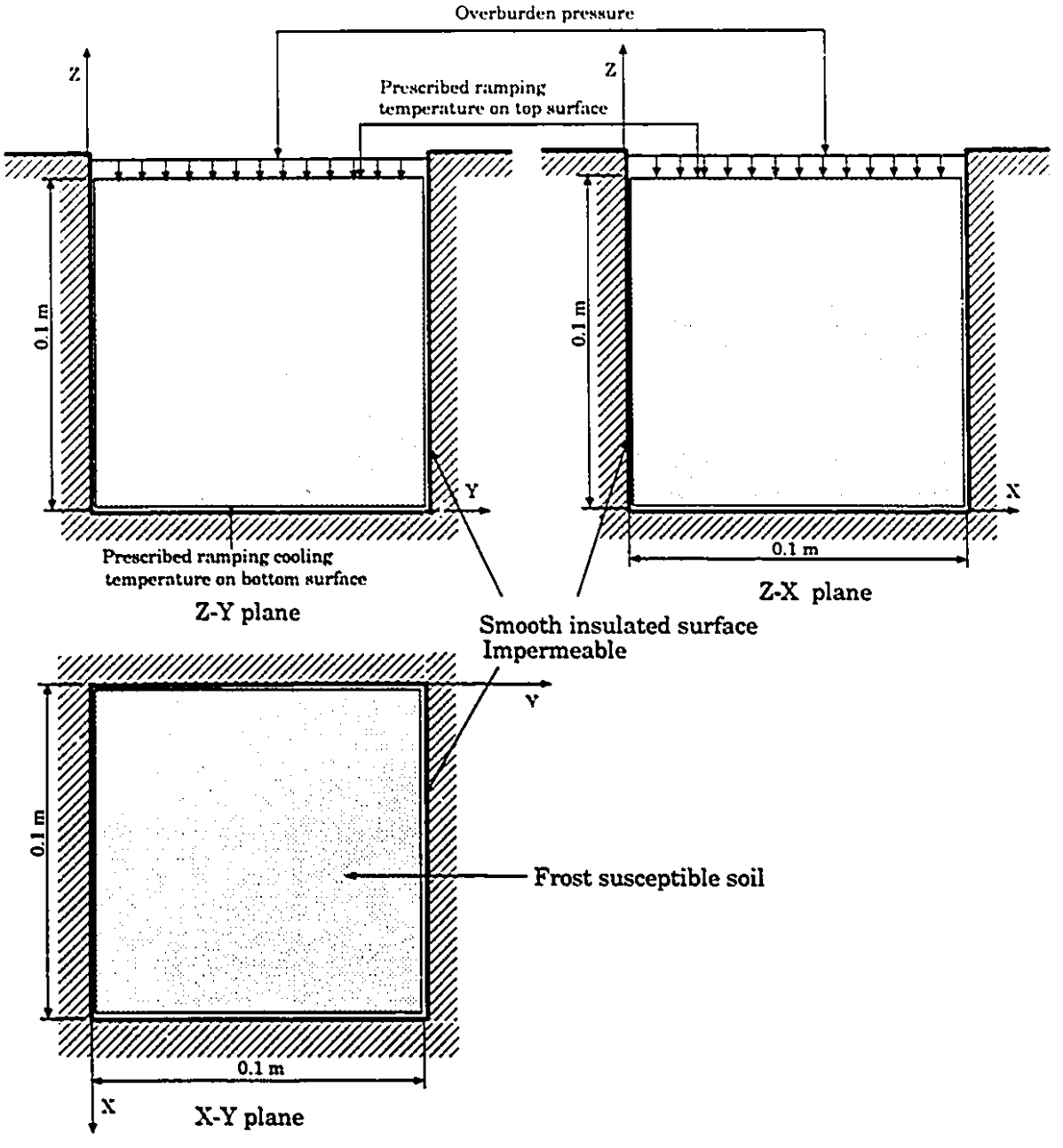

Figure 2.2: One-dimensional frost heave generation in a cuboidal region

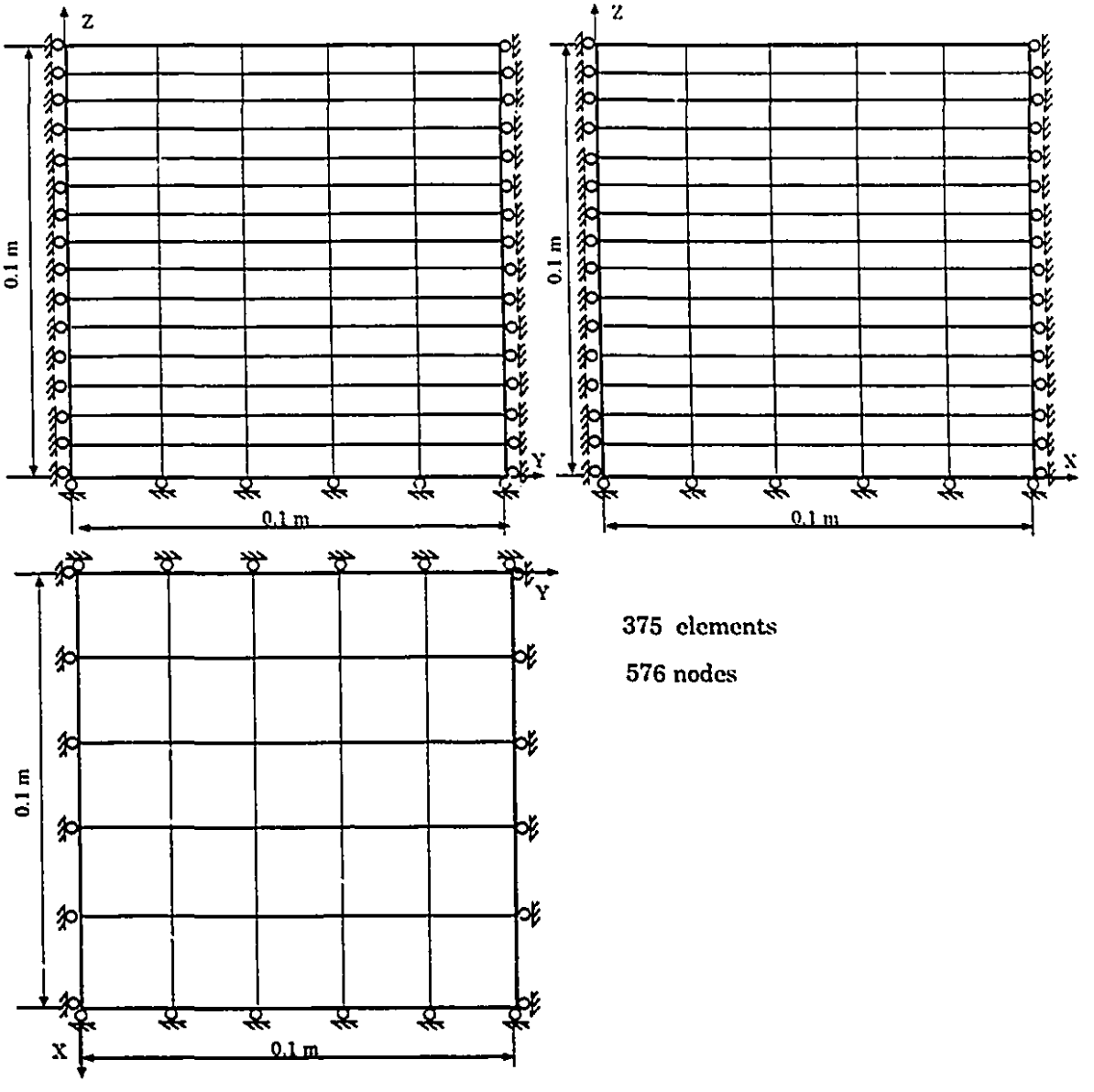

Figure 2.3: Finite element discretization of the cuboidal element

$$\lambda_s = 1.950 \quad \lambda_w = 0.602 \quad \lambda_i = 2.220 \quad (W m^{-1} {}^{o}C^{-1}) \tag{2.44}$$

The self weight of the soil is taken as 19 kN/m^3. $E = 12,000\ kPa$; $\nu = 0.3$.

The hydraulic conductivity of the frozen soil is modelled as a temperature dependent property. An example of such a variation was given by Horiguchi and Miller (1983).

$$k = \begin{cases} 3.072 \times 10^{-11} e^{13.438T} & -0.3^{o}C < T < T_f; \\ 5.453 \times 10^{-13} & T \leq -0.3^{o}C \end{cases} \quad m/sec \tag{2.45}$$

Since the hydraulic conductivity of the frost susceptible soil is an important parameter in the problem, its value is varied according to

$$k = \begin{cases} 3.072N \times 10^{-11} e^{13.438T}\ m/sec & -0.3^{o}C < T < T_f; \\ 5.453N \times 10^{-13}\ m/sec & T \leq -0.3^{o}C \end{cases} \tag{2.46}$$

where $N \in (1, 10)$.

Figure 2.4 shows the comparison of the results of the finite element technique proposed in this study with the results obtained by Penner (1986). These results have been matched by varying the value the hydraulic conductivity and the specific value used in the computations corresponding to the case where the constant N occurring in Equation (2.46) is set equal to 6. Figure 2.5 illustrates the influence of k on the magnitude of frost heave. As is evident, the reduction in the hydraulic conductivity results in a corresponding reduction in the magnitude of the frost heave.

A simulation was also performed by taking the coefficient of permeability of Caen silt as the value given by Shen and Ladanyi (1991) (Caen silt was the silty soil used in a large scale laboratory test involving a pipeline in a frost heave zone conducted at the Centre de Geomorphologie at Caen, France); i.e.

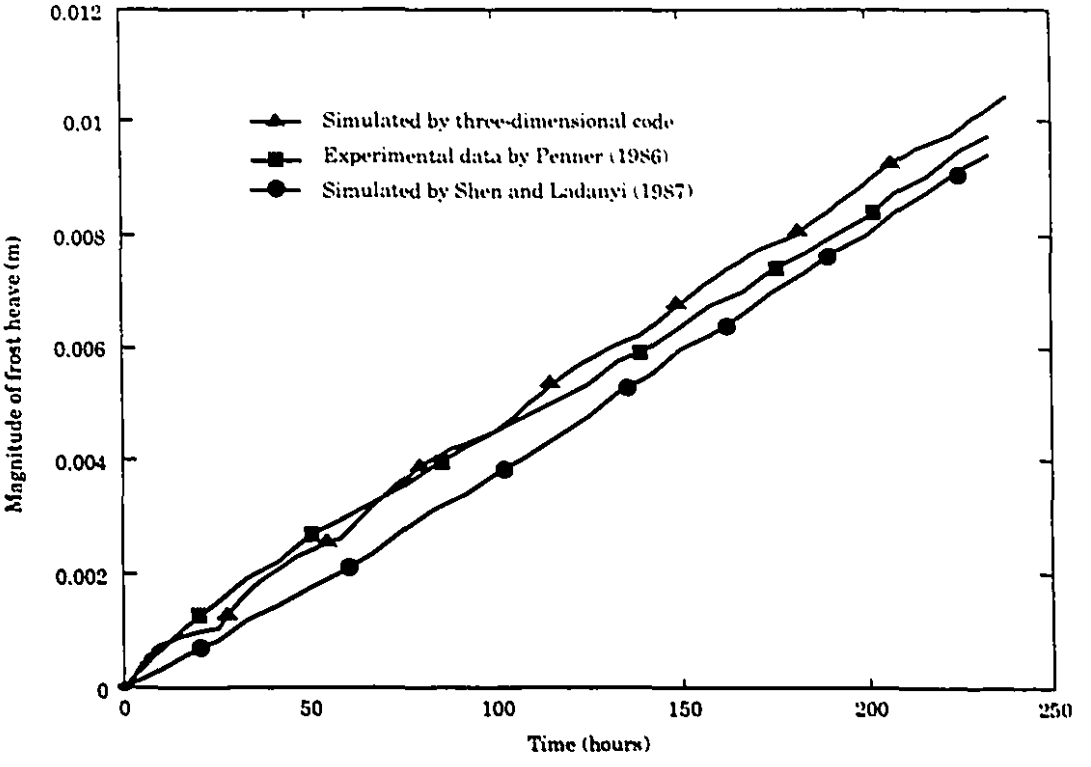

Figure 2.4: Frost heave generation in a sample of silty clay

$$k = \begin{cases} 1.075 \times 10^{-9} e^{23.39T} & -0.3^{o}C < T < T_f; \\ 8.0499 \times 10^{-13} & T \leq -0.3^{0}C \end{cases} \quad m/sec \qquad (2.47)$$

Figure 2.6 shows the time-dependent evolution of one-dimensional frost heave in a cuboidal element measuring 10 cm × 10 cm × 10 cm. The results obtained by Shen and Ladanyi (1987) for the specific case when the permeability is defined by Equation (2.47) and the experimental results obtained by Penner (1986) are also shown for purposes of comparison. The results given in Figure 2.6 indicate that the development of frost heave under one-dimensional conditions obtained by the computational modelling can be matched reasonably well with observations of one-dimensional experiments. In particular, the trends of the computational results agree

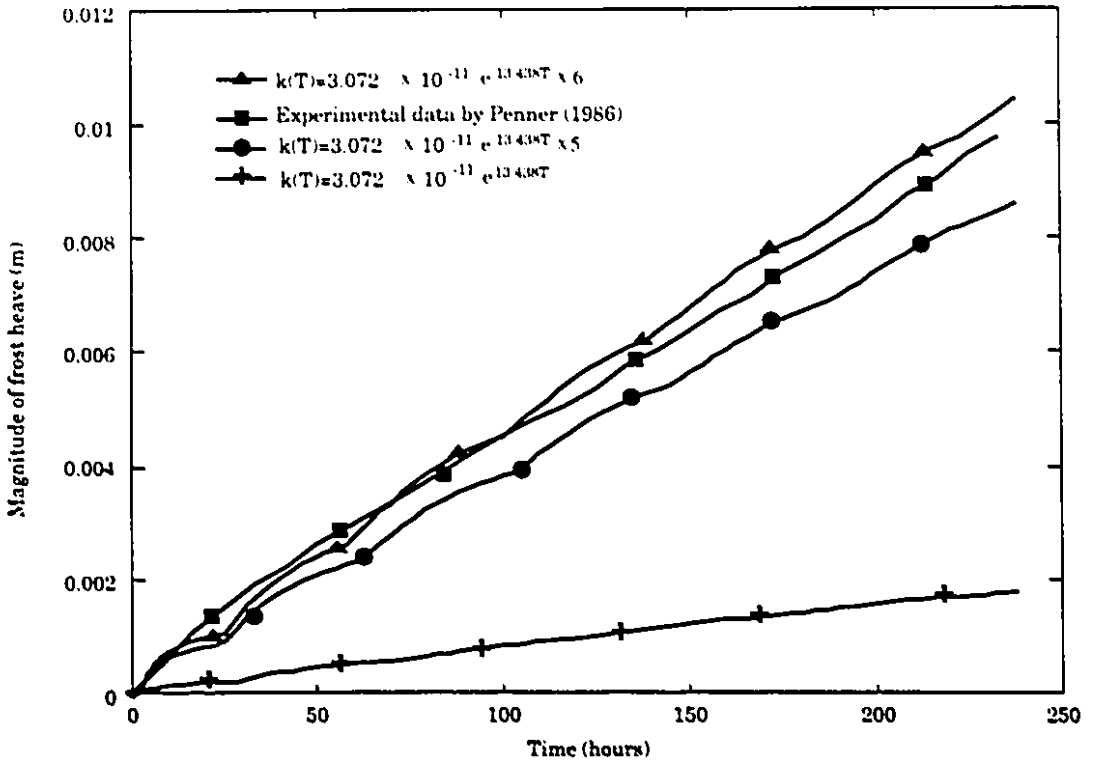

Figure 2.5: Influence of hydraulic conductivity on the generation of frost heave

very closely with experimental results.

(2) Frost heave test at Carleton University

In the test conducted at the Geotechnical Science Laboratory, Carleton University, a cylindrical soil sample was 110 *mm* long and 102 *mm* in diameter. The sample was prepared by the consolidation of a 50 percent soil-water slurry in a test cell (Dallimore, 1985). The one-dimensional freezing was conducted with constant end temperature. The temperature at the top of the sample was 1.8 ^0C and the temperature at the base of the sample was -5 ^0C.

We adopt the finite element configuration shown in Figure 2.3 and thermal constants which were assigned to the simulation of Penner's test. By modifying the

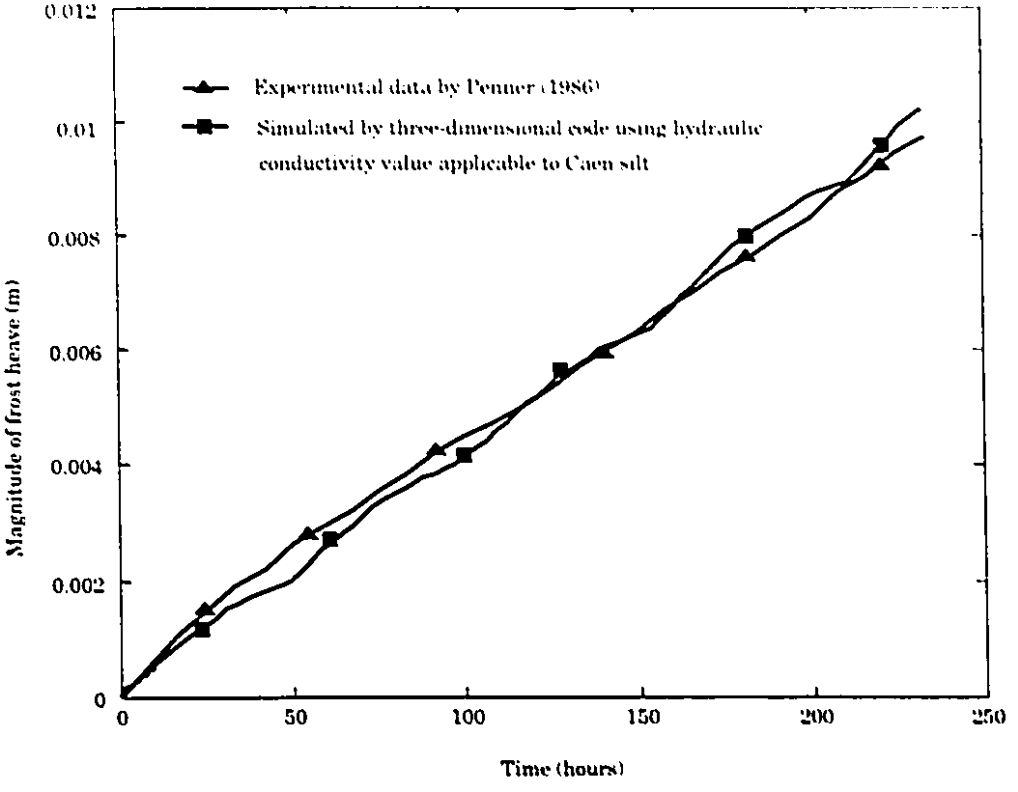

Figure 2.6: Frost heave generation in a sample of silt clay

coefficient of permeability to

$$k = \begin{cases} 26.25 \times 10^{-9} e^{23.99T} & -0.3^{0}C < T < T_f; \\ 12.07 \times 10^{-12} & T \leq -0.3^{0}C \end{cases} \quad m/sec \qquad (2.48)$$

the results of the computational modelling can reasonably match the results of the experiment (Figure 2.7).

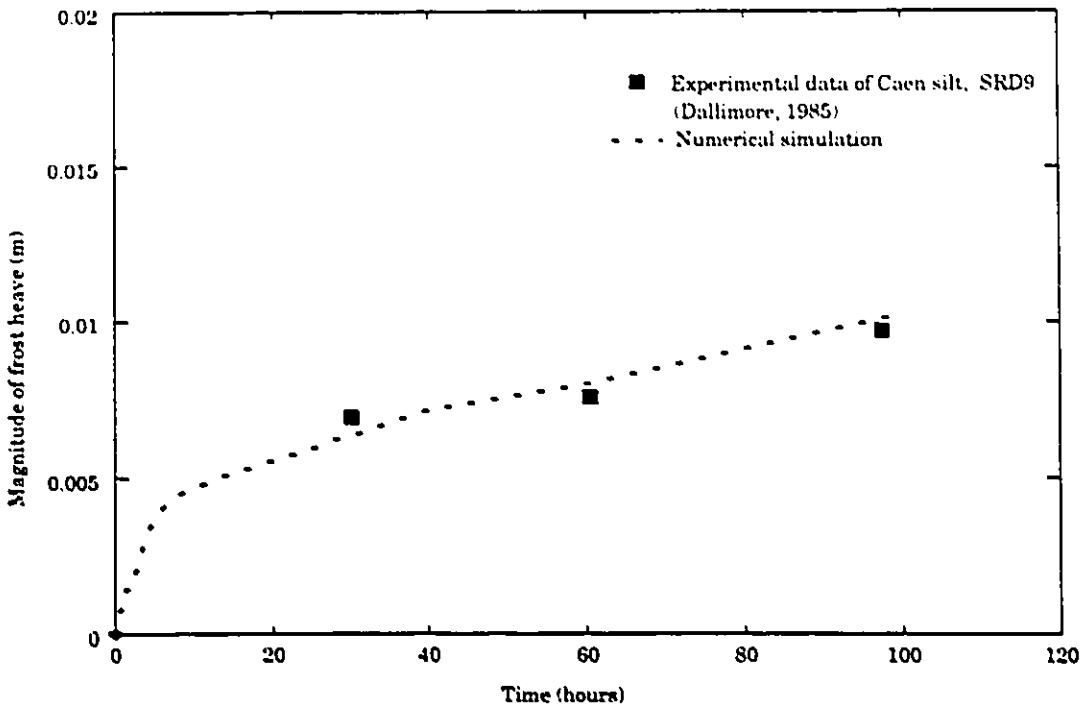

Figure 2.7: One-dimensional generation of frost heave in a sample of Caen silt

2.5.2 The two-dimensional problem of frost heave development

The computational modelling procedure was used to examine the problem of two dimensional development of frost heave in a cuboidal element of dimensions 10 cm × 10 cm × 10 cm. The two-dimensional nature of the frost heave development was achieved by allowing the freezing action to develop along a line of elements located at the edge of the cuboidal element (see Figure 2.8). The initial freezing temperature was -0.35^0C and the initial temperature at the top of the sample was 0.55^0C. These temperatures were ramped at 0.02^0C /day in the freezing period. The thermal and mechanical properties of the soil are identical to those used in the one-dimensional modelling and permeability is defined by the value applicable to Caen silt in Equation

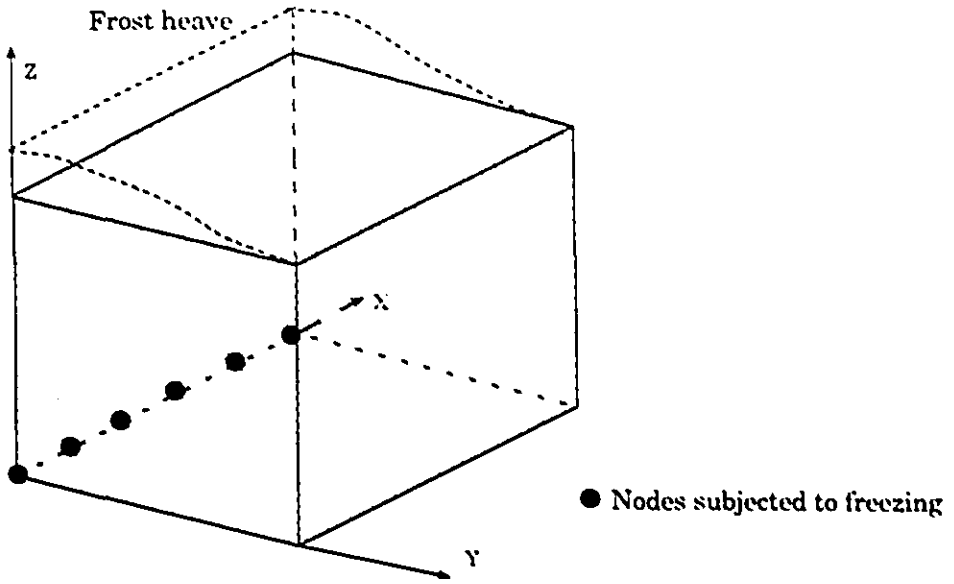

Figure 2.8: Nodes subjected to freezing at two-dimensional case

(2.47). Figures 2.9 and 2.10 illustrate the temperature contours within one plane (x=0) of the cuboidal element for lapsed times of t = 100 hours and 233 hours respectively. It is evident that the pattern of heat transfer is consistent with the imposed thermal boundary conditions.

We now focus attention on the development of frost heave at the surface of the element due to the internal cooling along a line of nodes located along the base of the element. Figures 2.11 and 2.12 illustrate the development of frost heave at the surface of the cuboidal element for lapsed times of 50 hours and 233 hours respectively. Again, the frost heave profiles are consistent with the boundary conditions associated with the cuboidal element. The surface heave above the line of nodes subjected to freezing, by virtue of symmetry, has a zero slope.

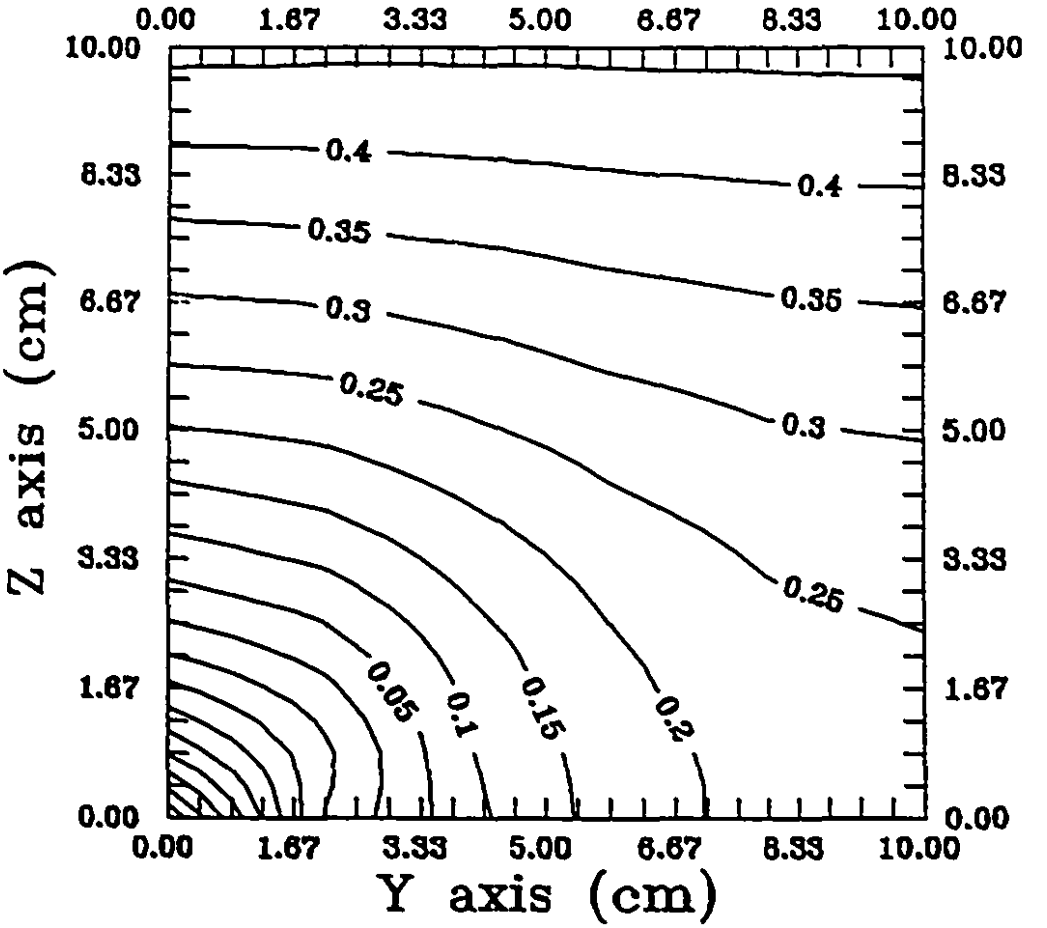

Figure 2.9: Temperature contour (^0C) within a cuboidal Caen silt region at 100 hours

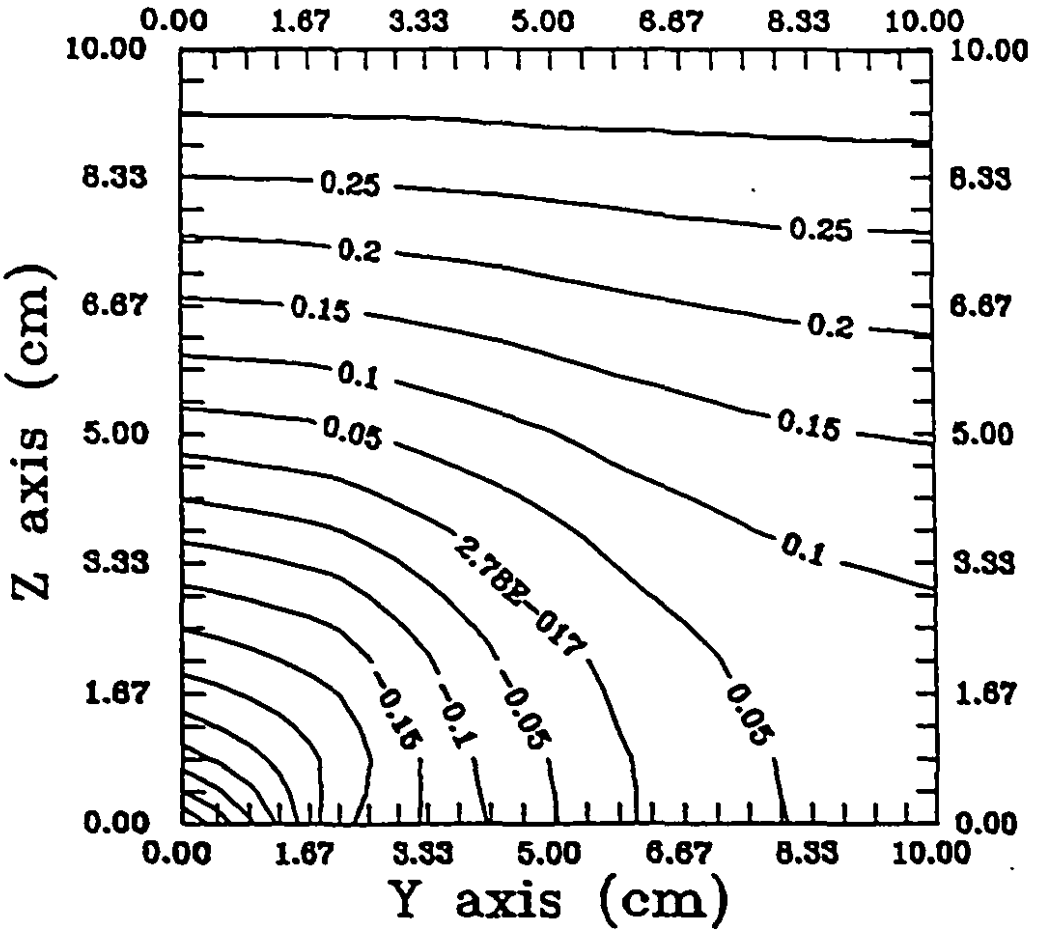

Figure 2.10: Temperature contour (^oC) within a cuboidal Caen silt region at 233 hours

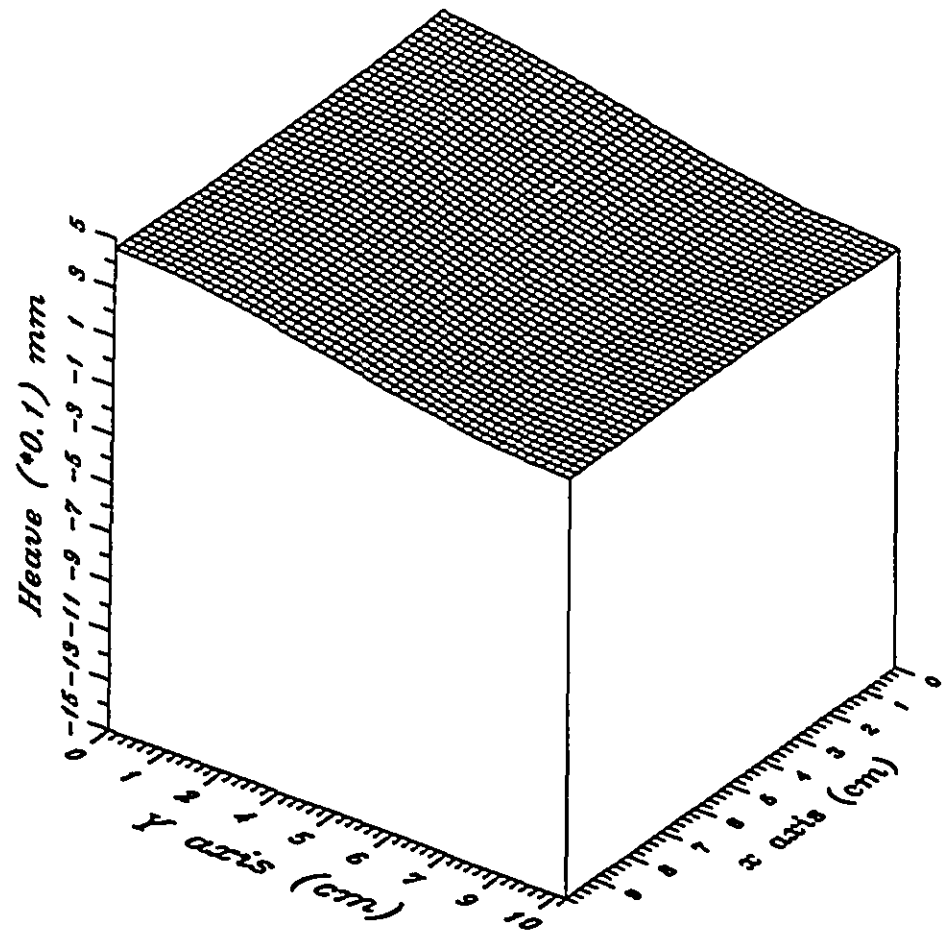

Figure 2.11: Surface heave of a cuboidal element subjected to base freezing along a line of edge nodes at 50 hours: Maximum heave = 0.465 mm

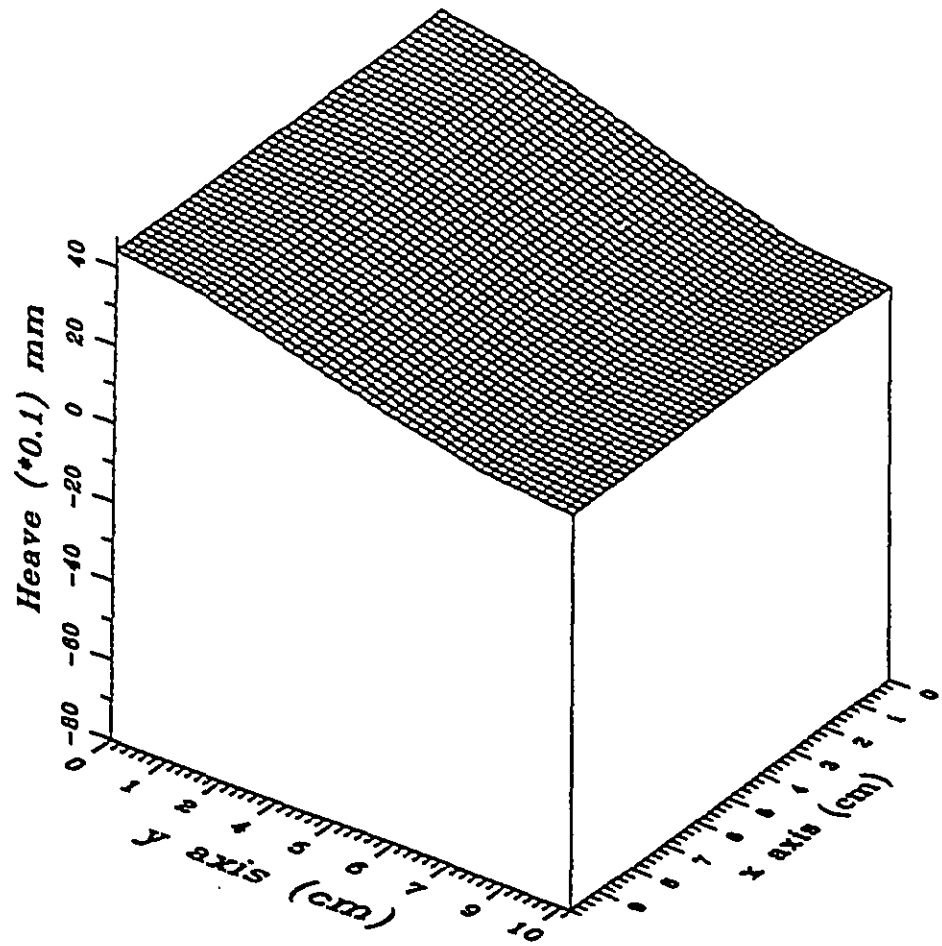

Figure 2.12: Surface heave of a cuboidal element subjected to base freezing along a line of edge nodes at 233 hours: Maximum heave = 4.78 mm

2.5.3 The three-dimensional problem of frost heave development

We now consider the three dimensional problem where the cuboidal element is subjected to cooling at the base of the element at two nodes locations (see Figure 2.13). The Figures 2.14 and 2.15 illustrate the development of frost heave at the surface of the cuboidal element. Again it is evident that the trend indicated in the development of frost heave is consistent with the cooling of isolated nodes located at the base of the cuboidal element.

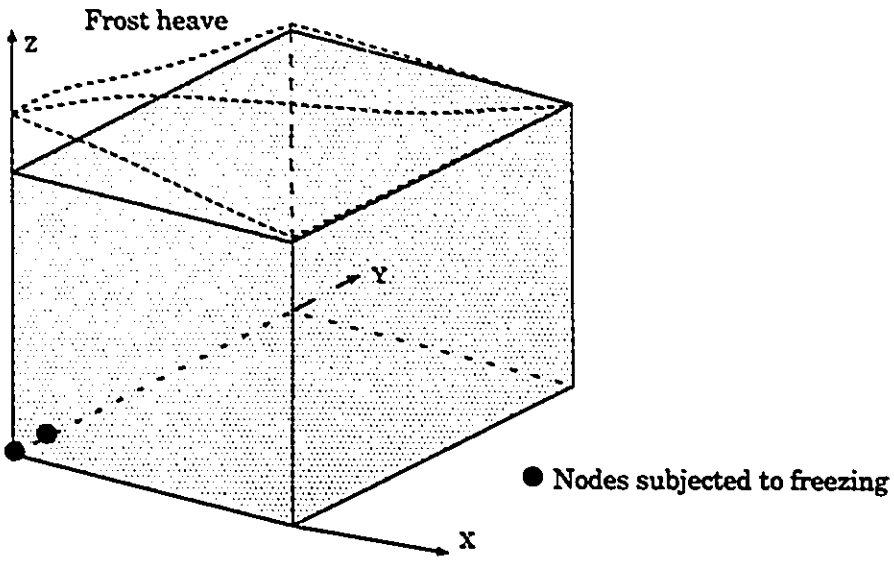

Figure 2.13: Nodes subjected to freezing at three-dimensional case

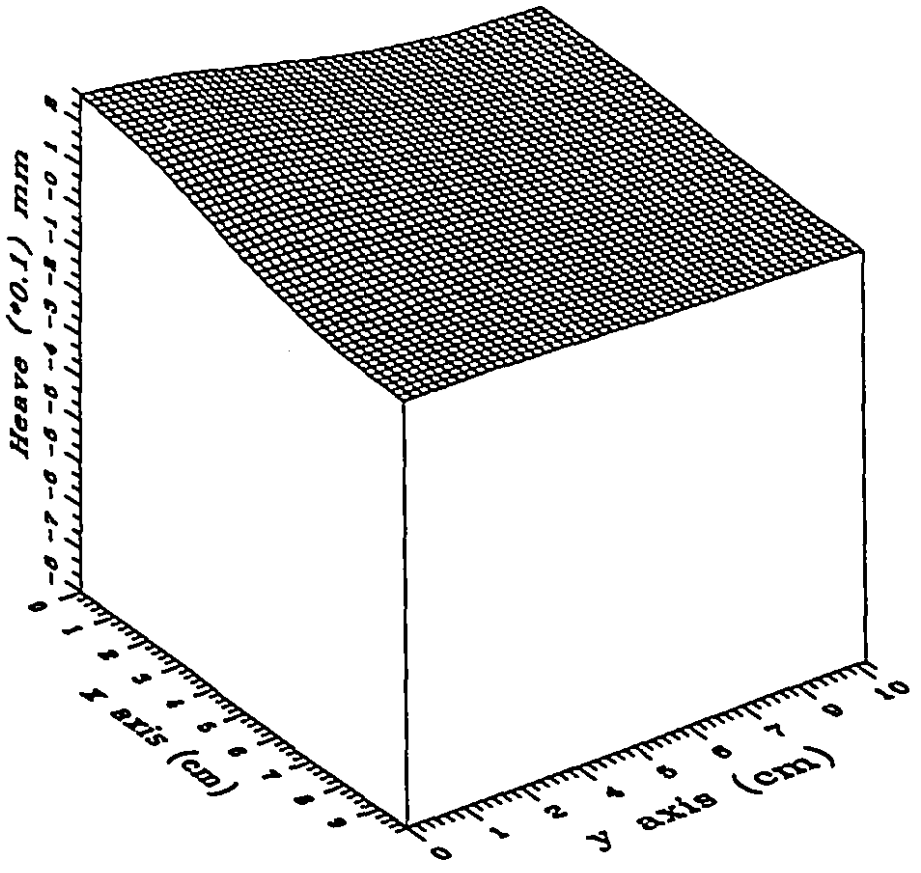

Figure 2.14: Surface heave of a cuboidal element subjected to base freezing at two edge nodes at 50 hours: Maximum heave = 0.211 mm

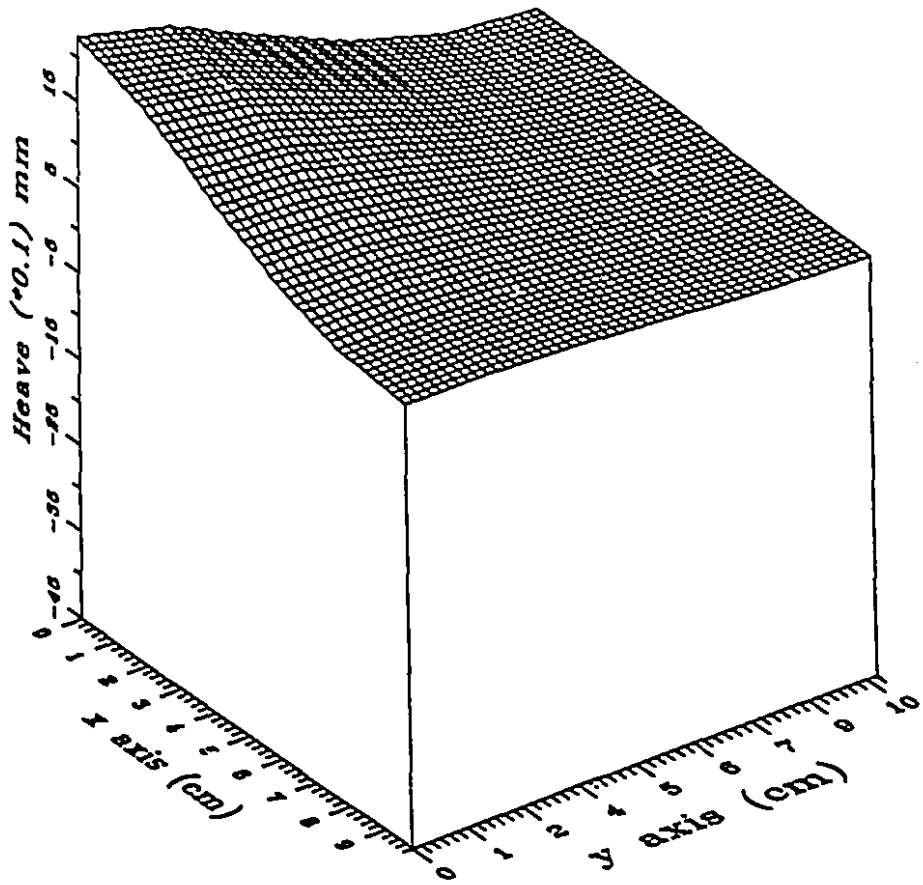

Figure 2.15: Surface heave of a cuboidal element subjected to base freezing at two edge nodes at 233 hours: Maximum heave = 2.26 mm

Chapter 3

Mechanical Modelling of Frozen Soils

3.1 General

Creep characteristics feature dominantly in the mechanical behaviour of a frozen soil owing to the presence of ice and unfrozen water within it. Creep behaviour of a frozen soil has three characteristic stages involving primary, secondary and tertiary creep. The creep rate strongly depends upon the temperature and applied stress.

During the past four decades, the modelling of creep in frozen soils has received considerable attention. The interests in such creep processes stem from the involvement in engineering in the northern environments where geomaterials such as permafrost can be predominant. Many models and empirical relationships have been put forward to describe the creep behaviour of frozen soils. Earlier research in this area focused largely on the description of mainly the creep behaviour in the primary stage. Examples of such models include the power function relationships proposed by Vyalov (1963), Assur (1963), Sayles (1973) and the exponential function representations given by Andersland and AlNouri (1970). In subsequent studies, creep behaviour in the secondary stage was taken into consideration in modelling. A purely secondary creep model which uses a power function was proposed by Hult (1966) and Ladanyi (1972) to represent creep responses in which the stage of the secondary creep

dominates the complete creep curve and the creep strain rate was approximated by a linear function. Ting and Martin (1979) employed Andrade's equation to represent the creep in the secondary stage. Complete creep models were proposed by Fish (1980, 1983), Ting (1983) and Gardner et al. (1984). These models all utilize a single equation and they belong to the family of creep curves characterized by a rate process theory. It is noted that these complete creep models can only represent primary and tertiary creep stages and the secondary stage degenerates to an inflexion point of the complete creep curve. Secondary creep behaviour, however, does exist and it is a recognizable component in the constitutive behaviour of many frozen soils.

Comparisons of creep models mentioned above were made by Hampton et al. (1985) and Sayles (1988). These studies found that a power function is able to predict the creep behaviour of frozen soil at primary stage, but it is not applicable to the latter two stages. The engineering model proposed by Ladanyi (1972) is only applicable to situations where the secondary creep stage dominates the complete creep curve. The models by Fish (1980) and Gardner et al. (1984) greatly overestimate the creep strain in the early portion of the curve but give better agreement in other stages of the creep response. The model by Ting (1983) fits well the early part of the creep curve, but under-predicts the strain for other ranges of creep. From these observations, it would appear that the available models are only capable of describing, at most, only one or two stages of the total creep behaviour. There is no single *complete model* that can accurately predict all three stages of creep behaviour. It may even be questioned whether it is reasonable to use a single equation to represent the three distinct mechanisms inherent in a typical creep curve.

3.2 A Complete Creep Model for Frozen Soils

A complete creep model is proposed as a method for characterizing the complete creep behaviour of a frozen soil which exhibits all three stages of creep behaviour. It is well known that the initiation of tertiary creep implies the generation of creep failure within the frozen soil. It is assumed that the occurrence of tertiary creep in a frozen soil does not imply the complete collapse of the region, however, it can induce relatively large creep deformations. In the proposed model, instead of using a single equation to describe a complete creep curve, three separate creep equations are used to characterize, individually, primary, secondary and tertiary stages of creep behaviour. The model is made complete by prescribing criteria for transition from one stage of creep behaviour to another.

3.2.1 Primary stage

The power law representations have been one of the most popular procedures for characterizing creep constitutive phenomena and as such has been widely accepted for the description of primary creep, i.e. the primary creep behaviour is modelled by the power law:

$$\dot{\epsilon}_{ij}^{cp} = \frac{3}{2} A C \sigma_e^{B-1} t^{C-1} s_{ij} \tag{3.1}$$

where $\dot{\epsilon}_{ij}^{cp}$ is the creep strain rate in the primary stage;

$\sigma_e = \sqrt{\frac{3}{2} s_{ij} s_{ij}}$ is equivalent stress ;

$s_{ij} = \sigma_{ij} - \frac{1}{3}\sigma_{kk}\delta_{ij}$ is the stress deviator tensor;

A, B and C can be temperature dependent material parameters.

3.2.2 Secondary stage

The secondary creep stage is also described by a power law of the form

$$\dot{\epsilon}_{ij}^{cs} = \frac{3}{2} A_2 \sigma_e^{B_2 - 1} s_{ij} \tag{3.2}$$

where $\dot{\epsilon}_{ij}^{cs}$ is the creep strain rate in the secondary stage; A_2 and B_2 can also be temperature dependent material parameters.

Primary creep parameters A, B, C and secondary creep parameters A_2 and B_2, can be evaluated from the creep curves of a uniaxial constant stress creep test by a graphical method. The detail of these procedures are given by Andersland et al (1978).

3.2.3 Tertiary stage

In this study, tertiary creep is modelled using a phenomenological theory of creep damage mechanics. The theory of damage mechanics has been used to examine the stress induced progressive deterioration of engineering materials such as concrete, ice, composites, etc. (Kachanov, 1986; Lemaitre and Chaboche, 1974; Boehler and Khan, 1991; Selvadurai and Au, 1991; Selvadurai, 1994). In the phenomenological theory of creep damage, the damage is identified as the time-dependent stress induced accumulation and growth of micro-voids within a material. The strain rate acceleration in the tertiary stage and the process of creep rupture are explained by appeal to the degradation of the material. Consider a material element in a body, with undamaged original area A_0. As damage evolves, the effective load carrying area diminishes with the creation of voids. The area of voids induced by damage is defined by A_D (Figure 3.1). A damage variable (ω) applicable to a uniaxial stress state can be:

$$\omega = \frac{A_D}{A_0} \tag{3.3}$$

The damage process reduces the load-bearing area of material. Consequently the

net stress $\overline{\sigma}$ in a damaged material is defined as:

$$\overline{\sigma} = \frac{\sigma_0}{1-\omega} \tag{3.4}$$

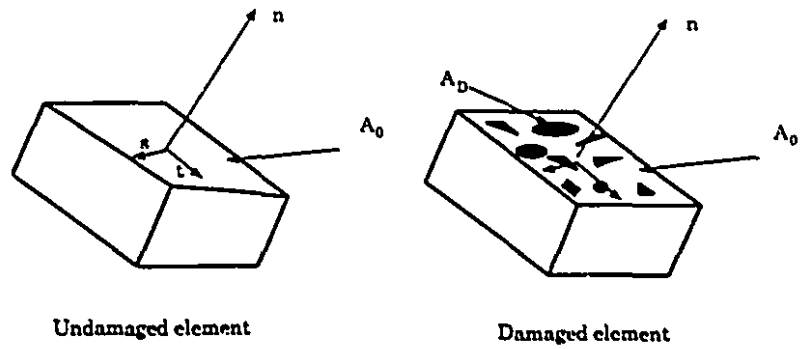

Figure 3.1: Evolving damage in element

The parameter ω is understood to be an evolving internal variable of the system. For a given stress state at a given time, the evolution of damage will be a property of the material.

Such damage evolution criteria can either be postulated or determined by recourse to creep experiments which are carried out to include the tertiary stage. In the current study we assume that the rate of evolution of damage can be determined by a power law of type:

$$\dot{\omega} = D\left(\frac{\sigma_0}{1-\omega}\right)^k \tag{3.5}$$

where D and k are temperature dependent constants.

Damage evolution is generally anisotropic (Lemaitre and Chaboche, 1974; Chow and Wang, 1987). Here we adopt a simplified *isotropic* damage model. The creep

strain rate in the tertiary stage $\dot{\epsilon}_{ij}^{cr}$ derived from Equation (3.2) is therefore defined by

$$\dot{\epsilon}_{ij}^{cr} = \frac{3}{2} A_2 \left(\frac{\sigma_e}{1-\omega}\right)^{(B_2-1)} \left[\frac{s_{ij}}{(1-\omega)}\right] \tag{3.6}$$

where A_2, B_2 are temperature dependent constants referred to the *secondary* creep stage.

A new creep equation for the tertiary stage is derived from Equations (3.5) and (3.6)

$$\dot{\epsilon}_{ij}^{cr} = \frac{3}{2} A_2 (\sigma_e)^{(B_2-1)} [1-(k+1)D(\sigma_e)^k t]^{\frac{-B_2}{k+1}} s_{ij} \tag{3.7}$$

All four parameters A_2, B_2, D and k in Equation (3.7) can be determined from creep curves obtained from uniaxial constant stress creep tests. The procedures of determining D and k are as follows: (i) two sets of uniaxial creep tests are conducted at different but constant stress levels (σ_1, σ_2), (ii) the creep curves $\dot{\epsilon}_1$ vs t and $\dot{\epsilon}_2$ vs t are obtained, and (iii) Equation (3.7) is applied to each creep test giving rise to the following equations. The unknown parameters D and k can be obtained by solving the non-linear equations.

$$\left.\begin{aligned} \dot{\epsilon}_1 &= A_2 \left(\frac{\sigma_1}{[1-(k+1)D\sigma_1^k t]^{\frac{1}{k+1}}}\right)^{B_2} \\ \dot{\epsilon}_2 &= A_2 \left(\frac{\sigma_2}{[1-(k+1)D\sigma_2^k t]^{\frac{1}{k+1}}}\right)^{B_2} \end{aligned}\right\} \tag{3.8}$$

3.2.4 Transition of creep stages

In addition to the creep laws governing each stage it is necessary to specify the specific times at which transition occurs from one creep process to the other. In the proposed unified creep model, the function of *inflexion times* T_m and their corresponding equivalent stresses σ_e are established either by power law $T_m = E\sigma_e^{-F}$ with a least squares

technique (E and F are material parameters) or numerical interpolation, depending on available sets of experimental data. Numerical interpolation polynomial method is a simple and an effective means of approximation. In this modelling, Aitken and Neville's algorithm (Kopal, 1955) is suggested to represent the function.

Let $(\sigma_{e,0}, T_{m,0}), (\sigma_{e,1}, T_{m,1}), (\sigma_{e,j}, T_{m,j}), ...(\sigma_{e,n}, T_{m,n})$ be support points. Here $T_{m,j}$ and $\sigma_{e,j}$ represent respectively the jth set of experimental inflexion times and their corresponding equivalent stresses. The computing scheme for this algorithm is given by

$$I_{0,1,2,...n}(\sigma_e) = \frac{(\sigma_e - \sigma_{e,n})}{(\sigma_{e,0} - \sigma_{e,n})} I_{0,1,2,...n-1}(\sigma_e) + \frac{(\sigma_e - \sigma_{e,0})}{(\sigma_{e,n} - \sigma_{e,0})} I_{1,2,...n}(\sigma_e) \tag{3.9}$$

where

$$I_{0,1,2,...n-1}(\sigma_e) = W_{(n+1)}(\sigma_e) \sum_{j=0}^{n} \frac{T(\sigma_{e,j})(\sigma_{e,j} - \sigma_{e,n})}{(\sigma_e - \sigma_{e,j})(\sigma_e - \sigma_{e,n}) W'_{n+1}(\sigma_{e,j})} \tag{3.10}$$

$$I_{1,2,...n}(\sigma_e) = W_{(n+1)}(\sigma_e) \sum_{j=1}^{n} \frac{T_m(\sigma_{e,j})(\sigma_{e,j} - \sigma_{e,0})}{(\sigma_e - \sigma_{e,j})(\sigma_e - \sigma_{e,0}) W'_{n+1}\sigma_e} \tag{3.11}$$

$$W_{(n+1)}(\sigma_e) = (\sigma_e - \sigma_{e,0})(\sigma_e - \sigma_{e,1})(\sigma_e - \sigma_{e,2})...(\sigma_e - \sigma_{e,n}) \tag{3.12}$$

where $I_{0,1,2,...n}(\sigma_e)$ denotes the interpolation polynomial which coincides in value with $\sigma_{e,j}$ at $j = 1, 2, ...n$. The advantage of this algorithm rests on the fact that the nth polynomial can be directly derived by the $(n-1)$th polynomial and nth point. The scheme is summarized in Table 3.1.

Table 3.1

$\sigma_{e,0}$	$T_{m,0} = I_0$	
$\sigma_{e,1}$	$T_{m,1} = I_1$	$I_{0,1}$
$\sigma_{e,2}$	$T_{m,2} = I_2$	$I_{1,2}$ $I_{0,1,2}$
$\sigma_{e,3}$	$T_{m,3} = I_3$	$I_{2,3}$ $I_{1,2,3}$ $I_{0,1,2,3}$
:	:	:

Using the discrete experimental points of inflexion time T_m versus σ_e obtained from uniaxial creep test data (Gardner et al., 1984), the functions defined by Aitken and Neville's interpolation and power law procedures are shown in Figure 3.2. For any stress σ_e, its corresponding inflexion time T_m can be calculated by the interpolation subroutine or power function. It indicates that the creep process has entered the next stage when the actual time is greater than the inflexion time. Figure 3.2 illustrates that the interpolation technique may give better modelling when available experimental data are limited (only 3 sets of data are used in the above example). However a power law with least square technique is recommended when adequate sets of inflexion times T_m versus σ_e are presented.

By the simulation of creep stage transition, the complete creep model is able to examine, depending on the stress levels, both individual and combinations of the creep processes (e.g. the primary stage, the secondary stage, the primary and the tertiary stages, secondary and tertiary stages and the combination of all three stages).

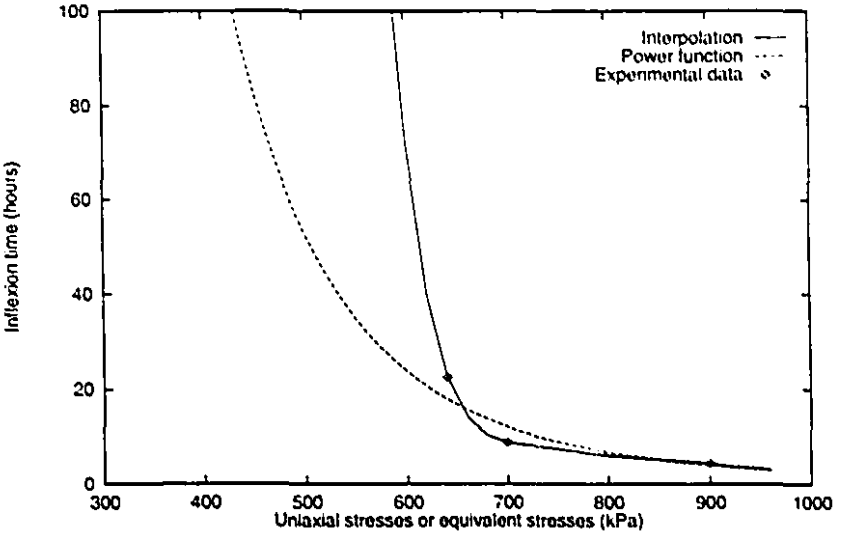

Figure 3.2: Modelling of stage transitions

3.3 Example: Description of Complete Creep Curve

A family of creep test data under three different stress levels is shown in Figure 3.3, (Gardner et al., 1984). All parameters determined from experimental data are listed in Table 3.2.

The experimental results and predictions by creep models are compared in Figure 3.3. Figure 3.3 also gives the set of predictions at other stress levels. The numerical results demonstrate that the complete model is able to provide satisfactory trends in characterizing the creep behaviour of frozen soils.

Table 3.2

Creep model	Parameters
Primary creep model	$A = 0.00002115$, $B = 1.05$, $C = 0.29$
Secondary creep model	$A_2 = 0.00014611$, $B_2 = 1.111$
Tertiary creep model	$D = 0.00013712$, $k = 0.7649$

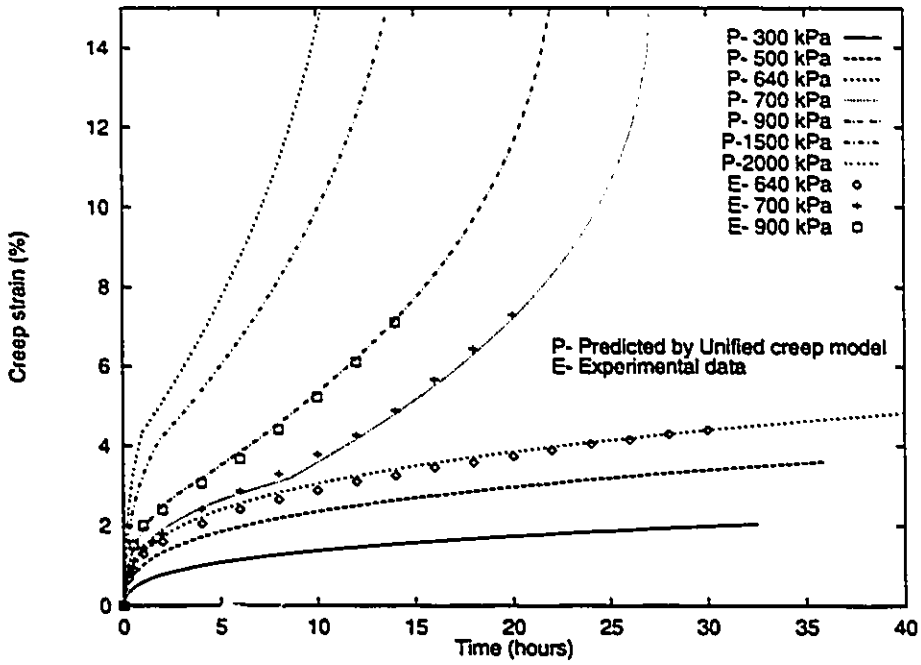

Figure 3.3: One-dimensional creep curves predicted by the complete creep model

3.4 Finite Element Implementation

3.4.1 Creep analysis algorithm

Details of the finite element modelling of media susceptible to creep are given by Zienkiewicz (1977) and in this section a brief account of the important elements is outlined. A general incremental constitutive relationship can be developed by assuming that the incremental strain rate is the sum of the incremental strain rate components associated with the respective stages, i.e.

$$\{d\dot{\epsilon}_{ij}\} = \{d\dot{\epsilon}^{e}_{ij}\} + \{d\dot{\epsilon}^{cp}_{ij}\} + \{d\dot{\epsilon}^{cs}_{ij}\} + \{d\dot{\epsilon}^{ct}_{ij}\} \tag{3.13}$$

where

$\{d\dot{\epsilon}_{ij}\}$ - total incremental strain rate;

$\{d\dot{\epsilon}^{e}_{ij}\}$ - incremental elastic strain rate;

$\{d\dot{\epsilon}^{cp}_{ij}\}$ - incremental creep strain rate in the primary stage;

$\{d\dot{\epsilon}^{cs}_{ij}\}$ -incremental creep strain rate in the secondary stage;

$\{d\dot{\epsilon}^{ct}_{ij}\}$ -incremental creep strain rate in the tertiary stage.

A fully implicit algorithm is used for creep analysis (Zienkiewicz, 1977). If $\{\epsilon^{c}_{ij}\}_{n+1}$ and $\{\epsilon^{c}_{ij}\}_{n}$ are respectively creep strain vectors at time t_{n+1} and t_n, then we can write

$$\{\epsilon^{c}_{ij}\}_{n+1} - \{\epsilon^{c}_{ij}\}_{n} = \Delta t_n \{\dot{\epsilon}^{c}_{ij}\}_{n+\alpha} = \Delta t_n \frac{\partial\{\dot{\epsilon}^{c}_{ij}\}}{\partial\{\sigma_{ij}\}}(\{\sigma_{ij}\}_{n+\alpha} - \{\sigma_{ij}\}_{n}) = \Delta t_n \frac{\partial\{\dot{\epsilon}^{c}_{ij}\}}{\partial\{\sigma_{ij}\}}\alpha\Delta\{\sigma_{ij}\}_{n} \tag{3.14}$$

where

$\Delta t_n = t_{n+1} - t_n$;

$\{\sigma_{ij}\}_n$ is stress vector at time t_n;

$\{\sigma_{ij}\}$ is current stress vector;

α is a conditioning parameter.

The governing finite element equation for this algorithm is given by

$$(\int [\mathbf{B}]^{T^*}[\mathbf{D}]^0[\mathbf{B}]dV)\ \{\Delta\delta_{ij}\}_{n+1} + \Delta\mathbf{F}_n - \int [\mathbf{B}]^{T^*}[\mathbf{D}]^0 \Delta t_n \frac{\partial\{\dot{\epsilon}^c_{ij}\}}{\partial\{\sigma_{ij}\}}\alpha\{\Delta\sigma_{ij}\}_n = 0 \quad (3.15)$$

where $\{\Delta\delta_{ij}\}_{n+1}$ is the vector of incremental nodal displacement; $\Delta\mathbf{F}_n$ are incremental loads applied during the time interval Δt_n.

The matrix $[\mathbf{D}]^0$ in Equation (3.15) can be derived as follows:

$$\{\Delta\sigma^c_{ij}\}_n = [\mathbf{D}](\{\Delta\epsilon_{ij}\}_n - \{\Delta\epsilon^{cp}_{ij}\}_n - \{\Delta\epsilon^{cs}_{ij}\}_n - \{\Delta\epsilon^{ct}_{ij}\}_n) \quad (3.16)$$

where $\{\Delta\sigma^c_{ij}\}_n$ is the increment of stress vector during the interval Δt_n and $[\mathbf{D}]$ is the elastic matrix: From Equations (3.14) and (3.16)

$$\{\Delta\epsilon_{ij}\}_n = [\mathbf{D}]^{-1}\{\Delta\sigma^c_{ij}\}_n + \{\Delta\epsilon^c_{ij}\}_n = ([\mathbf{D}]^{-1} + \Delta t_n \frac{\{\partial\dot{\epsilon}^c_{ij}\}}{\{\partial\sigma_{ij}\}}\alpha)\{\Delta\sigma^c_{ij}\}_n \quad (3.17)$$

$$\Delta\{\sigma^c_{ij}\}_n = \frac{1}{([\mathbf{D}]^{-1} + \Delta t_n \frac{\{\partial\dot{\epsilon}^c_{ij}\}}{\{\partial\sigma_{ij}\}}\alpha)}\{\Delta\epsilon^c_{ij}\}_n \quad (3.18)$$

Hence

$$[\mathbf{D}]^0 = \frac{1}{([\mathbf{D}]^{-1} + \Delta t_n \frac{\{\partial\dot{\epsilon}^c_{ij}\}}{\{\partial\sigma_{ij}\}}\alpha)} \quad (3.19)$$

If $\alpha \geq \frac{1}{2}$ the scheme is unconditionally stable (Zienkiewicz, 1977).

3.4.2 Procedure for post failure analysis

Consider the problem of a pipeline which is embedded in a frozen soil. Due to the process of discontinuous heave the pipe section can be subjected to an uplift force.

Such forces can initiate tertiary creep damage in limited zones of the frozen soil. With further loading there can occur distinct zones of failure or localized damage which ultimately will result in the development of cracking or separation. Consequently, the stress dependent tertiary creep damage can influence failure that can result from inelastic or plastic phenomena. This section considers the problem of failure development as a consequence of creep phenomena, which includes all three stages. In order to achieve this, constitutive equations which describe failure have to be introduced.

The initiation of failure of frozen soil is prescribed by appeal to the Mohr-Coulomb failure criterion with a tension cut off condition (Hill, 1950; Zienkiewicz, 1977; Desai and Siriwardane, 1984). The Mohr-Coulomb failure criterion, F in the compression range takes the form:

$$F = \frac{I_1}{3}sin\phi + \sqrt{J_2}(cos\theta - \frac{1}{\sqrt{3}}sin\theta sin\phi) - C_0 cos\phi = 0 \tag{3.20}$$

where

$$\theta = \frac{1}{3}sin^{-1}\{-\frac{3\sqrt{3}}{2}\frac{J_3}{J_2^{\frac{3}{2}}}\}, \quad (-\frac{\pi}{6} \leq \theta \leq \frac{\pi}{6}) \tag{3.21}$$

$$\begin{aligned} I_1 &= \sigma_{kk} \\ J_2 &= \frac{1}{2}\sigma_{ij}^D\sigma_{ij}^D\sigma_{ij}^D \\ J_3 &= \frac{1}{3}\sigma_{ij}^D\sigma_{jk}^D\sigma_{ki}^D \end{aligned} \tag{3.22}$$

$$\sigma_{ij}^D = \sigma_{ij} - \frac{1}{3}\sigma_{kk}\delta_{ij} \tag{3.23}$$

C_0 is the cohesion and ϕ is the angle of internal friction.

For the tensile failure criterion, F is given by

$$F = \{\sigma_1\} - R_T = 0 \tag{3.24}$$

where R_T is the tensile strength.

Incremental theory of plasticity is used to develop the constitutive relationships which describe post failure processes. We assume that the total incremental strain in the medium undergoing elasto-plastic failure takes the form

$$\{d\epsilon_{ij}\} = \{d\epsilon_{ij}^e\} + \{d\epsilon_{ij}^p\} \tag{3.25}$$

where elastic strain $\{d\epsilon_{ij}^e\} = [\mathbf{D}^e]^{-1}\{d\sigma_{ij}^e\}$ and $[\mathbf{D}^e]$ is an elastic matrix. It must be noted that the elasticity matrix $[\mathbf{D}^e]$ should correspond to that which relates to elastic behaviour at the particular level of damage $[\mathbf{D}_\omega^e]$. The limits of elastic behaviour are such that $[\mathbf{D}_\omega^e] \rightarrow [\mathbf{D}^e]$ when $\omega \rightarrow 0$ and $[\mathbf{D}_\omega^e] \rightarrow 0$ as $\omega \rightarrow 1$. In this study, however, we assume that, since $\omega \in (0,0.2)$, the elasticity matrix in the damaged state $[\mathbf{D}_\omega^e]$ is approximated by the initial elasticity matrix $[\mathbf{D}^e]$. The plastic strain increment $\{d\epsilon_{ij}^p\}$ can be obtained for a flow rule of the type

$$\{d\epsilon_{ij}^p\} = d\lambda \frac{\partial G}{\partial \sigma_{ij}}; \qquad F = 0; \quad dF > 0 \tag{3.26}$$

where G is the plastic potential function and $d\lambda$ is the positive scalar factor of proportionality.

The general elastic-plastic constitutive matrix $[\mathbf{D}^{ep}]$ can be written as

$$[\mathbf{D}^{ep}] = [\mathbf{D}^e] - [\mathbf{D}^p] = [\mathbf{D}^e] - \frac{[\mathbf{D}^e]\{\frac{\partial G}{\partial \sigma_{ij}}\}\{\frac{\partial F}{\partial \sigma_{ij}}\}^T[\mathbf{D}^e]}{A + \{\frac{\partial F}{\partial \sigma_{ij}}\}^T[\mathbf{D}^e]\{\frac{\partial G}{\partial \sigma_{ij}}\}} \tag{3.27}$$

where A is the hardening parameter.

The initial stress algorithm (Zienkiewicz, 1977) for non-linear analysis, used as the iteration procedure, will be summarized in the following: (i) Determine if an element has failed by applying the failure criteria at each time interval. (ii) For an element which has experienced failure, adjust the state of stress based on the corresponding post-failure constitutive relations and compute the initial stress $\{\sigma_0\}$. The initial stress of each element can be evaluated by the difference of stress before and after adjustment. In this analysis, we use an associated flow rule $G = F$ and the hardening parameter A is assumed to be 0 (perfectly plastic material). (iii) Compute the equivalent force induced by the initial stress σ_0 and repeat the above scheme till convergence ($\{\sigma_0\} \rightarrow 0$) is established.

3.4.3 Modelling of interface adfreezing

Adfreezing describes the mechanism of strength generation at a frozen soil-structure interface. In pipelines embedded in frozen soils or soils susceptible to freezing, adfreezing can generate strength at the interface. In the analysis of soil-pipeline interaction some accounts should be made to incorporate adfreezing. If interface adfreezing strength is sufficiently large, failure will initiate in the frozen soil. For the purposes of a generalized treatment, the effects of adfreezing will be modelled by considering interface mechanics of a zero thickness interface element (see e.g. Goodman et al. 1968; Desai et al. 1984; Soo et al. 1987; Selvadurai and Boulon, 1995).

In this interface element, stress has two components, a shear stress which is parallel to the bond interface and a normal stress which is normal to the bond interface. The constitutive relation at the bond interface is given by

$$\begin{pmatrix} \tau_s \\ \sigma_n \end{pmatrix} = \begin{pmatrix} K_s & 0 \\ 0 & K_n \end{pmatrix} \begin{pmatrix} d_s \\ d_n \end{pmatrix} \tag{3.28}$$

where shear stiffness K_s is the slope of curve of shear stress-displacement; Normal stiffness K_n is the slope of curve of normal stress-displacement; d_s is shear displacement and d_n is normal displacement to the bond interface.

When creep components are involved, the constitutive equation can be re-written as follows (Soo et al. 1987)

$$\begin{pmatrix} \tau_s \\ \sigma_n \end{pmatrix} = \begin{pmatrix} K_s & 0 \\ 0 & K_n \end{pmatrix} \begin{pmatrix} d_s - d_s^c \\ d_n - d_n^c \end{pmatrix} \tag{3.29}$$

where d_s^c and d_n^c are creep displacement components in shear and normal directions respectively. These displacement components can be calculated by the complete creep models which were developed in Section 3.2.

The interface element failure includes shear failure along the the length of interface and detachment of the interface element due to tensile failure. Post-failure analysis for an interface element follows the incremental plastic theory (Equation (3.27)) and initial stress algorithm which was previously stated. For shear failure along the interface, the Mohr-Coulomb failure criteria takes the form:

$$F = |\tau_s| - C_f + \sigma tan\phi_f = 0 \tag{3.30}$$

where C_f, ϕ_f- Cohesion and angle of internal friction of interface.

If $A = 0$ and $G = F$, the elastic-plastic constitutive equation (3.27) can be re-written in the form

$$[\mathbf{D}^{ep}] = \begin{pmatrix} K_s & 0 \\ 0 & K_n \end{pmatrix} - \frac{1}{S_0} \begin{pmatrix} {K_s}^2 & K_s S_1 \\ K_s S_1 & {S_1}^2 \end{pmatrix} \tag{3.31}$$

where

$S_0 = K_s + K_n tan^2\phi_f$;

$S_1 = K_n tan\phi_f$

3.5 Verification of Computational Procedures

This section presents an analytical solution of a classical problem, which is used for validating the accuracy and capabilities of the finite element procedures for creep analysis described in previous sections. Thereafter, the verified computer program can be applied to solve the problems of frozen soil-structure interaction in practical situations.

The problem of a simply supported frozen beam subjected to a concentrated vertical load at the midspan is considered. The frozen beam has a cross section measuring 0.15 m in height and 0.1 m in width and a span length of 1 m. The identical finite element configuration with Klein and Jessberger (1977) and Puswewala and Rajapakse (1990) is considered, in which only half of the beam is discretized with 50 plane stress elements, 66 nodes due to the symmetry of the problem (Figure 3.1).

(1) Purely primary creep

The investigation of creep behaviour of frozen soil in the primary stage is conducted by applying a 4 kN concentrated load on an artificially frozen Emscher-Marl beam (Klein and Jessberger, 1977) for which the creep parameters are $A = 7.6\times10^{-17}$, $B = 4$, $C = 0.1$. The analytical solution for the rate of vertical deflection at the midspan was given in the form (Odqvist, 1966; Puswewala and Rajapakse, 1990)

$$\dot{\delta} = \frac{K P^B L^{B+2} (\frac{1}{2})^{2B+2}}{B+2} C t^{C-1} \tag{3.32}$$

where

$$K = \frac{A}{[b(\frac{h}{2})^{2+\frac{1}{B}} \frac{2B}{2B+1}]^B} \tag{3.33}$$

in which $\dot{\delta}$ is the rate of the vertical deflection at the centre of the beam; P is the

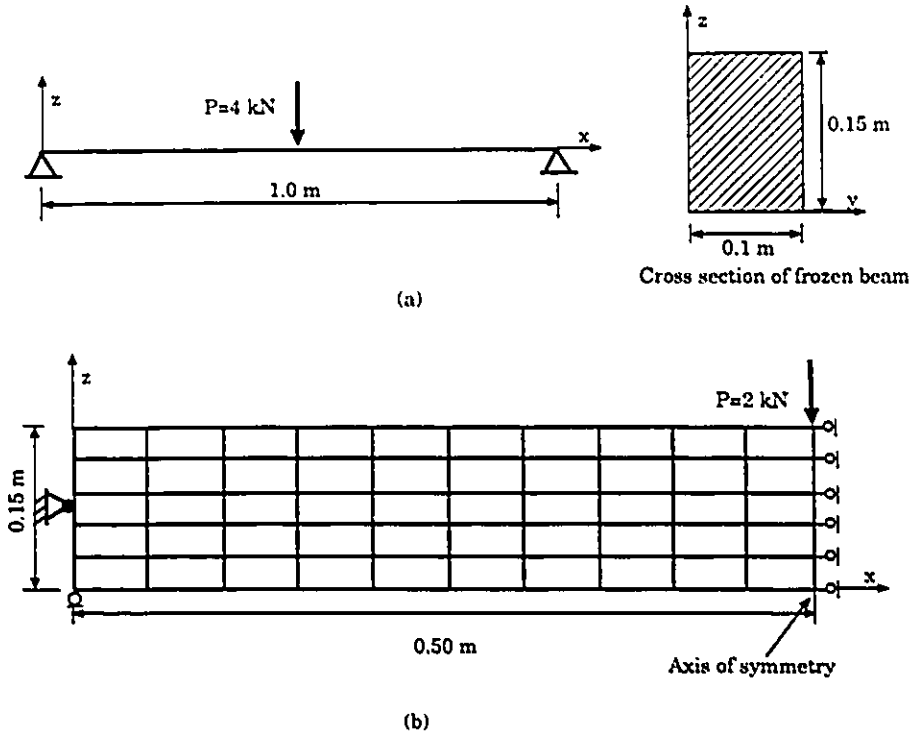

Figure 3.4: A simple supported frozen beam and its finite element model

applied vertical concentrated load (kN); L is beam span (m); h is beam height (m) and b is beam breadth (m); A, B and C are creep parameters.

Figure 3.5 indicates that the numerical simulation compares very accurately with the analytical solution (Equation (3.32)). The maximum discrepancy between the two sets of results is 2.2 % .

(2) Purely secondary creep

Creep parameters for secondary stage are not available for Emscher-Marl frozen beam. For purposes of calibration, the parameters governing the secondary creep

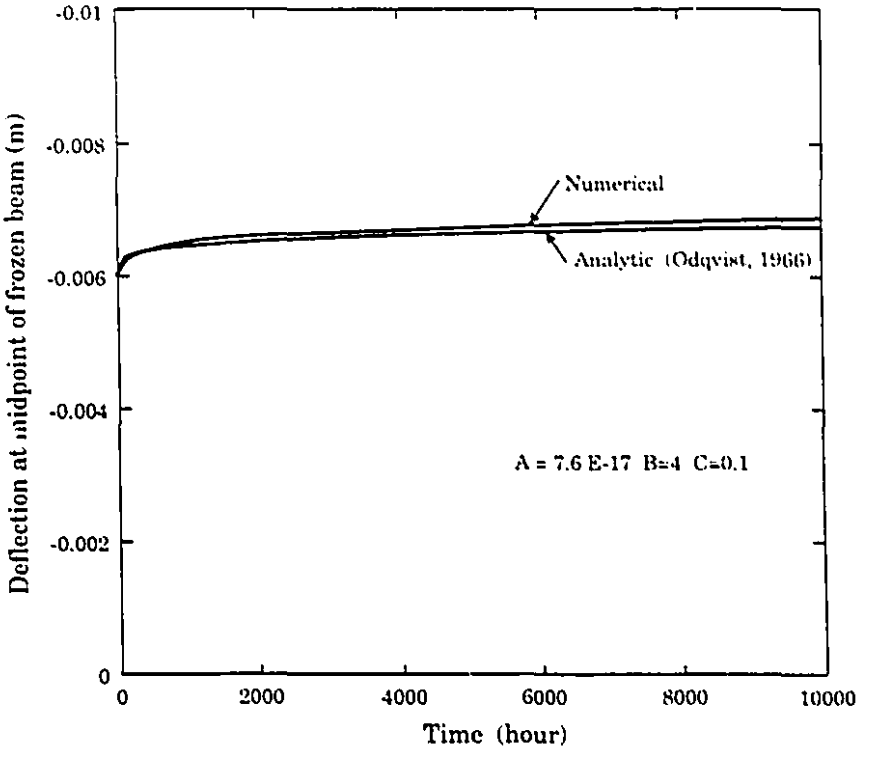

Figure 3.5: Creep deflection of frozen beam (primary stage only)

model can be obtained using the creep test data which closely approximate the steady stage for artificially frozen Emscher-Marl provided by Klein (1979), i.e. $A = 3.7 \times 10^{-10}, B = 1.08$. The analytical solution from Equation (3.32) ($C = 1$) gives a deflection rate at the center of the beam 1.954×10^{-6} m/h and the corresponding result for the numerical simulation is $1.7778 \times 10^{-6} m/h$.

The expression of steady-state stress distribution over a cross-section was given by Odqvist and Hult (1962) and Klein and Jessberger (1977).

$$\sigma_x = (4 + \frac{2}{B})(\frac{M}{bh^2})(\frac{2z}{h})^{\frac{4}{B}} \tag{3.34}$$

where M is the bending moment on the cross-section and z is the distance from the natural axis of the cross-section.

The stress distribution for a cross-section of frozen beam obtained by Equation 3.34 and finite element simulation are shown in Figure 3.6. It is noted that the parameter B in Equation (3.34) should be set equal to $B = 1.08$ for secondary model, not the value $B = 4$ for primary model (Klein and Jessberger, 1977). It verified this code can provide the satisfied numerical simulation for stress analysis.

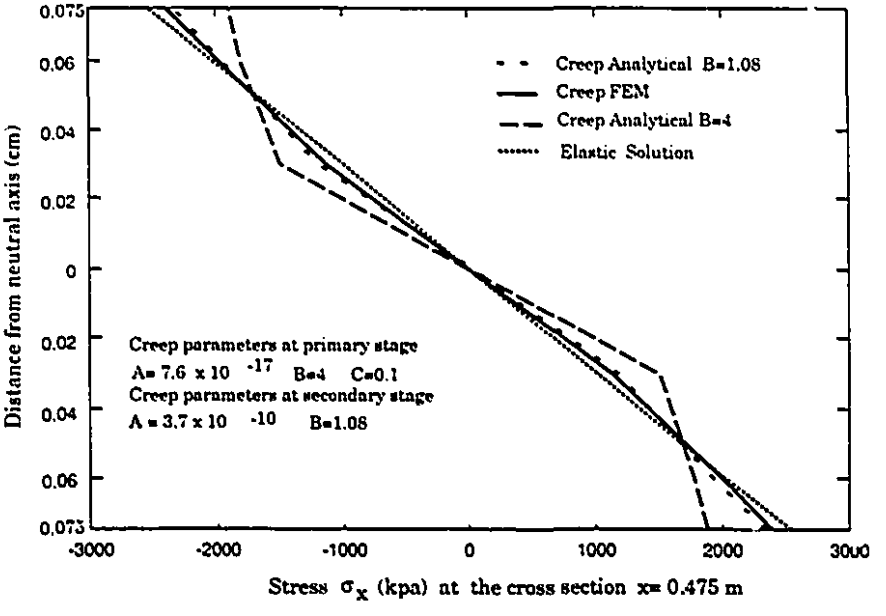

Figure 3.6: Stress redistribution at creep steady stage

(3) Primary and secondary creep

Strain rate continues to attenuate in primary stage ($\dot{\varepsilon}^{cr} = A_1\sigma^{B_1}(C_1t^{C_1-1})$ until the rate reaches a critical value which is determined by secondary creep model ($\dot{\varepsilon}^{cr} = A_2\sigma^{B_2}$). As the process continues into secondary stage, creep rate will keep constant.

Figures 3.7 compares the creep deflection curves obtained by purely primary creep, purely secondary creep and a model incorporating primary and secondary creep. It is observed that the results derived for a model which incorporates either primary creep or secondary creep will be significantly different to the results obtained for a material which exhibits both primary and secondary creep phenomena.

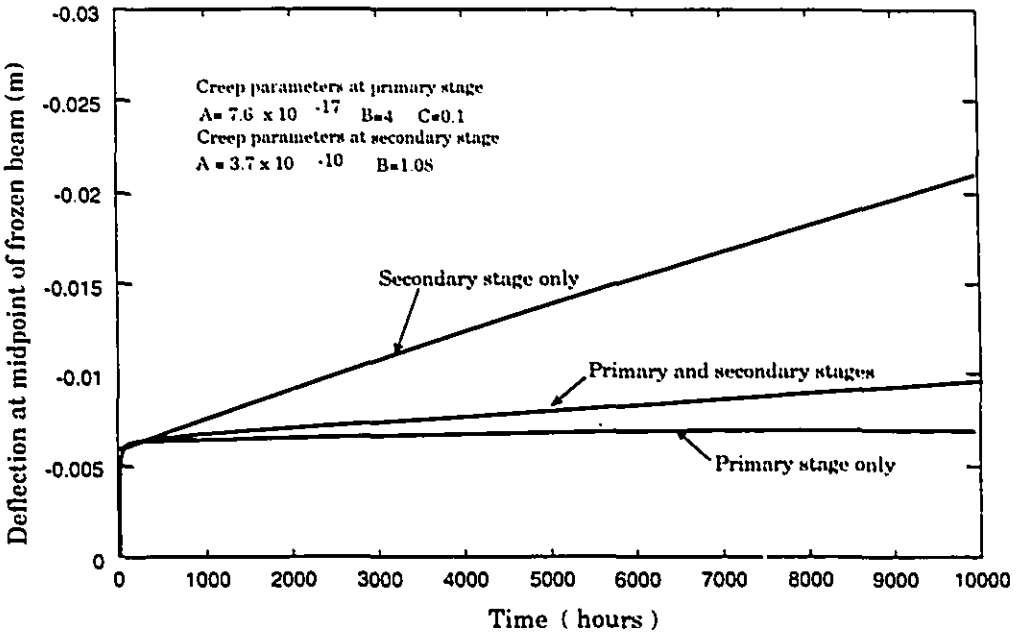

Figure 3.7: Creep deflection of frozen beam (Primary and secondary creep)

(4) Creep failure

From Equation (3.7), the time to failure from the initiation of tertiary stage can be obtained by setting ($\dot{\varepsilon}_{ij}^{cf} \rightarrow \infty$). Assuming that $\sigma_e, s_{ij}, A_2, B_2$ and k are finite, for

$\dot{\varepsilon}_{ij}^{c}$ to become unbounded we require

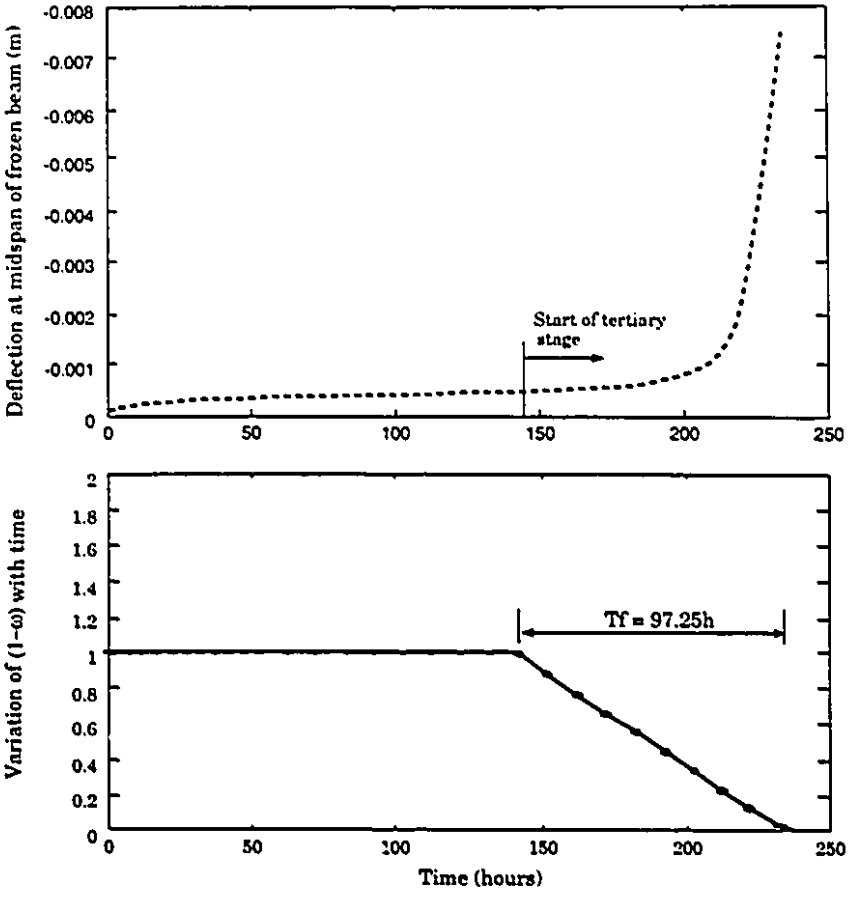

Figure 3.8: Complete creep deflection of frozen beam

$$t_f = [(k+1)D\sigma_e{}^k]^{-1} \tag{3.35}$$

Now consider the problem of the flexure of a beam examined previously. Substituting Equation (3.34) in Equation (3.35) the analytical solution for the time from the initiation of tertiary stage to failure of the beam can be written as

$$t_f = \left\{(k+1)D[(4+\frac{2}{B})(\frac{M}{bh^2})(\frac{2z}{h})^{\frac{1}{B}}]^k\right\}^{-1} \tag{3.36}$$

By incorporating the creep parameters in Table 3.2, Figure 3.8 illustrates the complete creep deflection curve at midspan of the frozen beam. Figure 3.8 also shows the variation of damage parameter ω with time. Creep failure initiates at the point $z = \frac{h}{2}$, of cross-section at the midspan of the beam. The time for failure from the commencement of tertiary creep derived via Equation (3.36) is 91.9 hours. The corresponding time obtained via the computational modelling is 97.25 hours (Figure 3.8).

Chapter 4

Mechanical Modelling of Pipeline

4.1 General

Pipelines are generally shell-type flexible structures. In any computational modelling, the pipeline should be represented by thin/thick shells or solid regions which can accommodate all axial, flexural, shear and torsional effects. The extent to which such processes would dominate will depend on the relative dimensions of the pipeline. In long distance pipelines the predominant effects are bound to be those induced by flexural and axial effects, where the interaction processes take place over shorter distance (e.g. transition and overbends, sharp change in curvature) or where the loading patterns are localized. The axial, shear and torsional effects could be independent. Many investigations have adopted beam and shell models to describe the behaviour of long distance pipeline (see e.g. Selvadurai and Pang, 1988; Selvadurai and Shinde, 1993)

4.2 One-dimensional Bernoulli-Euler Beam Element

In the recent study of frost heave induced flexural interaction, Selvadurai and Shinde (1993) examined three representations of pipeline behaviour by appeal to (i) a beam

model (ii) a shell model and (iii) a solid element model. In all three cases, the flexural stiffness of the pipeline and its outer dimension was kept constant by suitably adjusting the effective static modulus of the pipeline. These investigations showed that with a range of relative stiffness values of practical interest, the beam model of the pipeline gives flexural moments which are consistent with a shell idealization (Figure 4.1). These results were derived for the case where the embedded pipeline was subjected to a uniform surface load of finite extent. The results nevertheless indicate that the representation of the pipeline by an elementary Bernoulli-Euler beam model is a useful first approximation in the examination of soil-pipeline interaction problem.

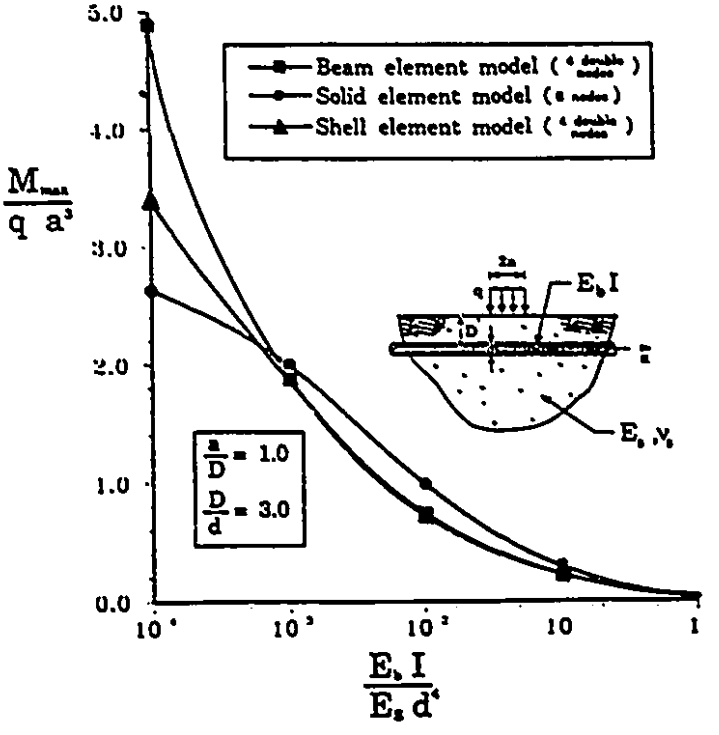

Figure 4.1: Surface loading induced flexural moments in buried pipeline: Comparison of models of pipeline response (after Selvadurai and Shinde, 1993)

The soil-pipeline interaction is modelled by representing the pipeline as a flexible

circular beam element of stiffness EI. The continuity between the beam and the surrounding soil medium is achieved by assuming continuity of displacement between nodal points of the beam element and the nodal points of the elements representing the soil region. To achieve compatibility between the 8-noded three-dimensional continuum element which has 24 degrees of freedom, the one-dimensional beam elements must be incorporated with a double node at each nodal point. The four nodes of this new beam element has six degrees of freedom at each node including three displacements and three rotations. The continuity between the continuum elements and the beam elements is achieved through the three displacement components. The finite element formulation for a beam element can be written as

$$\{\mathbf{u}\} = [\mathbf{K}]\{\mathbf{F}\} \tag{4.1}$$

where the vector of nodal deflections $\{\mathbf{u}\}$ and the vector of nodal forces $\{\mathbf{F}\}$ are defined, respectively, as

$$\{\mathbf{u}\}^{T^*} = \{\, u_1 \quad u_2 \quad u_3 \quad \theta_1 \quad \theta_2 \quad \theta_3 \,\} \tag{4.2}$$

$$\{\mathbf{F}\}^{T^*} = \{\, F_1 \quad F_2 \quad F_3 \quad M_1 \quad M_2 \quad M_3 \,\} \tag{4.3}$$

$[\mathbf{K}]$ is beam element stiffness matrix and takes the form

$$[\mathbf{K}] = \begin{bmatrix} \mathbf{K_{11}} & \mathbf{K_{12}} \\ \mathbf{K_{12}^{T^*}} & \mathbf{K_{21}} \end{bmatrix} \tag{4.4}$$

where the submatrices are

$$\mathbf{K_{11}} = \begin{bmatrix} \frac{EA}{l} & 0 & 0 & 0 & 0 & 0 \\ 0 & \frac{12EI}{l^3} & 0 & 0 & 0 & \frac{6EI}{l^2} \\ 0 & 0 & \frac{12EI}{l^3} & 0 & \frac{-6EI}{l^2} & 0 \\ 0 & 0 & 0 & \frac{GJ}{l} & 0 & 0 \\ 0 & 0 & \frac{-6EI}{l^2} & 0 & \frac{4EI}{l} & 0 \\ 0 & \frac{6EI}{l^2} & 0 & 0 & 0 & \frac{4EI}{l} \end{bmatrix} \tag{4.5}$$

$$\mathbf{K_{22}} = \begin{bmatrix} \frac{EA}{l} & 0 & 0 & 0 & 0 & 0 \\ 0 & \frac{12EI}{l^3} & 0 & 0 & 0 & \frac{-6EI}{l^2} \\ 0 & 0 & \frac{12EI}{l^3} & 0 & \frac{6EI}{l^2} & 0 \\ 0 & 0 & 0 & \frac{GJ}{l} & 0 & 0 \\ 0 & 0 & \frac{6EI}{l^2} & 0 & \frac{4EI}{l} & 0 \\ 0 & \frac{-6EI}{l^2} & 0 & 0 & 0 & \frac{4EI}{l} \end{bmatrix} \tag{4.6}$$

$$\mathbf{K_{12}} = \begin{bmatrix} \frac{-EA}{l} & 0 & 0 & 0 & 0 & 0 \\ 0 & \frac{-12EI}{l^3} & 0 & 0 & 0 & \frac{-6EI}{l^2} \\ 0 & 0 & \frac{-12EI}{l^3} & 0 & \frac{-6EI}{l^2} & 0 \\ 0 & 0 & 0 & \frac{-GJ}{l} & 0 & 0 \\ 0 & 0 & \frac{6EI}{l^2} & 0 & \frac{2EI}{l} & 0 \\ 0 & \frac{-6EI}{l^2} & 0 & 0 & 0 & \frac{2EI}{l} \end{bmatrix} \tag{4.7}$$

where E is Young's modulus; G is shear modulus; I and J are the second moments of area about the axis of flexure and the polar moment of inertia respectively and A is effective cross-section area. For a typical cross section of pipeline, I, J and A are defined as (see Figure 4.2).

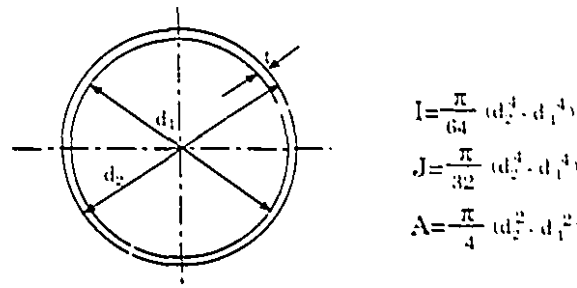

Figure 4.2: A cross section of pipeline

4.3 Shell Element

In this study, the shell is idealized as a series of flat plate elements. The flat plate elements can be subjected to both in-plane forces and bending effects which can occur independently. Since attention is restricted to owing linear elastic behaviour of the pipeline, the stretching and flexural effects can be superposed. The flat plate element representation of the shell behaviour has been extensively reported in the literature (see e.g. Greene et al. 1961; Clough and Johnson, 1964; Zienkiewicz and Cheung, 1965; Zienkiewicz, 1977). The elements that are used quite frequently in the modelling of flat elements are rectangular and triangular elements. A shell with sharp changes in curvature can be better approximated by a triangular element. For pipelines which are of the long distance type, the shell element can be represented by rectangular element.

4.3.1 Stiffness matrix of a typical flat element

Consider a typical rectangular flat element which subjects to in-plane forces and bending (see Figure 4.3). For in-plane stretching action, the strain can be defined in terms of the u and v displacement components in the x and y directions of each node i. Therefore the stiffness relation is given by

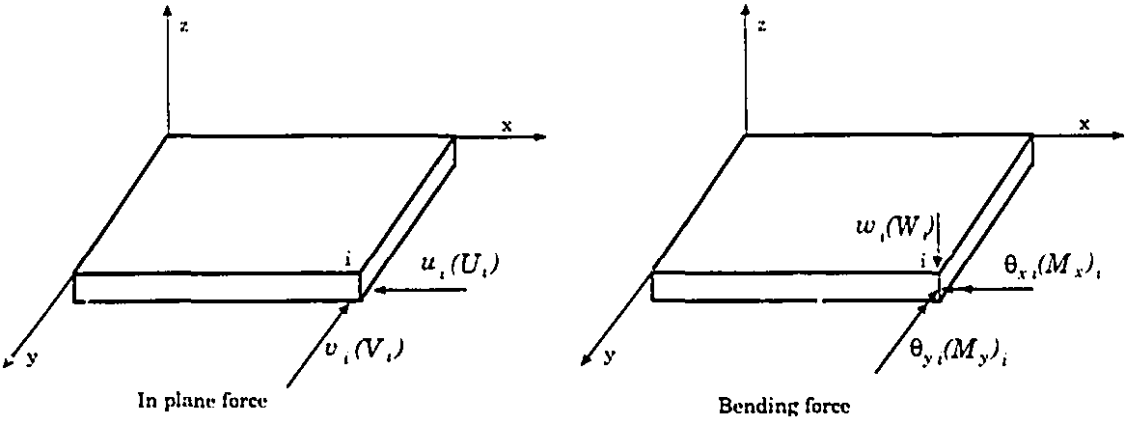

Figure 4.3: A typical rectangular flat element

$$\{F_i^p\} = [\mathbf{K_p}]\{\delta_i^p\} \tag{4.8}$$

where $\{F_i^p\}$ is the vector of in-plane forces

$$\{F_i^p\} = \begin{Bmatrix} U_i \\ V_i \end{Bmatrix} \tag{4.9}$$

$\{\delta_i^p\}$ is the vector of in-plane displacements

$$\{\delta_i^p\} = \begin{Bmatrix} u_i \\ v_i \end{Bmatrix} \tag{4.10}$$

and $[\mathbf{K_p}]$ is stiffness matrix of plane stress element.

Taking a bending action, the strain is defined in terms of w, the displacement in z direction and two rotations θ_x and θ_y. The stiffness relation for bending can be written as

$$\{F_i^b\} = [\mathbf{K_b}]\{\delta_i^b\} \tag{4.11}$$

where the vector of generalized forces is defined by

$$\{F_i^b\} = \begin{Bmatrix} W_i \\ M_{xi} \\ M_{yi} \end{Bmatrix} \tag{4.12}$$

and the vector of generalized displacements

$$\{\delta_i^b\} = \begin{Bmatrix} w_i \\ \theta_{xi} \\ \theta_{yi} \end{Bmatrix} \tag{4.13}$$

Details of the documentation of the stiffness matrices for plane stress ($[\mathbf{K^p}]$) and bending ($[\mathbf{K^b}]$) are given by Zienkiewicz (1977).

The combined stiffness relationship can be expressed in the form

$$\{F_i\} = [\mathbf{K}]\{\delta_i\} \tag{4.14}$$

where the combined stiffness matrix $[\mathbf{K}]$ is given by

$$[\mathbf{K}] = \begin{bmatrix} \mathbf{K_{11}^p} & \mathbf{K_{12}^p} & 0 & 0 & 0 & 0 \\ \mathbf{K_{21}^p} & \mathbf{K_{22}^p} & 0 & 0 & 0 & 0 \\ 0 & 0 & \mathbf{K_{11}^b} & \mathbf{K_{12}^b} & \mathbf{K_{13}^b} & 0 \\ 0 & 0 & \mathbf{K_{21}^b} & \mathbf{K_{22}^b} & \mathbf{K_{23}^b} & 0 \\ 0 & 0 & \mathbf{K_{31}^b} & \mathbf{K_{32}^b} & \mathbf{K_{33}^b} & 0 \\ 0 & 0 & 0 & 0 & 0 & 0 \end{bmatrix} \tag{4.15}$$

The combined generalized force vector is given by

$$\{F_i\}^{T^*} = \{\, U_i \quad V_i \quad W_i \quad M_{xi} \quad M_{yi} \quad M_{zi} \,\} \tag{4.16}$$

and the combined generalized displacement vector is given by

$$\{\delta_i\}^{T^*} = \{\, u_i \quad v_i \quad w_i \quad \theta_{xi} \quad \theta_{yi} \quad \theta_{zi} \,\} \tag{4.17}$$

It has to be noted that rotation θ_{zi} does not enter as a parameter in definition of deformations in either plane stress or bending mode. M_{zi} always equals to 0.

4.3.2 Local co-ordinates and global co-ordinates of a rectangular shell element

The development in the previous section is formulated in a local frame of reference. To express the appropriate equilibrium equations and to conduct assembly of the elements, it is necessary to transform the stiffness matrix in local co-ordinates to that in global co-ordinates.

Considering a local co-ordinate system (x', y', z') and the global co-ordinate system (x, y, z) (see Figure 4.4), the transformation of the generalized displacements is given by

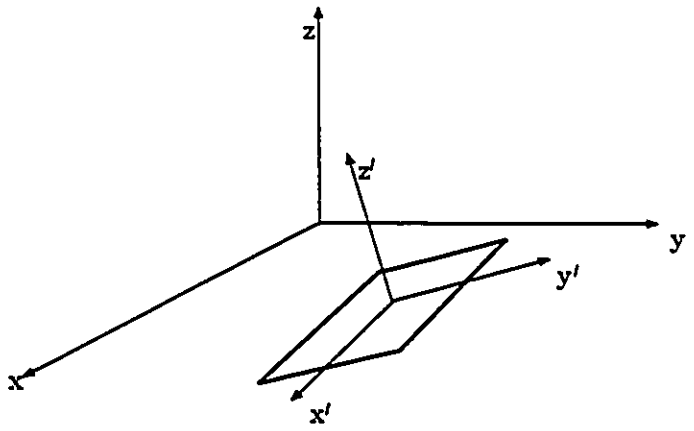

Figure 4.4: Local co-ordinates and global co-ordinates of a rectangular shell element

$$\{\delta_i'\} = [\mathbf{L}]\{\delta_i\} \tag{4.18}$$

and the transformation of the vector of generalized forces take the form

$$\{F_i'\} = [\mathbf{L}]\{F_i\} \tag{4.19}$$

in (4.18) and (4.19)

$$[\mathbf{L}] = \begin{bmatrix} \lambda & 0 \\ 0 & \lambda \end{bmatrix} \tag{4.20}$$

where λ is a 3×3 matrix of direction cosines of angles formed by the two sets of axes (x, y, z) and (x', y', z').

$$\lambda = \begin{bmatrix} \lambda_{x'x} & \lambda_{x'y} & \lambda_{x'z} \\ \lambda_{y'x} & \lambda_{y'y} & \lambda_{y'z} \\ \lambda_{z'x} & \lambda_{z'y} & \lambda_{z'z} \end{bmatrix} \tag{4.21}$$

and $\lambda_{x'x}$ refers to the cosine of angles between x and x' axes, etc.

For the entire set of nodes of an element, the transformation relation for the generalized displacements, generalized forces and the generalized stiffness matrix can be written as

$$\{\delta\}_e' = [\mathbf{M}]\{\delta\}_e \tag{4.22}$$

$$\{F\}_e' = [\mathbf{M}]\{F\}_e \tag{4.23}$$

$$[\mathbf{K}] = [\mathbf{M}]^{\mathbf{T}}[\mathbf{K}]_e[\mathbf{M}] \tag{4.24}$$

where [M] is given as

$$[\mathrm{M}] = \begin{bmatrix} [L] & 0 & 0 & 0 \\ 0 & [L] & 0 & 0 \\ 0 & 0 & [L] & 0 \\ 0 & 0 & 0 & [L] \end{bmatrix} \tag{4.25}$$

4.4 Validation of the Shell Element Formulation

The accuracy of the flat plate model for the representation of a shell has been investigated by a number of authors including Zienkiewicz and Cheung (1964). In this section a verification procedure is adopted to test the accuracy of the flat plate element.

We consider the problem of cylindrical tank made of a thin cylindrical shell with uniform wall thickness. The shell is fixed at the base and is subjected to pressure by a retained fluid. As illustrated in Figure 4.5, the dimensions of tank are: the radius $a = 9.144\ m$, the height $h = 8\ m$ and the thickness $th = 0.356\ m$. The Poisson's ratio of steel is 0.25. The weight per unit volume of the liquid γ is 9.8 kN/m^3.

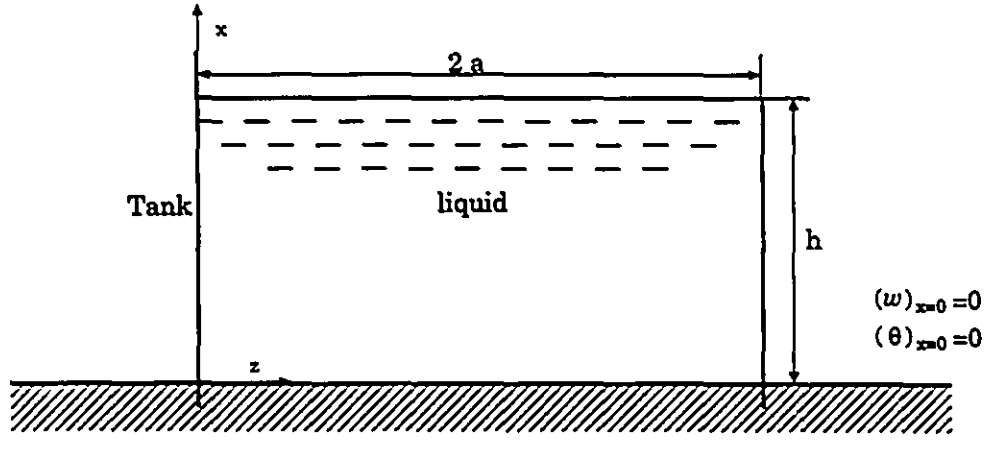

Figure 4.5: A cylindrical tank subjected to liquid pressure

The analytical solutions for the variations of deflection w and the bending moment M_x along a generator of the shell is given by Timoshenko and Woinowsky-Krieger (1959)

$$w = -\frac{\gamma a^2 d}{Eh}[1 - \frac{x}{d} - \theta(\beta x) - (1 - \frac{1}{\beta d})\zeta(\beta x)] \tag{4.26}$$

$$M_x = \frac{\gamma a d h}{\sqrt{12(1-\nu^2)}}[-\zeta(\beta x) + (1 - \frac{1}{\beta d})\theta(\beta x)] \tag{4.27}$$

where

$$\beta = (\frac{3(1-\nu^2)}{a^2 h^2})^{\frac{1}{4}} \tag{4.28}$$

$$\theta(\beta x) = e^{-\beta x} cos\beta x \tag{4.29}$$

$$\zeta(\beta x) = e^{-\beta x} sin\beta x \tag{4.30}$$

Taking into account the symmetry of the problem it is convenient to adopt the finite element discretization of the quarter tank, where appropriate displacement and shear boundary conditions are invoked. The finite element discretization is shown in Figure 4.6. The variation of deflection along the shell obtained via the analytical solution (Timoshenko and Woinowsky-Krieger, 1959) and via numerical modelling are shown in Figure 4.7. Figure 4.8 illustrates the variation of bending moment along the shell as derived from the analytical solution and from the finite element scheme. The maximum discrepancy between the results is less than 10 %.

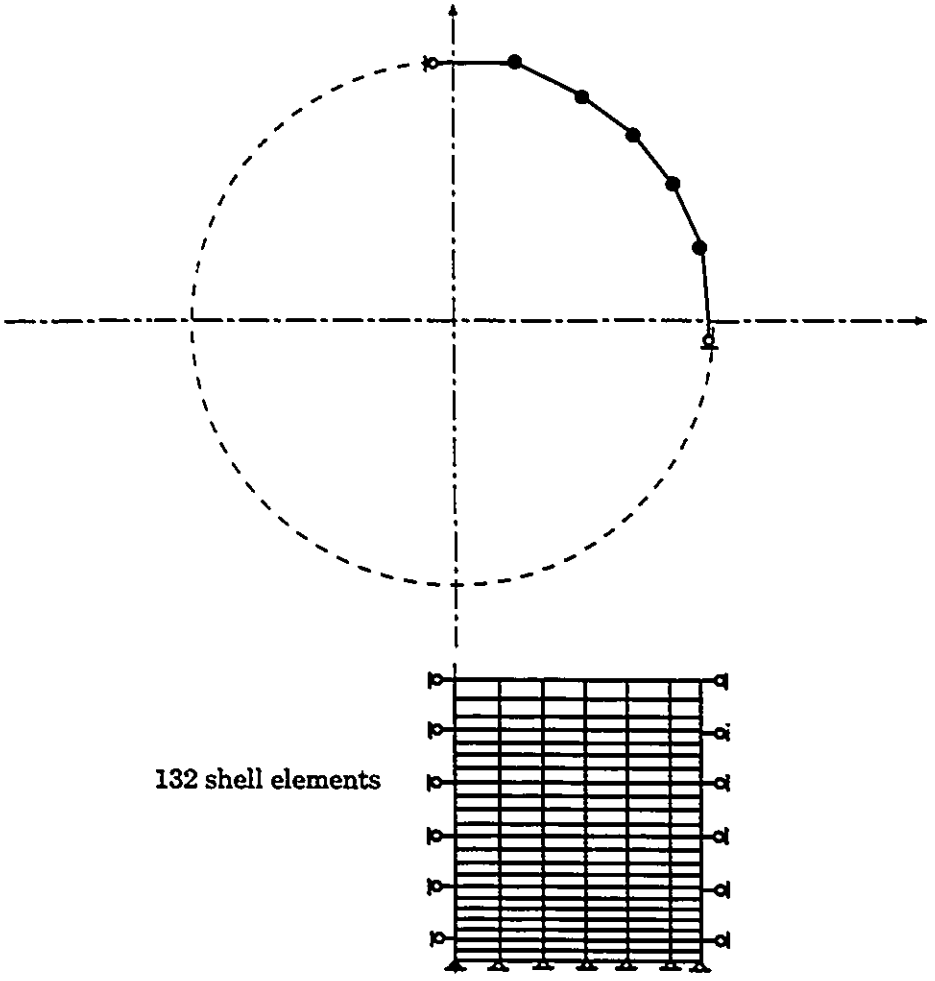

Figure 4.6: Finite element configuration of the cylindrical Tank

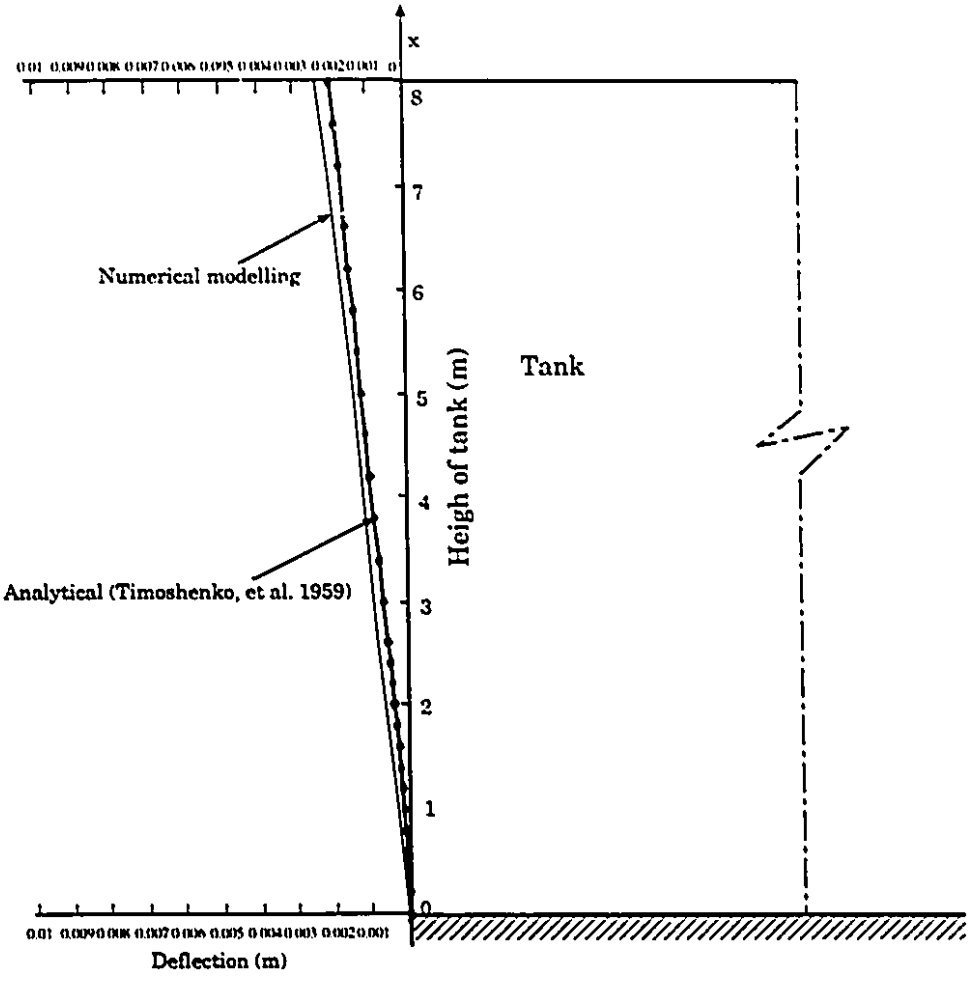

Figure 4.7: Variation of deflection along the wall of tank

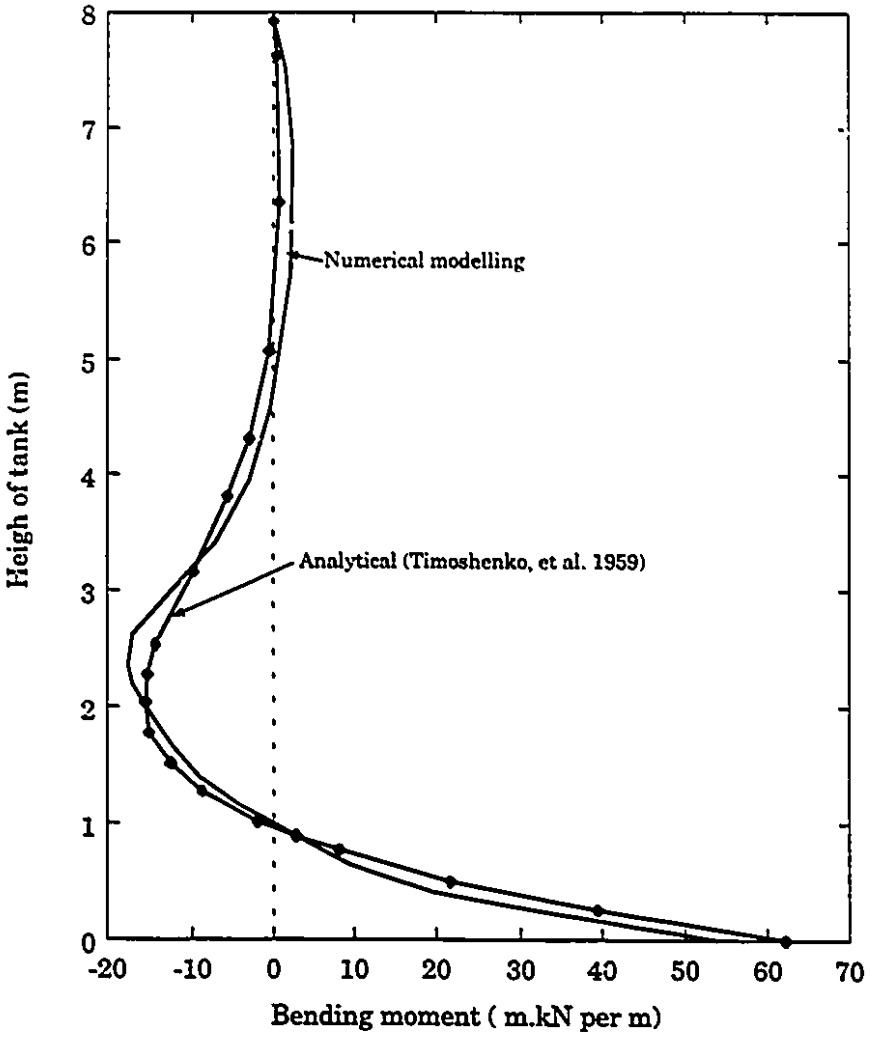

Figure 4.8: Bending moment distribution along the wall of tank

Chapter 5

Computational Analysis of Structure-Frozen Soil Interaction

5.1 General

Several numerical simulations of structure-frozen soil interaction involving creep modelling can be found in the literature. Most creep models used in such analysis employ power laws, which are valid only for describing the primary or secondary creep stages (Ladanyi, 1972, 1981, 1985). Examples of these include the investigation of creep behaviour of frozen tunnel walls (Klein, 1979) and the analysis of the settlement of vertically loaded cylindrical footings embedded in frozen soil (Puswewala and Rajapakse, 1990, 1991). Using the creep model proposed by Fish (1983), Puswewala and Rajapakse (1990) also examined the creep curve of a pressuremeter test, a plate load test and laterally loaded rigid cores. However, the unified creep model proposed by Fish (1983) incorporates only primary and tertiary creep stages and secondary stage is not included.

In this chapter the finite element method is used to investigate the complete creep behaviour of certain problems related to structure-frozen soil interaction, where the creep response is modelled by a complete creep model which accounts for all three stages (see Section 3.2). The structures used in the computational modelling deal with problems related to an embedded cylindrical footing and an embedded pile in the

frozen ground. The loadings can take the forms of either an axial load, a lateral load, a multi-step load or a quasi-static cyclic load. Other problems examined include a pipe section subjected to uplift loads and an embedded footing which has an interface effect.

5.2 Embedded Cylindrical Footing Subjected to Axial Load

We consider the axisymmetric problem of a cylindrical concrete footing which is embedded in a frozen soil and bonded to the surrounding frozen soil medium. Due to the axial symmetry of the footing and the loading, only the discretization in the r, z plane need be considered. The finite element discretization of the domain, which involves 400 four-noded isoparametric elements, is shown in Figure 1.2. The boundary conditions applicable to the problem are also indicated in Figure 1.2. The interface between the footing and the frozen soil is assumed to be bonded. The dimensions of the concrete footing are as follows: diameter=1 m, embedded depth=1 m, and the material properties are $E_c = 20\ GPa$, $\nu_c = 0.3$. The self-weight of the concrete is taken as 25 kN/m^3 and that of frozen soil is taken as 19 kN/m^3. The frozen soil is characterized by the creep parameters given in Table 3.2 and $E = 520\ MPa$ and $\nu = 0.3$ (Klein et al., 1979). All above parameters used in computational modelling are also shown in Figure 1.2. A set of vertical compressive loadings of magnitude, 400, 500, 625, 750 kPa, are applied in sequence to observe the general responses of creep behaviour.

The two creep settlement curves at the basal centre of a circular footing, under different compressive loading, are compared in Figure 1.2 to Figure 1.5 (it is noted

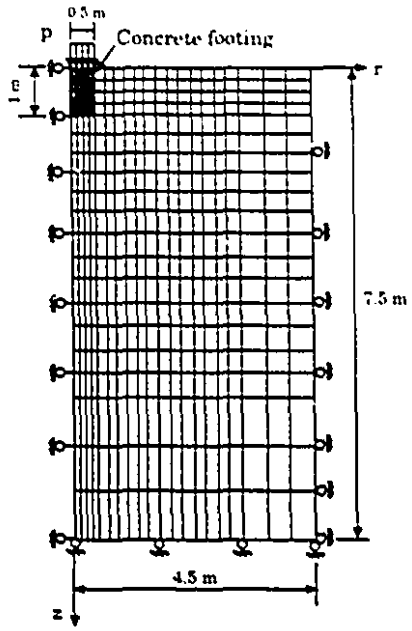

Concrete	E_c	20 GPa
	ν_c	0.3
	γ_c	25 kN/m^3
Frozen soil	E	520 MPa
	ν	0.3
	γ	19 kN/m^3
	Primary	A=0.00002118 B=1.05 C=0.29
	Secondary	A_2=0.00014611,B_2=1.111
	Tertiary	D=0.00013712 k=0.7649

Figure 5.1: Finite element discretization of circular footing embedded in frozen soil

that since E_c/E is large, the footing essentially behaves as a rigid body and the deflections at the basal centre also correspond to the overall settlement of the footing). In these Figures, one creep curve incorporates the complete creep model and the other incorporates the primary creep model. It is evident that when compressive pressure (p) is below 400 kPa, all locations within the frozen soil remain in primary creep stage. Therefore creep strain rates exhibit attenuating behaviour. At $p = 400$ kPa, elements in the vicinity of the base of the footing enter tertiary stage at $t = 2860$ days. The tertiary effects are not sufficiently dominant to allow one to distinguish between the results for the two material models. When the load is increased to $p = 500$ kPa, the displacement behaviour for the tertiary model shows an accelerated response. The creep curves display *failure* behaviour at 1950 days when $p = 625$ kPa and at $t = 1000$ days when $p = 750$ kPa (Figures 5.4 and 5.5).

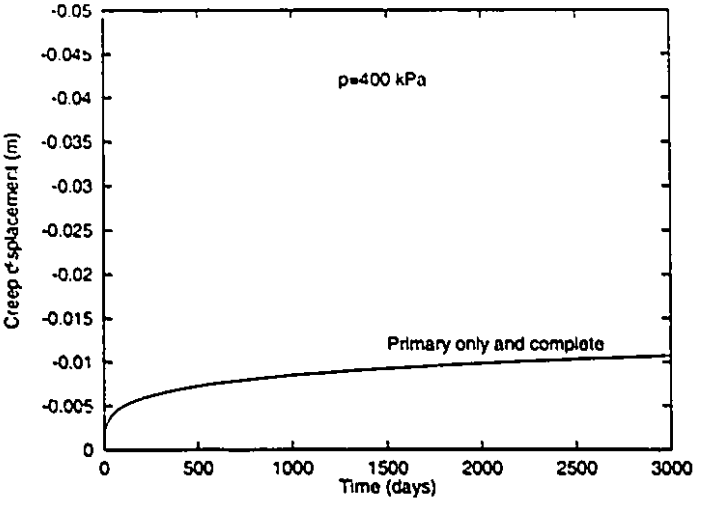

Figure 5.2: Creep displacements of cylindrical footing subjected to compressive loading

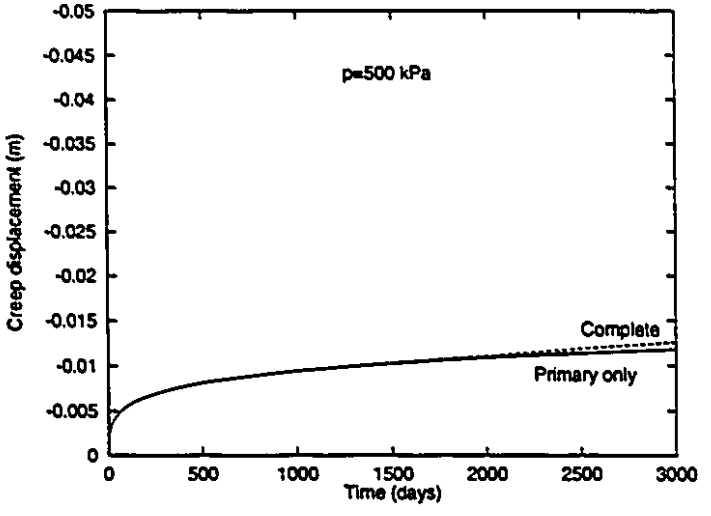

Figure 5.3: Creep displacements of cylindrical footing subjected to compressive loading

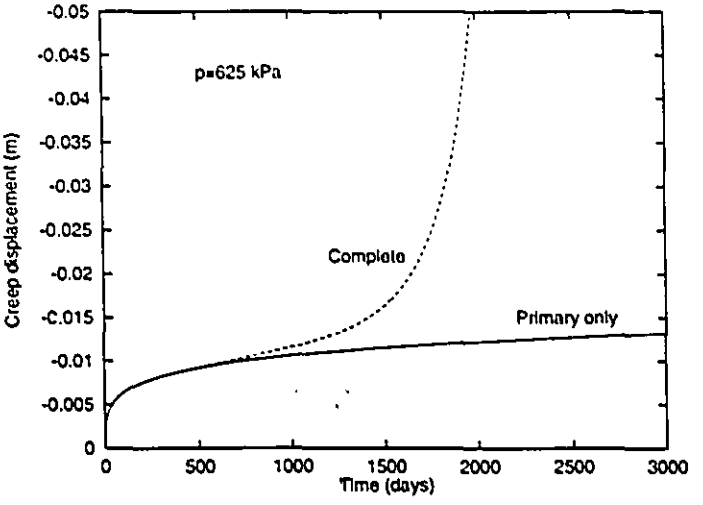

Figure 5.4: Creep displacements of cylindrical footing subjected to compressive loading

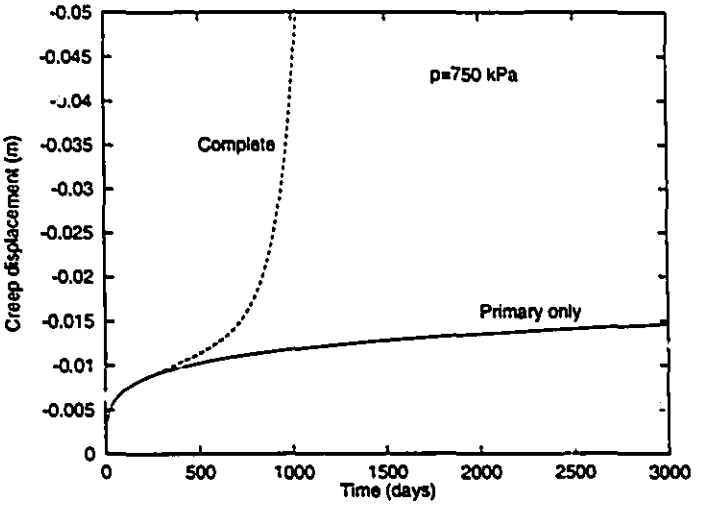

Figure 5.5: Creep displacements of cylindrical footing subjected to compressive loading

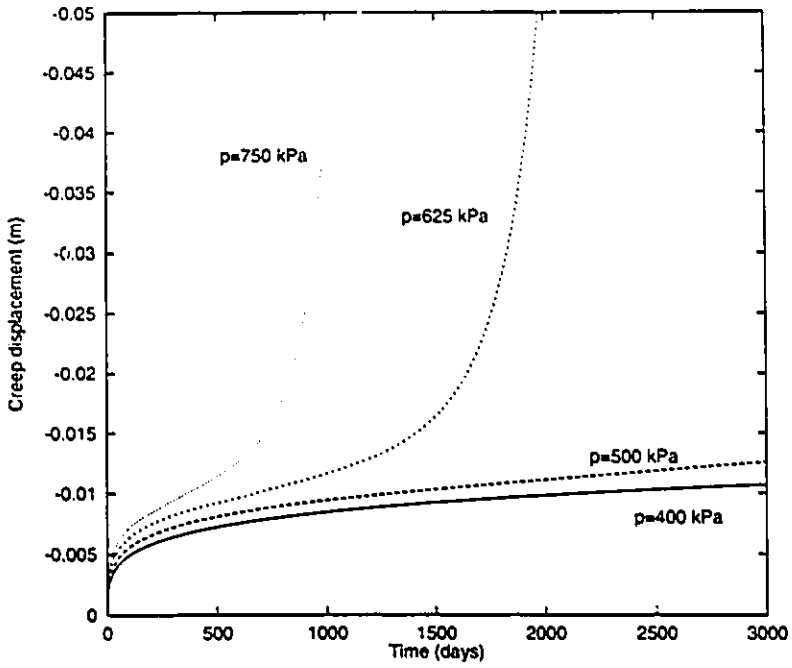

Figure 5.6: Creep displacements of cylindrical footing subjected to compressive loadings: influence of load level

Figure 5.6 compares the complete creep curves for the cylindrical foundation which is subjected to axial loadings. The computational results indicate that different magnitude of the applied load results in significantly different creep responses.

The creep curves for footings with different diameter to embedded depth ratios and for different creep responses (primary creep effects or complete creep effects) are illustrated in Figure 5.7 to Figure 5.10. If the embedded depth is kept constant ($h = 1\ m$), the footings with a lower diameter to depth ratio may yield a greater creep deformation. If the diameter of footing is kept constant ($d = 1\ m$), the creep curves indicate that the larger the footing embedded depth the lower the creep settlement. It is also observed that when compressive loading is held constant the time for the onset of the tertiary stage is sensitive to the diameter to embedded depth ratio.

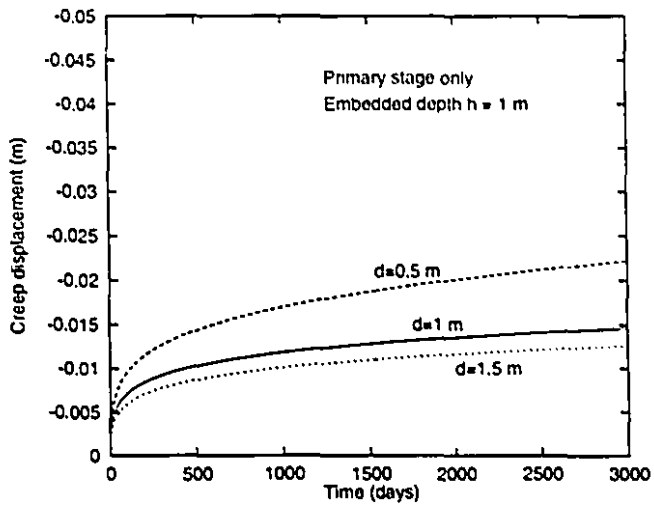

Figure 5.7: Creep displacements of cylindrical footing subjected to compressive loading: influence of aspect ratio of footing

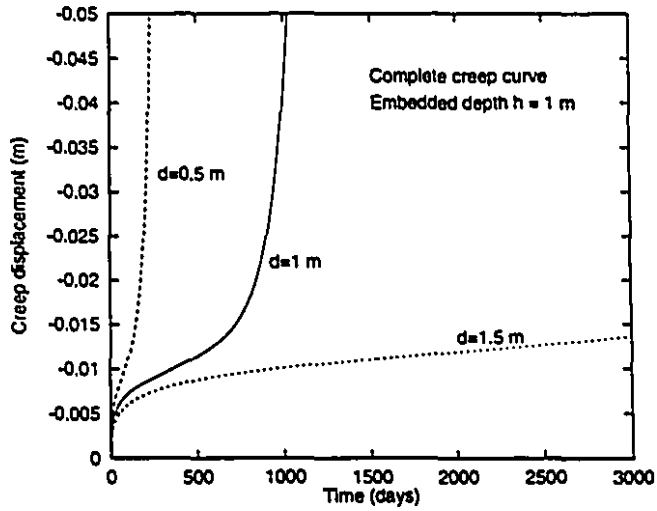

Figure 5.8: Creep displacements of cylindrical footing subjected to compressive loading: influence of aspect ratio of footing

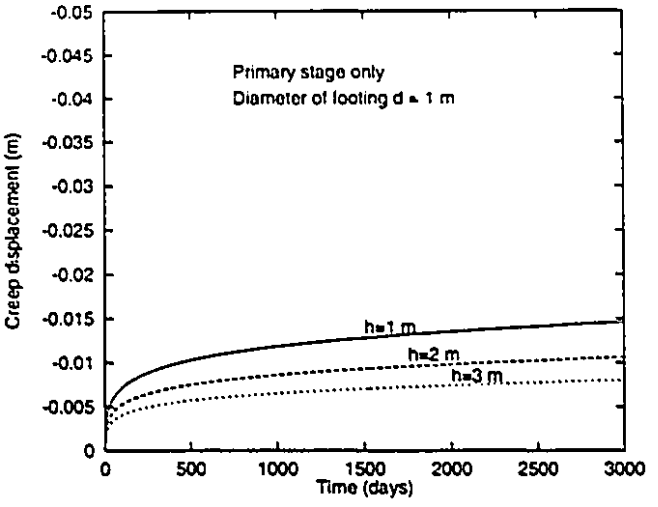

Figure 5.9: Creep displacements of cylindrical footing subjected to compressive loading: influence of aspect ratio of footing

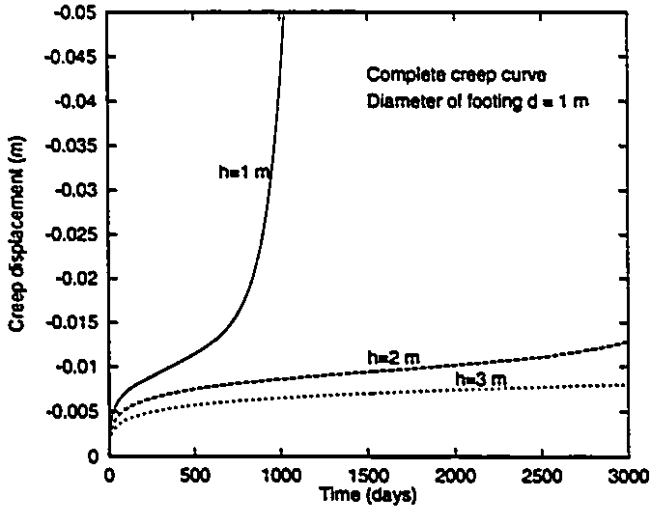

Figure 5.10: Creep displacements of cylindrical footing subjected to compressive loading: influence of aspect ratio of footing

5.3 Uniform circular Loading

As a second example we consider the problem of the indentation of a halfspace region of frozen soil by a uniform circular loading. The finite element mesh used in Figure 5.2 was modified to simulate the above problem, in that the embedded concrete footing region in Figure 5.2 was replaced by frozen soil. A set of loading intensities, $p = 100, 200, 300$ and $500\ kPa$, corresponding to total loads of $P = 78.5, 157, 235.5$ and $392.5\ kN$ respectively were applied.

Figure 5.11 illustrates the general creep displacement at the centre of the loading determined by using the complete creep model. For a uniform loading of stress intensity $100\ kPa$, the general response of complete creep curve attenuated and the result was similar to the curve obtained with the primary stage only for 3000 days. When $p = 200\ kPa$, the complete creep curve accelerated at 2000 days (i.e. the time at which a deviation from the displacement behaviour observed with purely primary creep model). It can be observed that under a load of stress intensity $300\ kPa$ the creep curve displays *an accelerated displacement* behaviour at 500 days. For a load of $500\ kPa$, the creep curve accelerates at 14 days.

Figure 5.12 illustrates the evolution of time-dependent creep damage for the stresses of $p = 500\ kPa$ and $p = 200\ kPa$. It illustrates that for a load of $500\ kPa$ larger regions of the frozen soil experience tertiary creep and tertiary creep occurs much sooner.

It may be noted that the magnitude of load initiating the onset of the acceleration of creep curve when circular loading is applied on the frozen ground is about half of the load on the footing with same diameter embedded in frozen soil (where embedded depth is 1 m).

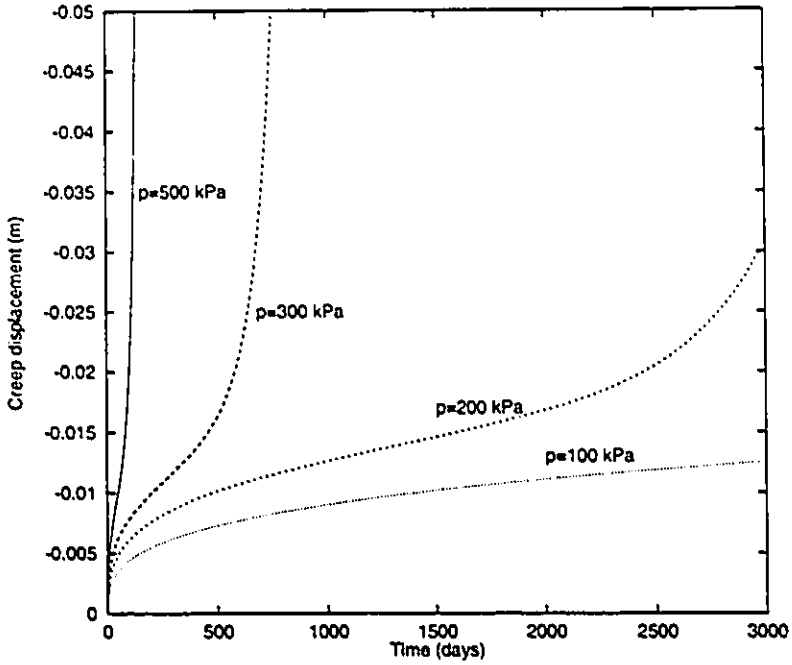

Figure 5.11: Creep displacements of frozen soil subjected to uniform circular loadings: influence of load level

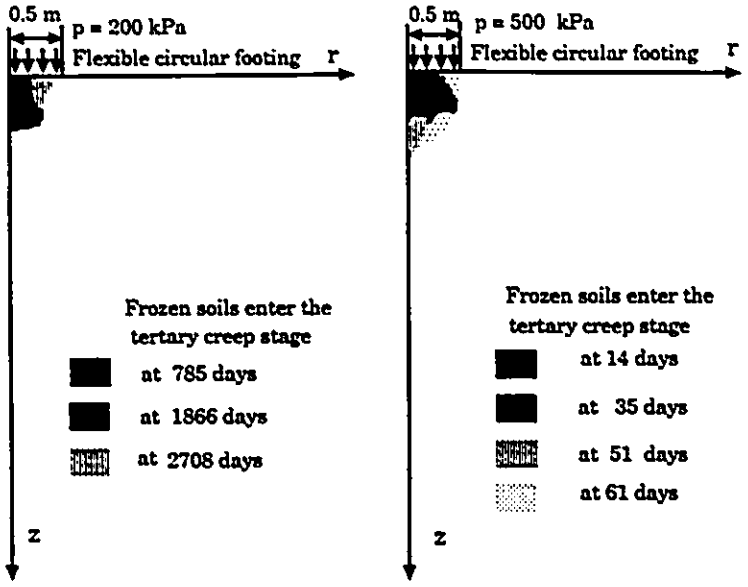

Figure 5.12: Evolution of time-dependent creep damage of frozen soil

5.4 Circular Flexible Footing Subjected to Variable Loading

In engineering practice, loading conditions are much more complicated than that of a load which remains constant with time. The loading cases may include step-loading, loading-unloading and quasi-static cyclic loading. Variable loadings can induce a sharp, discontinuous variation of both the stress and the creep strain rate. To simulate the creep behaviour under multi-step loading, a modification of the creep model is required.

In reviewing the complete creep model, it may be noted that creep phenomena are dependent on the current stress state and the time from latest applied external loading. Puswewala and Rajapakse (1992) assumed that the prevailing deformation resulting from the previous load attenuates sufficiently and exerts no influence on further creep development by a new step loading. Therefore the primary creep model may be given in the form where t refers to current time; t_i refers to time at which latest load is applied, i.e.

$$\dot{\epsilon}_{ij}^{cp} = \frac{3}{2} A C \sigma_e^{B-1} (t - t_i)^{C-1} s_{ij} \tag{5.1}$$

Puswewala et al. (1992) examined the primary creep behaviour of step-loading. In this thesis, the complete creep behaviour under step-loading, load-unloading and quasi-static cyclic loading cases were investigated. Based on the assumption for the primary creep stage (Equation (5.1)), the creep model for the tertiary stage can be modified to the following form:

$$\dot{\epsilon}_{ij}^{ct} = \frac{3}{2} A_2 (\sigma_e)^{(B_2-1)} [1 - (k+1) D (\sigma_e)^k (t - t_i)]^{\frac{-B_2}{k+1}} s_{ij} \tag{5.2}$$

where all parameters are defined in Chapter 3. The determination of stage transition is based on the following assumptions: when a new load is applied, if the elements are in primary creep stage by previous loading, the transition times are re-calculated using a stage transition function (see Section 3.2.4). All elements in the tertiary stage will remain in the tertiary stage regardless of loading condition.

Figures 5.13 and 5.14 show respectively the applied step loadings with time (up to a peak value of 300 kPa) and the resulting total displacements (including creep and elastic displacements) at the centre of the flexible circular footing. Figures 5.13 and 5.14 also indicate, for purpose of comparison, the load-time and displacement-time history for the case where the stress of 300 kPa is applied instantly. For the step loading case 1, each increment 150 kPa was applied separately at $t = 0$ and $t = 100$ days. For the step loading case 2, the magnitude of load at $t = 0$ is 100 kPa. At $t = 100$ days and $t = 200$ days, further compressive loads of 100 kPa were applied. From Figure 5.14, it is evident that the creep curves of step loadings are considerably different from the case where load was applied as a single step. The creep curve for the latter case displays failure behaviour at 550 days. In contrast, the creep curve by step loading 1 accelerates at 1600 days. The creep curve shows failure behaviour at 2000 days for the step loading case 2. These phenomena imply that the load applied in steps can reduce the creep deformation and delay the time of acceleration of displacement. This can be attributed to the occurrence of appreciable stress relaxation before application of subsequent step loadings.

Figure 5.15 indicates the loading history where loading, unloading in a step fashion takes place between 0 and 500 kPa, which is followed by a constant loading at the 500 kPa level. The creep settlement of the cylindrical footing subjected loading-

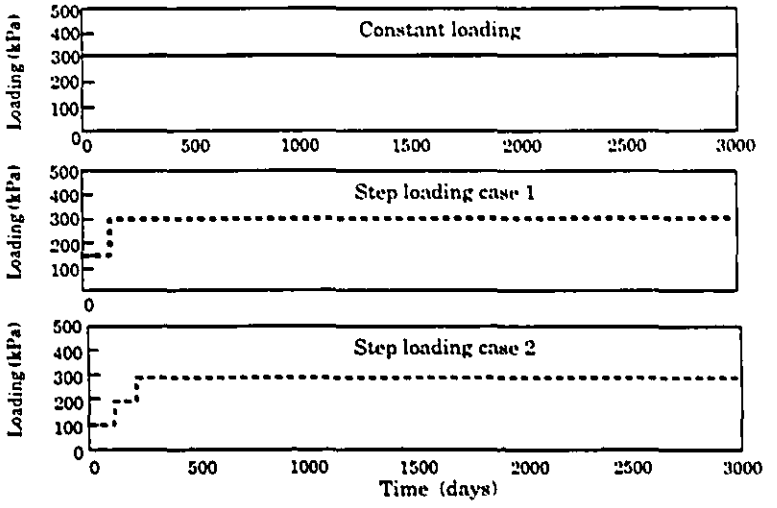

Figure 5.13: Time-dependent step loading history

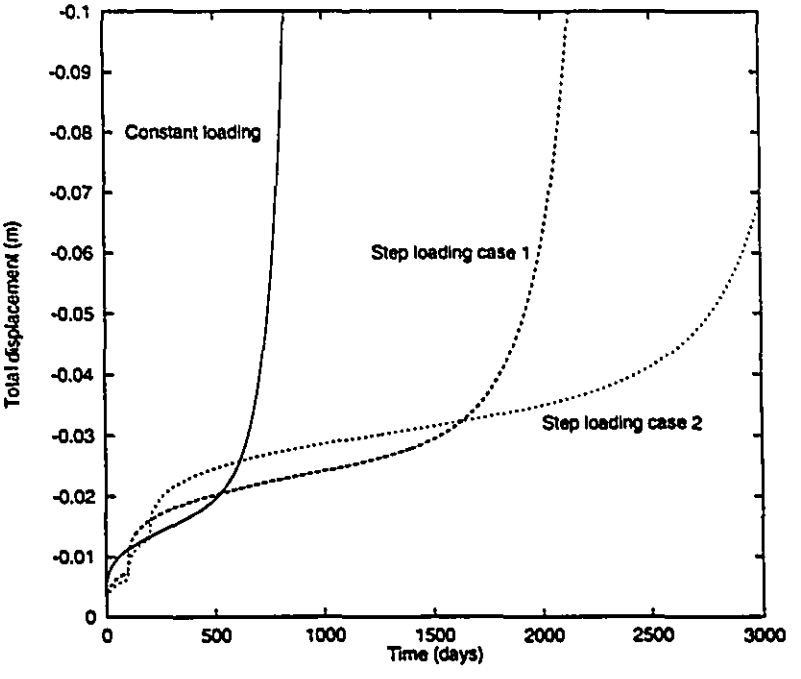

Figure 5.14: Creep displacement of circular flexible footing subjected to step loading

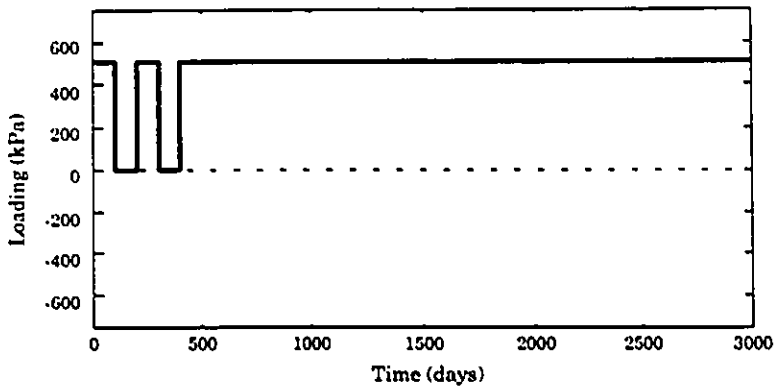

Figure 5.15: Time-dependent loading and unloading history

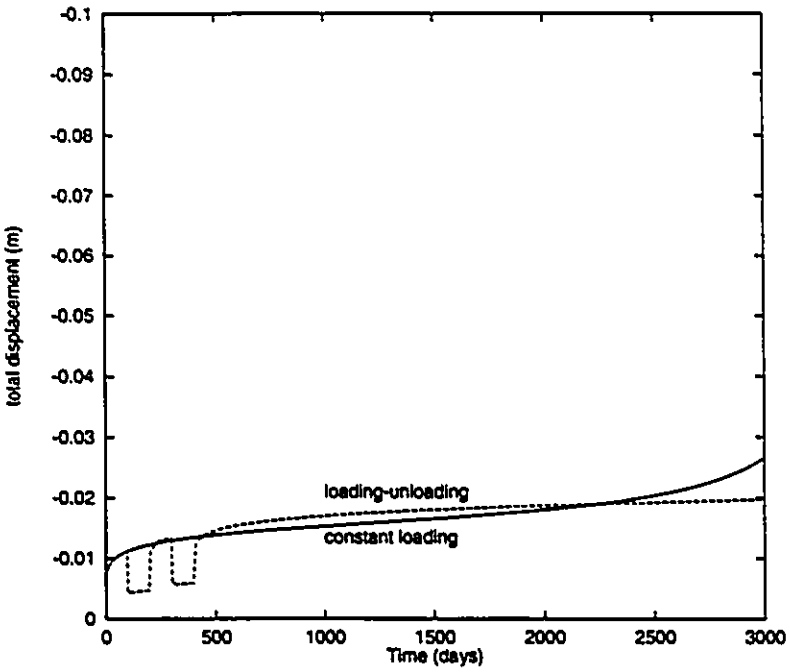

Figure 5.16: Creep displacement of circular flexible footing subjected to loading and unloading

-unloading-reloading is illustrated in Figure 5.16. Unlike the creep displacement induced by constant loading at $p = 500\ kPa$ from $t = 0$, for which the tertiary stage

initiated at t = 2200 days, the creep displacement curve under loading-unloading would not accelerate for a duration of 3000 days.

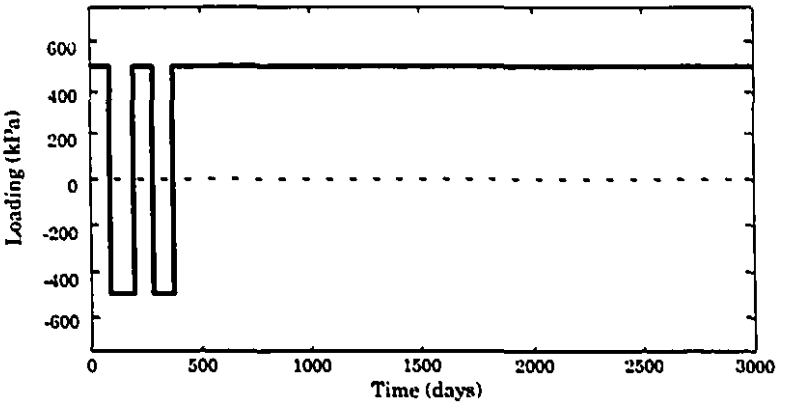

Figure 5.17: Time-dependent quasi-static cyclic loading history

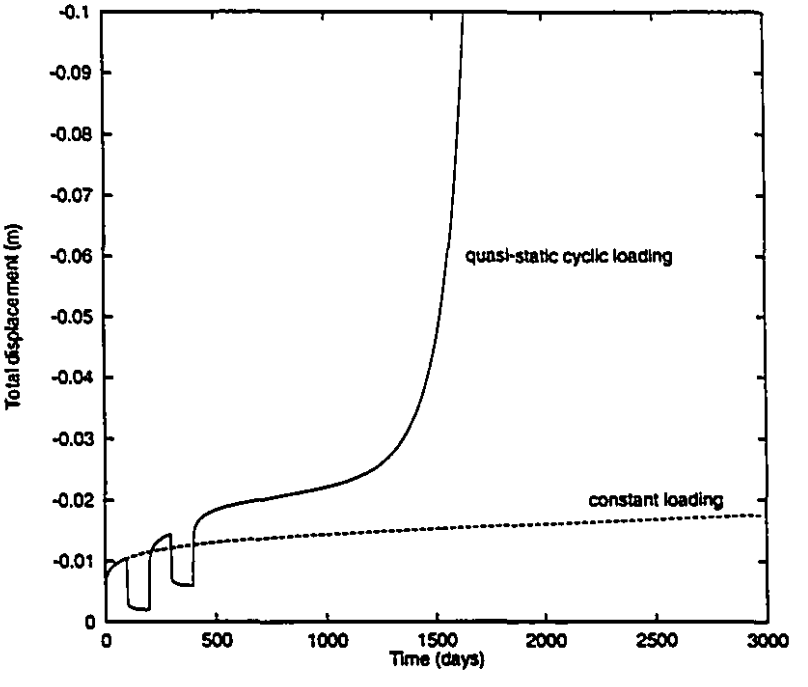

Figure 5.18: Creep displacement of circular flexible footing subjected to quasi-static cyclic loading

The simulation of quasi-cyclic loading $P = 500\ kPa$ including stress reversal is shown in Figure 5.17 and Figure 5.18. It shows that with cyclic load reversal, the displacement is more sensitive to activation of tertiary creep.

5.5 Pile Subjected to Lateral Load

In this section we consider the problem of a flexible pile which is embedded in bonded contact with a creep susceptible soil. The flexural behaviour of the steel pile is modelled by the Bernoulli-Euler beam theory. The geometry of the problem and the finite element discretization are shown in Figure 5.19. The steel pile has a Young's modulus of 210 GPa and a Poisson's ratio of 0.3. Different flexural rigidities of pile are represented by varying the diameter of pile from 15 cm to 30 cm. Simulations are carried out for a set of lateral loadings, applied at the top of the pile. The magnitude of the loadings are 125, 250, 500, 650 and 1000 kN. Results shown in Figure 5.20 illustrate the variation in the lateral displacements of the pile with time. The creep curves indicate that remarkably different shapes of displacement responses are displayed under the varying magnitudes of lateral loadings. The creep deflection accelerates at the very beginning when the applied load is 1000 kN. For an applied load of 125 kN, the creep curve enters a near steady state at 825 hours.

Figure 5.21 compares the elastic pile deflection with creep deflection in the case of 1000 kN. Larger creep deflection takes place on the top of the pile. In view of Figure 5.22, The bending moment along the length of pile shows that creep of frozen soil may increase the moment of the pile. Figures 5.23 and 5.24 give the deflection profile and bending moment along the pile respectively in the case of diameter 30 cm at the loading of 2500 kN. The results also illustrate the expected trend that different flexural rigidities can significantly change the shapes of the pile deflection and bending moment profiles.

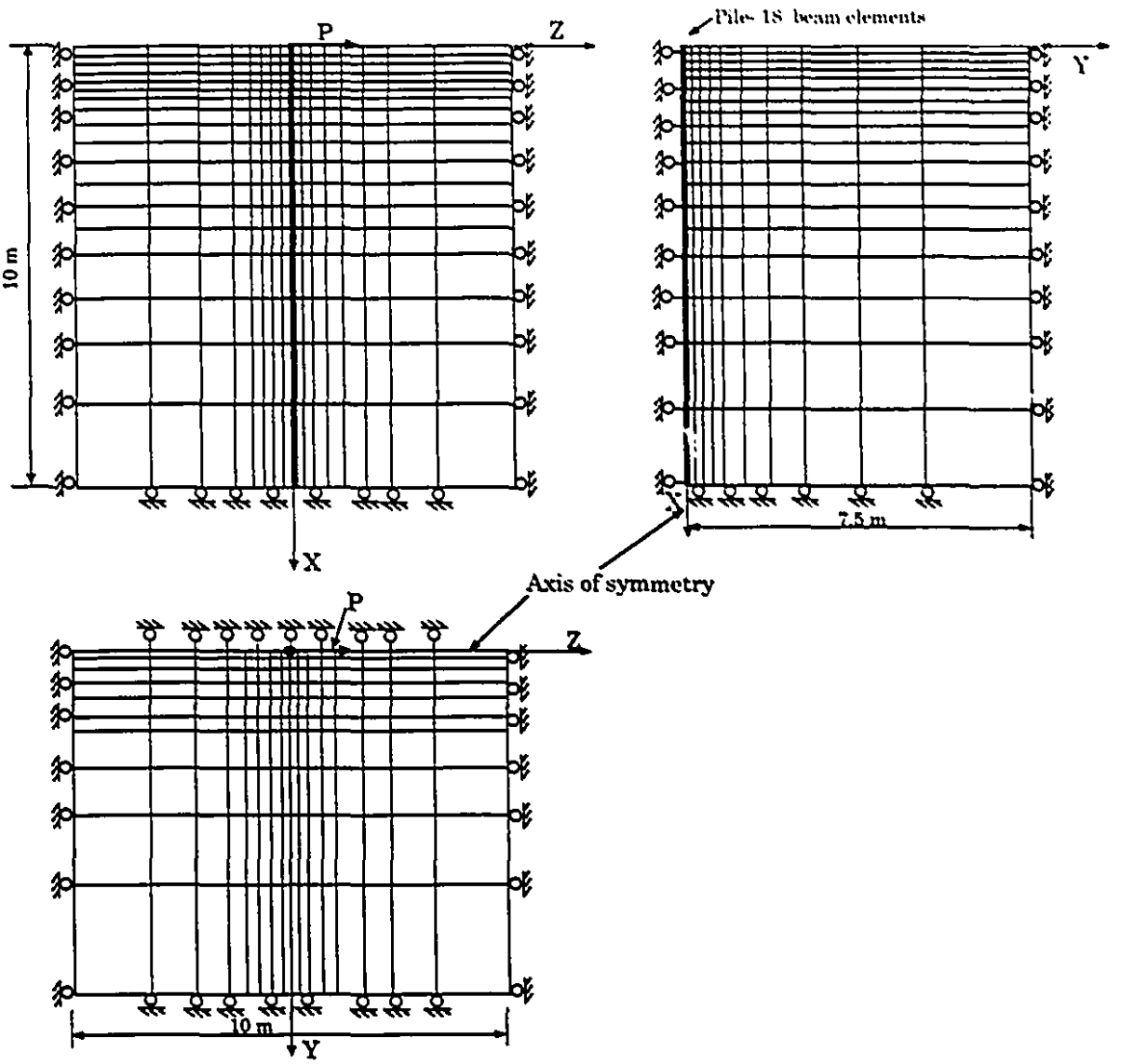

Figure 5.19: Finite element configuration of frozen soil-pile system

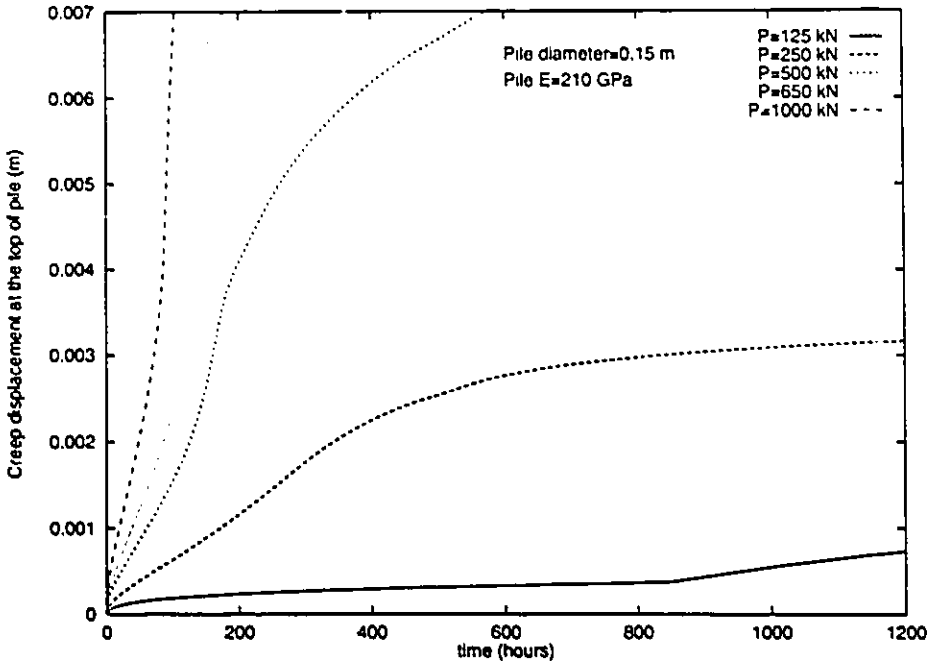

Figure 5.20: Creep displacement with time

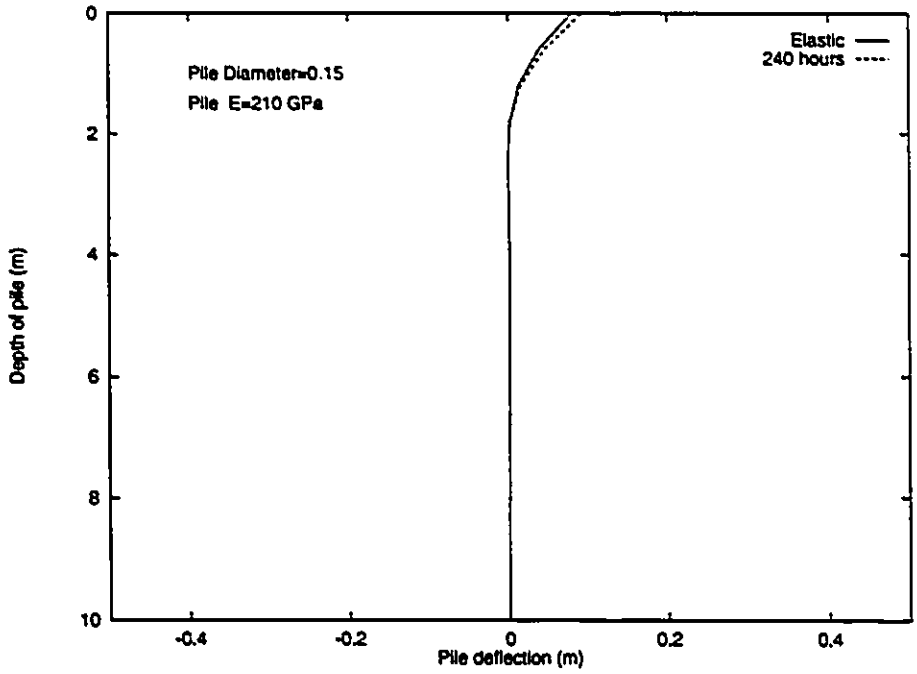

Figure 5.21: Pile deflection profile

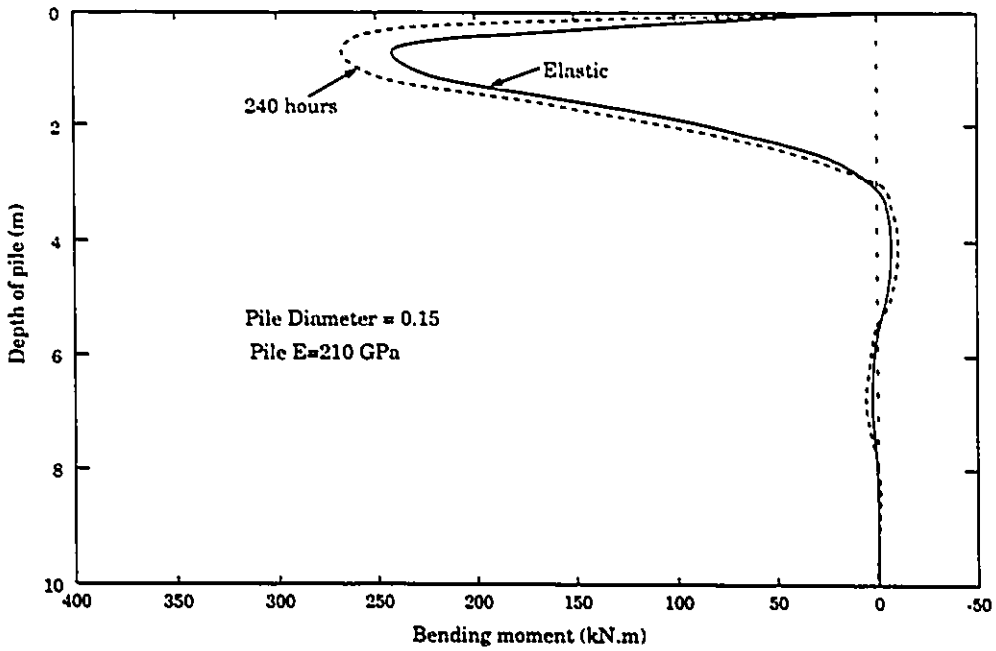

Figure 5.22: Bending moment along the length of pile

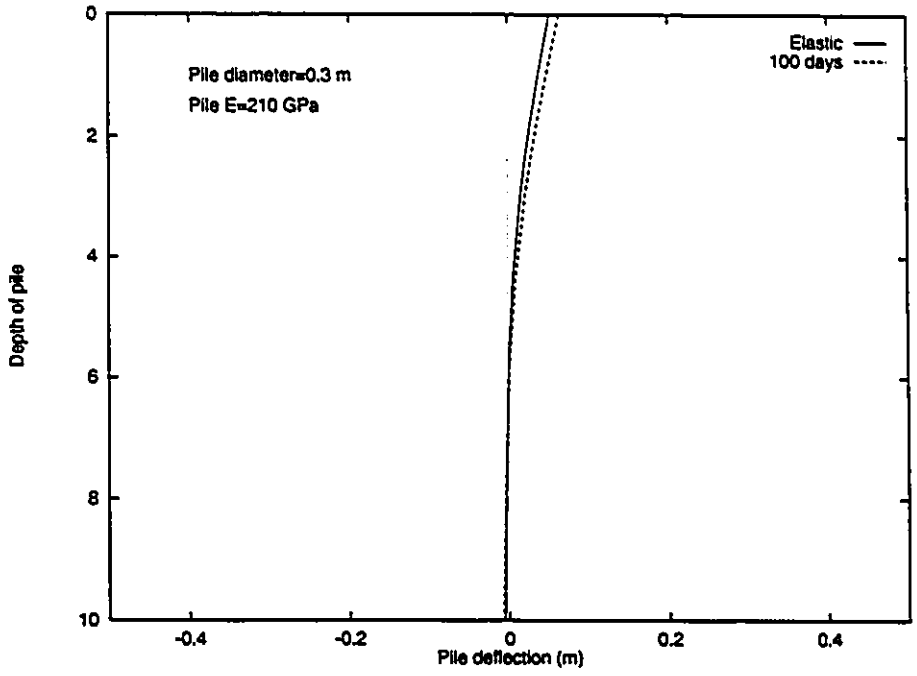

Figure 5.23: Pile deflection profile

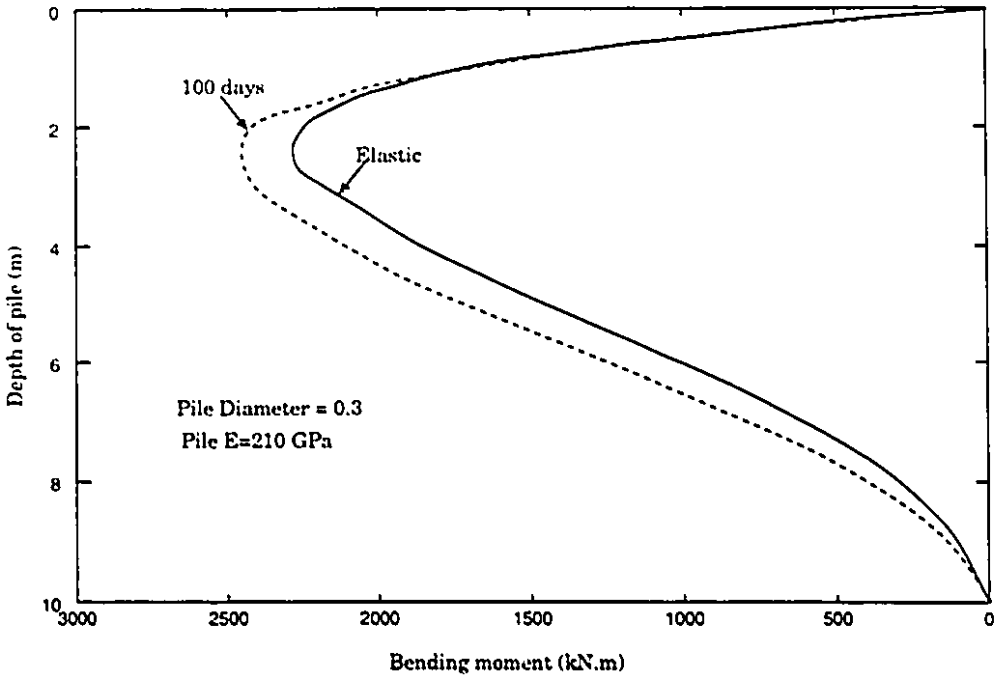

Figure 5.24: Bending moment along the length of pile

5.6 A Pipeline Subjected to Uplift Load

Pipelines which convey chilled gas which are located in discontinuous frost susceptible regions can be subjected to non-uniform displacements. The non-uniform displacements can create uplift in transition regions in which the frozen soils are either frost susceptible or non-frost susceptible. The mechanics of the soil-pipeline interaction in such discontinuous regions are influenced by the creep characteristics of the frozen soil. In this section, finite element technique is used to examine an idealized two-dimensional plane strain problem of the time-dependent displacement of a pipe which is subjected to uplift loads which are kept constant with time. The modelling also focusses on the time-dependent evolution of creep failure zones within the frozen soil.

A pipeline of diameter 50 cm and wall thickness 0.5 cm is located at a depth of 175 cm below the surface of a frozen layer. The mechanical parameters of pipe and frozen soil were assumed as follows: Pipe: $E_p = 200\ GPa$, $\nu_p = 0.3$; Frozen soil: $E = 520\ MPa$, $\nu = 0.3$, $C_0 = 1.5\ MPa$, $\phi = 30^0$. The tensile strength of frozen soil was assumed to be 0.5 MPa. The weight of the frozen soil was taken as 19 kN/m^3. The mesh discretization with 152 elements and 182 nodes is shown in Figure 5.25. The creep parameters used for simulation are given in Table 3.2.

Case 1: An uplift load $P = 80\ kN$ is applied to the pipe and this load is maintained constant with time. The magnitude of load was chosen in order to initiate detachment of elements in the vicinity of the base of the pipe, upon application of the load. Figure 5.26 illustrates the influence of the post failure analysis on the time dependent displacement of the pipe section. The influence of tertiary creep failure of the medium on the rate and magnitude of the displacement is clearly evident in the results given in Figure 5.26. A tertiary creep analysis which incorporates the development of post failure detachment gives a much larger value of total displacement after 6300 hours than for simulation where post failure detachment is not included. Figure 5.27 also indicates the time-dependent evolution of failure in the frozen soil which couples tertiary creep with failure development.

Case 2: In this problem, a 60 kN load is applied to the pipe and this load is maintained constant with time. At this load level there is no initiation of detachment of the pipe from the frozen soil. At the time of application of the 60 kN load, however, failure is allowed to develop by the initiation and evolution of tertiary creep. The elements in the vicinity of the base of the pipe enter the tertiary stage at $t = 1010$ hours. The maximum tensile stresses in these elements are attained and failure occurs at $t = 3100$ h, due to material degradation and reduction of loading-bearing area within frozen soils. Figure 5.28 shows the resulting total displacement and creep displacement with time. Figure 5.29 illustrates the contour of the progressive failure

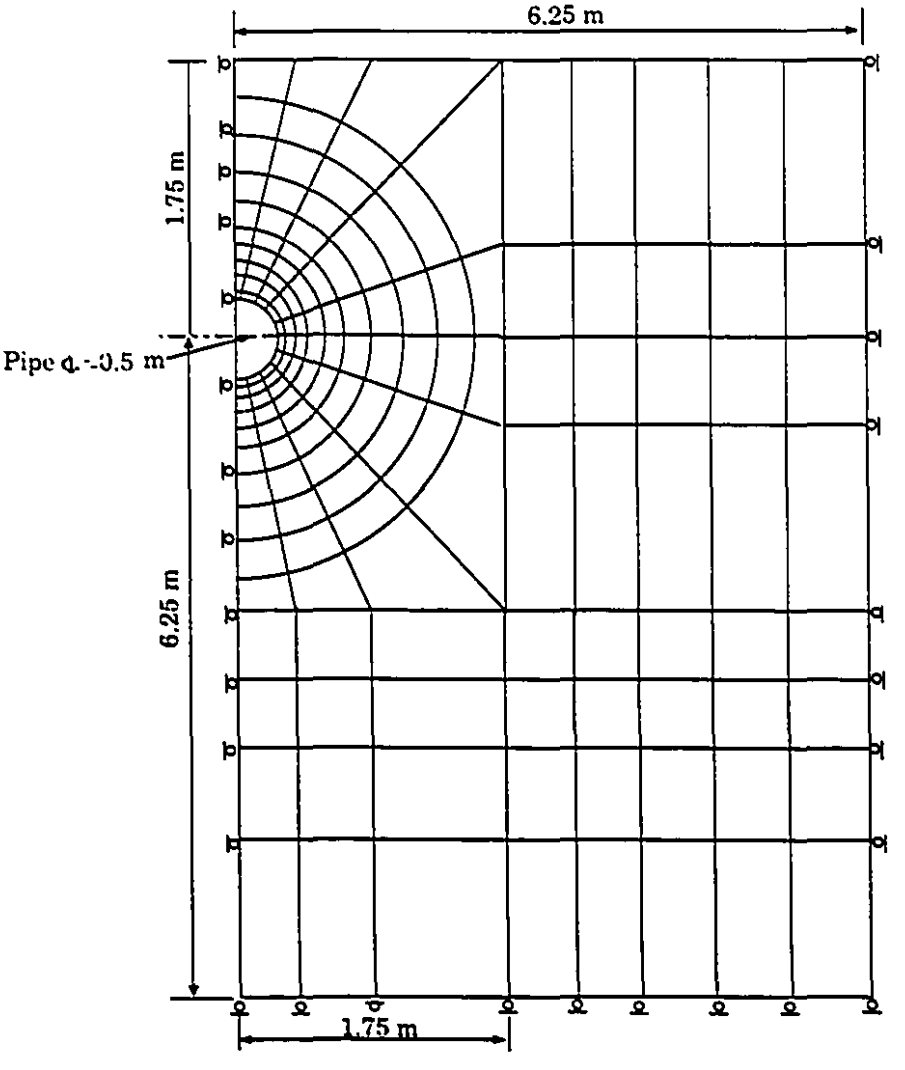

Figure 5.25: Discreted finite element mesh of pipe embedded in a layer of frozen soil

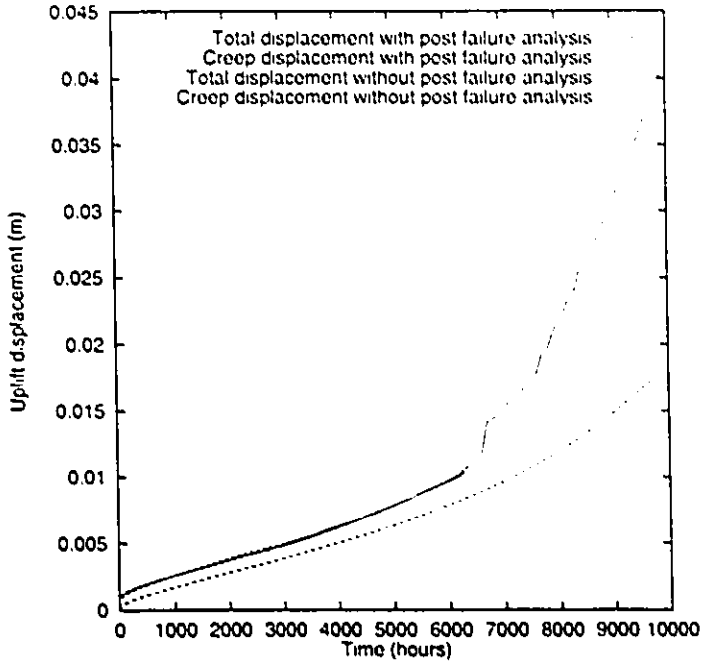

Figure 5.26: Uplift displacement of the pipe when P=80 kN

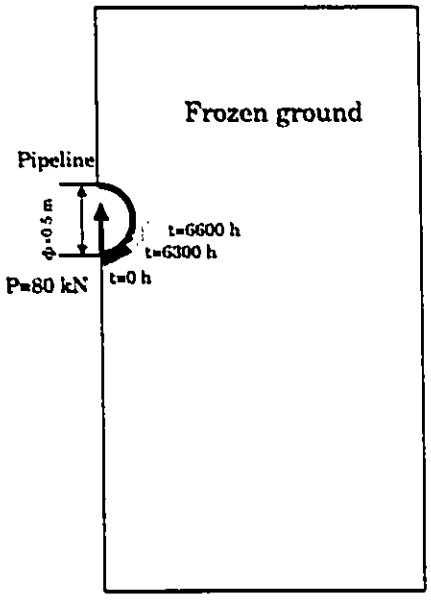

Figure 5.27: Evolution of failure in the frozen soil when P=80 kN

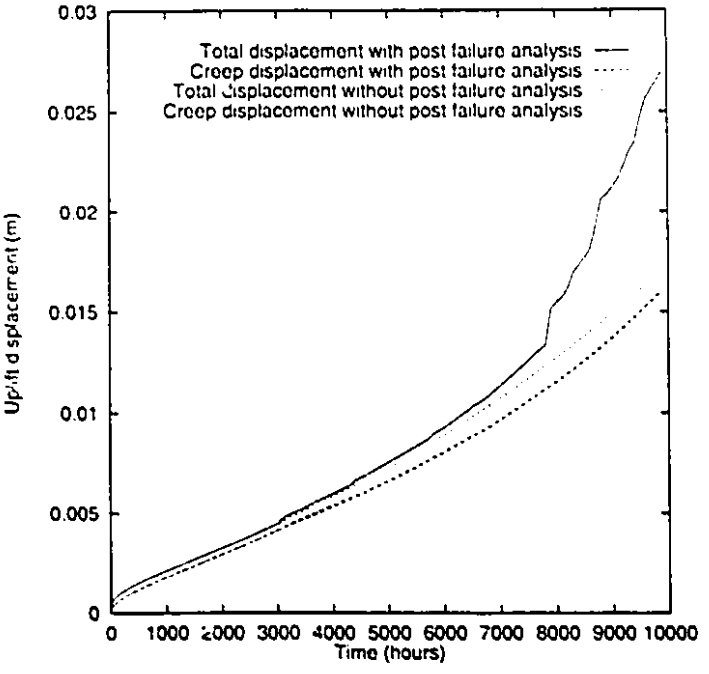

Figure 5.28: Uplift displacement of the pipe when P=60 kN

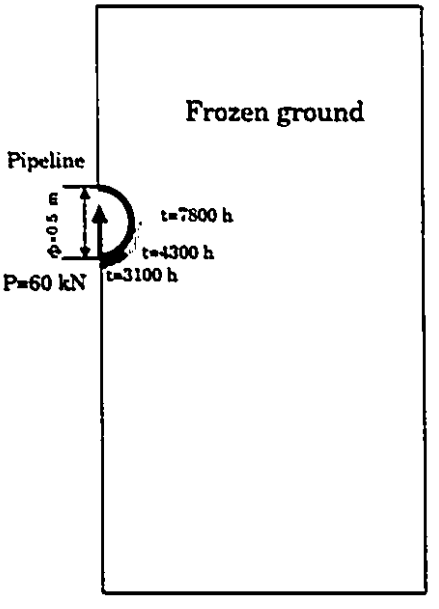

Figure 5.29: Evolution of failure in the frozen soil when P=60 kN

zone. As can be observed, the failure zone initiates at 3100 hours after the application

of the uplift load. The failure zone gradually expanded thereafter and the displacement curve accelerated markedly at 7800 hours. Further computations also indicate that the frozen medium remains in the primary stage, without evolution of tertiary creep and failure, when the uplift load is 40 kN. The 40 kN load can be identified as the peak loading in the range for a duration of 10000 hours (approximately 1.14 years).

5.7 Embedded circular footing with the effect of interface

In this section, we examine the problem of the rigid cylindrical foundation embedded in a creep susceptible region. The interface between the rigid foundation and the creep susceptible medium is incorporated with a non-linear interface element which is developed in Section 3.4.3. Figure 5.30 shows the interface element configuration incorporated at the interface. The constitutive parameters of interface are assumed as follows: $K_n = 1\ GPa$, $K_s = 25\ MPa$, $C_f = 0.5\ MPa$ and $\phi_f = 30^0$.

An axial compressive load $P = 1500\ kN$ is applied at the surface of the footing. The induced creep settlement and total settlement (which includes elastic and creep deformations) are shown in Figures 5.31 and 5.32. The results indicate the modelling which includes interface elements can give a larger total settlement and lower creep settlement than the analysis in which the footing was assumed to be completely bonded with surrounding soils. In the analysis of incorporated with interface failure modelling, it is observed that shear failure occurs at interface 1, which gives considerably larger total settlements and creep settlements in comparison with the analysis where interface failure is not involved.

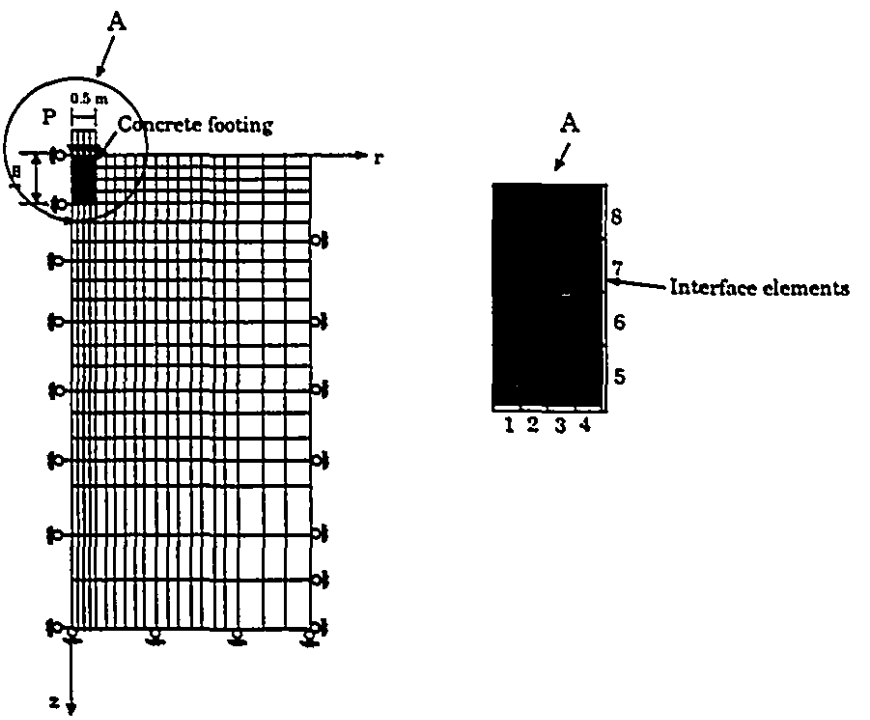

Figure 5.30: Finite element configuration with interface element

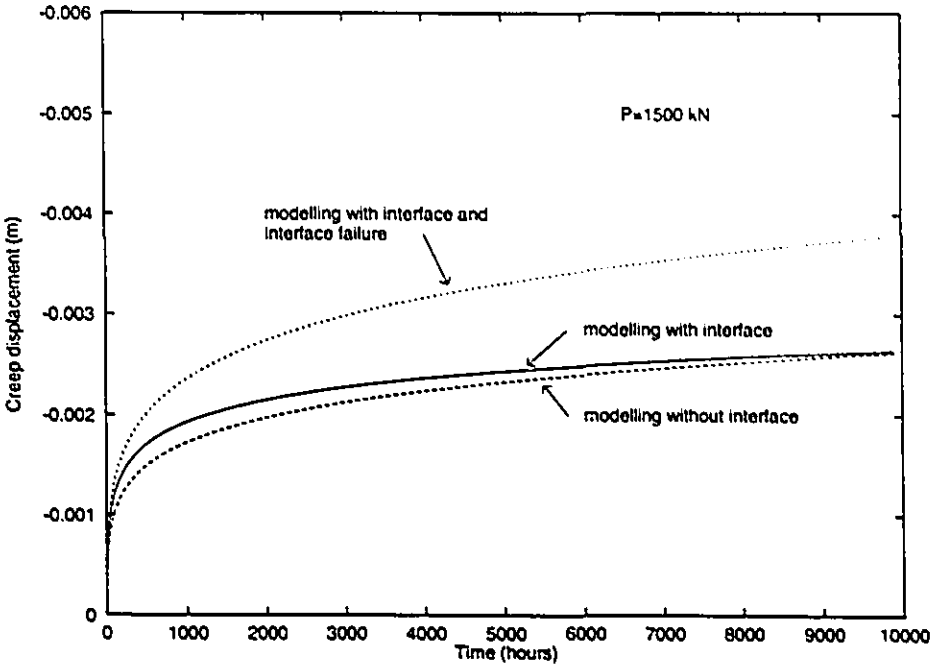

Figure 5.31: Modelling of interface and adfreezing creep

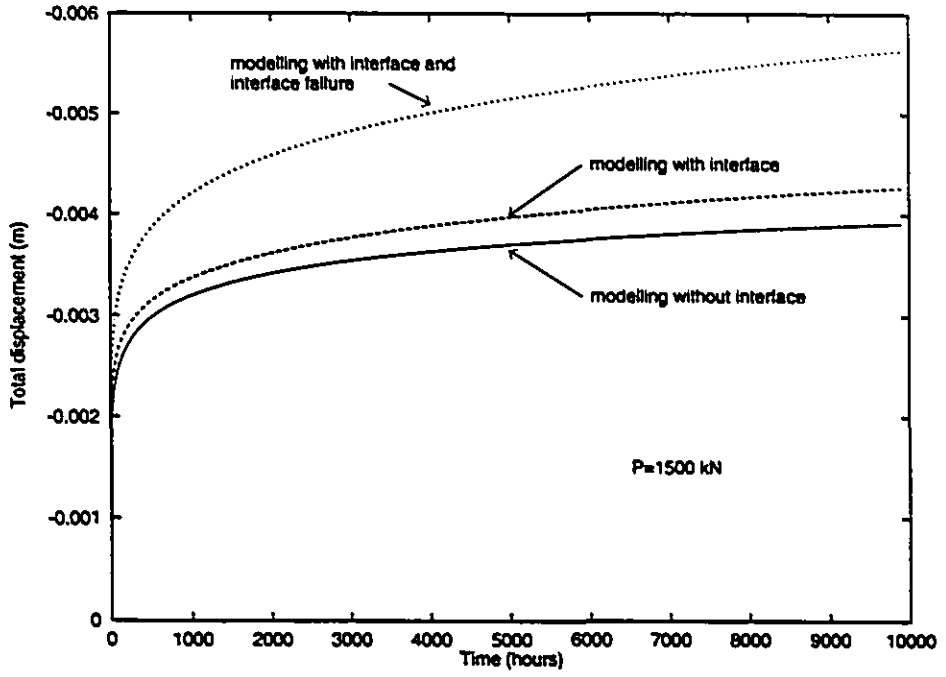

Figure 5.32: Modelling of interface and adfreezing creep

Chapter 6

Numerical Modelling of Soil-Pipeline Interaction

6.1 General

The structural analysis and design of a buried chilled gas pipeline should take into consideration the interaction between the soil and the pipeline induced by thermo-hydro-mechanical processes associated with soil freezing. The simulation of these processes should include the modelling of frost heave, constitutive behaviour of frozen and unfrozen soils, mechanical response of the pipeline and the constitutive response of the interface between the pipeline and the frozen and unfrozen soils. In this chapter, we apply the finite element procedures which were developed in the previous chapters to conduct a numerical modelling of the Canada-France pipeline freezing test which was carried out at *Station de Gel* at the *Centre de Geomorphologie* at Caen, France.

The Caen pipeline test is a multi-disciplinary investigation involving many aspects, including, fundamental studies related to soil freezing and thawing of soil and the study of soil-pipeline interaction, including the measurement of deformations and stresses induced in both the pipeline and surrounding soils, for the situation where a full scale chilled pipeline was buried at a transition zone between a highly frost susceptible soil and a non-frost susceptible soil. The physical, thermal and moisture influx conditions at the test facility were controllable.

The freezing experiment consisted of two major stages. The first stage commenced in September, 1982 with four freezing periods. The purpose of this stage was to examine the behaviour of a buried chilled pipeline passing through the boundary between two initially unfrozen soils with significantly different responses to frost susceptibility. The experimental data on this phase of the test was presented by Dallimore (1985).

The second stage was designed to investigate the behaviour of a buried chilled pipeline crossing a transition zone between prefrozen and unfrozen frost-susceptible soils. The details of this stage refer to the *Preliminary Database Report* (National Energy Board, 1994) for the Caen frost heave test facility.

6.2 Test Facility

The test facility consisted of a temperature-controlled hall with the following dimension: 18 m in length, 8 m in width and 5 m in height, which was originally designed for the study of freeze-thaw problems encountered in highways. The base of trough of the temperature controlled hall can isolate the thermal and hydraulic regime from the natural ground conditions and the trough can be filled with soil to a depth of 2 m. A steel pipeline measured 18 m in length and 273 mm in diameter was buried in the trough at a depth of 33 cm from the surface. This pipeline can be subjected to independent refrigeration temperature. In order to model a pipeline of substantial length, both ends of the pipeline were maintained free of constraint. The wall thickness of pipe was 0.5 cm.

Longitudinal and transverse sections of the Caen test facility are shown in Figures 6.1 and 6.2.

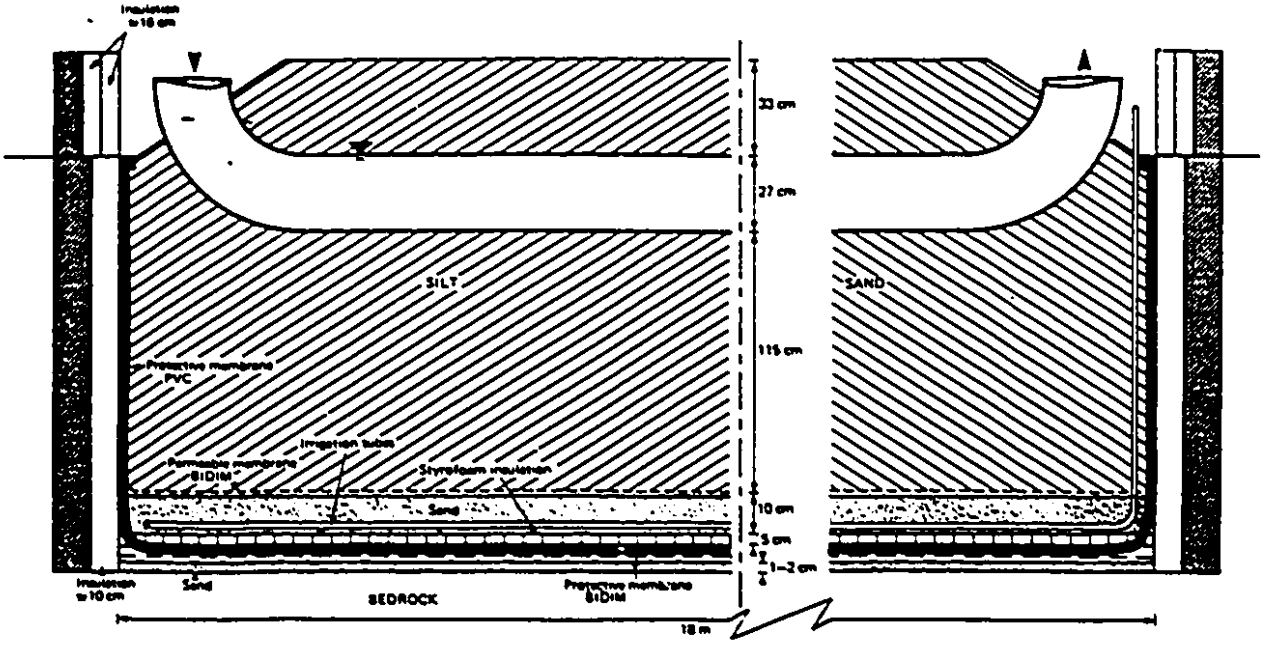

Figure 6.1: Longitudinal section of Caen test facility (after Dallimore et al. 1984)

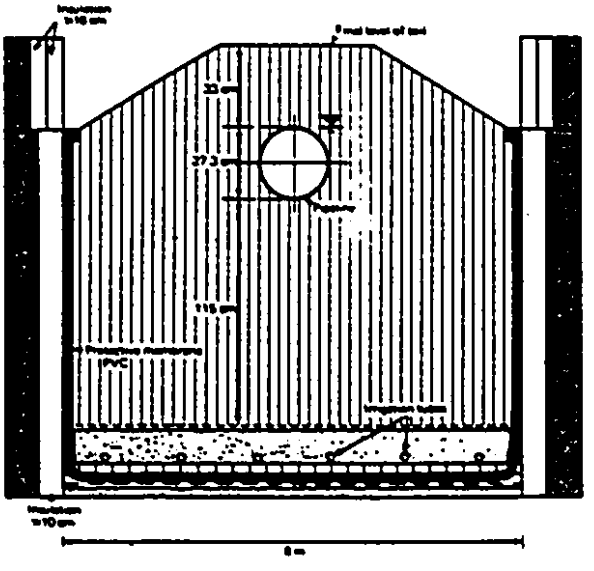

Figure 6.2: Transverse section of Caen test facility (after Dallimore et al. 1984)

In the experiments conducted at this facility, two types of soils with contrasting frost susceptibilities, were placed in each half of the trough. The soil with high susceptibility to frost heave was Caen silt (Dallimore, 1985). A grain size analysis of the Caen silt gave the following: 13 to 20% clay, 65 to 75% silt and 10 to 20% sand. The soil with low susceptibility to frost heave used in the experiments was the SNEC sand. A grain size analysis indicated that the SNEC sand has a composition of approximately 10% silt and 90% sand. The water table in the test facility was maintained at 30 *cm* below the base of the pipeline.

6.3 Instrumentation

Extensive instrumentation was incorporated in the Caen pipeline test facility to measure thermal regimes, moisture regimes, internal soil displacements, soil surface heave, earth pressure, pipe movements, strains and stresses in the pipeline. For the measurement of heave, more than 400 test points, were installed. The test points measured the time dependent heave of the surface of the entire soil.

The temperature profiles were collected automatically by 160 thermocouples, 20 thermistors and several heat flux meters located at critical locations. Additional portable thermistors were used manually to collect the temperature data. The moisture regimes were measured with time domain reflectometry probes (TDR) and the water table was measured by piezometer wells. The change of apparent dielectric constant of the soil due to soil freezing was measured by time domain reflectometry probes and the resulting change was related to the unfrozen water content. Internal soil deformation was measured by sets of magnet heave measurement systems and telescoping tubes. Soil surface heave was measured by a grid of surveying nails which were fixed to the ground surface. The earth pressure was measured via Gloetzl total

pressure cells which were buried in both the Caen silt and the SNEC sand.

Pipe displacement was monitored by conducting an optical survey of vertical rods which were welded to the crown of the pipe. The vertical rods were 0.5 m in length and they were installed at intervals of 0.5 m along the length of pipe. The strain gauges mounted on the pipe were used to record the strain in the pipeline at important locations and these strains were used to compute the stresses in the pipeline.

6.4 Finite Element Modelling

The methodologies described in the previous chapters were used to carry out exercises in computational modelling of the experiments conducted at the Caen test facility. The finite element discretization of the soil mass in test basin measuring 18 m × 8 m × 1.75 m is shown in Figure 6.3. A total of 3360 continuum elements and 24 beam elements were used in the computation.

Properties of soils and pipeline used in the computational modelling are given as follows:

(1) Caen silt

The Geotechnical Science Laboratory at Carleton University conducted a series of laboratory tests of Caen silt samples. The measured thermal conductivity and heat capacity at 5 ^0C were 1.97 $[Wm^{-1}(^0C^{-1})]$ and 2.72 $[MJm^{-3}(^0C^{-1})]$ respectively. The unfrozen water at -1^0C is about 18% by volume.

The coefficients of permeability of Caen silt were determined with a specially devised frost heave cell (Wood and Williams, 1985). The relationships between the coefficient of permeability and temperature were generalized as (Shen and Ladanyi, 1991)

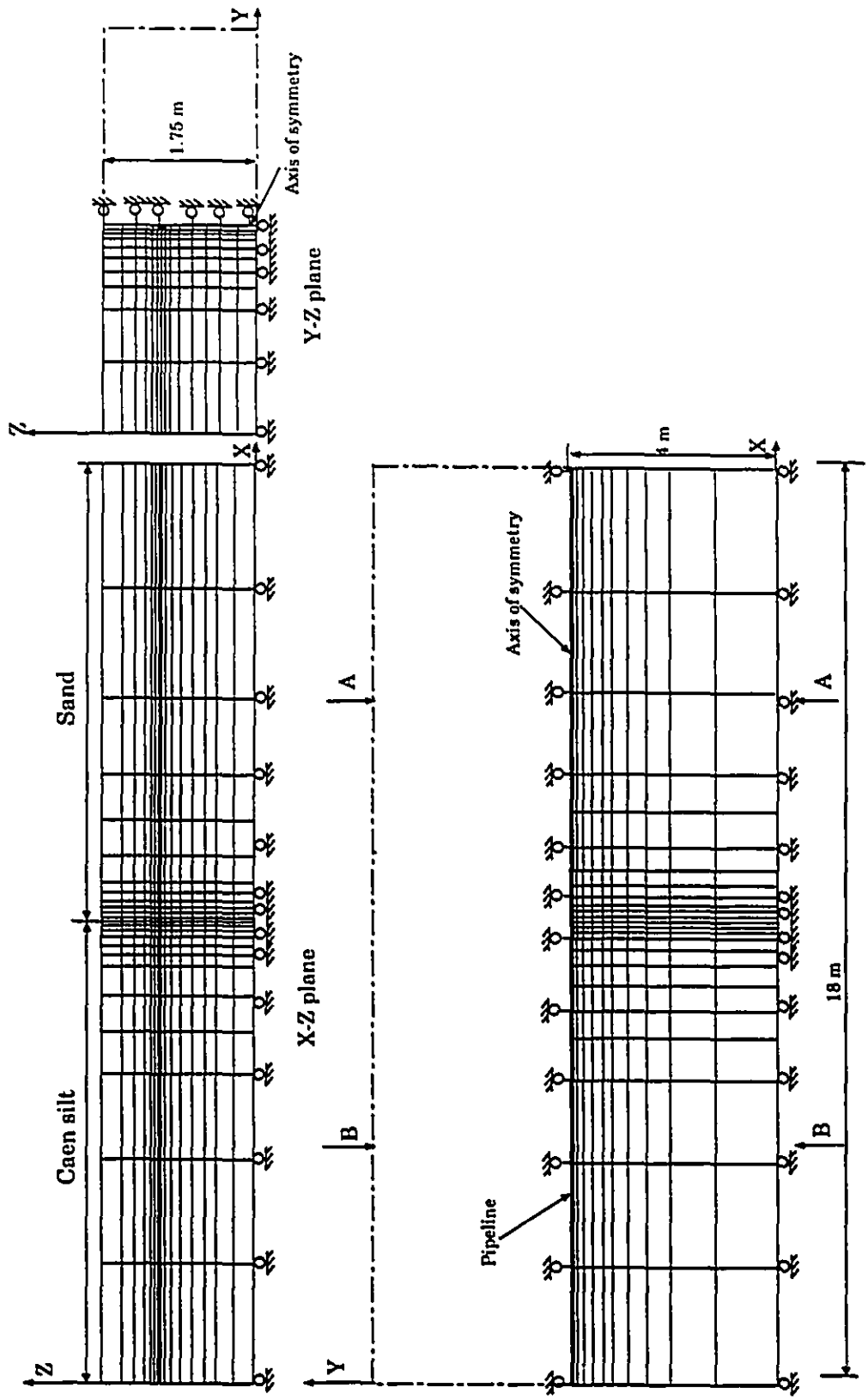

Figure 6.3 Finite element discretization of soil-pipeline system: with beam elements

$$k = \begin{cases} 1.075 \times 10^{-9} e^{23.39T} & -0.3^0C < T < T_f; \\ 8.0499 \times 10^{-13} & T \leq -0.3^0C \end{cases} \quad m/sec \tag{6.1}$$

Young's modulus of unfrozen silt was taken as 11.2 MPa. In general, Young's modulus of frozen Caen silt was considered to be a function of temperatures below the freezing point. In the following modelling, the temperature-dependent Young's modulus of the frozen Caen silt was accounted for by utilizing the relationship (Shen and Ladanyi, 1991)

$$E = 13.75(\frac{T}{T_r})^{1.18} \quad (MPa) \tag{6.2}$$

where T_r $(= -1^oC)$ is the reference temperature.

The unit weight of the Caen silt was taken as 15 kN/m^3. The initial moisture content was 40% .

(1) SNEC sand

The thermal conductivity and heat capacity of the sand were taken as 2.5 $[Wm^{-1}(^0C^{-1})]$ and and 2.5 $[MJm^{-3}(^0C^{-1})]$ respectively according to Harlan and Nixon (1978). The unfrozen permeability of the sand was determined as 1.5×10^{-5} m/s at a test density of 1.9×10^3 kg/m^3 (Dallimore, 1985). The experiment also indicated that the unfrozen water content drops off sharply below 0^0C and the permeability below freezing temperature is very low. Young's modulus of unfrozen sand was taken as 20 MPa. The temperature-dependent Young's modulus of the frozen SNEC sand was assumed in the form

$$E = 24.75(\frac{T}{T_r})^{1.18} \quad (MPa) \tag{6.3}$$

The unit weight of the SNEC sand was taken as 19 kN/m^3. Poisson's ratios for all soils were set equal to 0.3.

(3) Pipeline

Young's modulus of the steel pipeline was taken as 200 GPa and Poisson's ratio was set to 0.3. The moment of inertia of the pipeline I was $3.688 \times 10^{-5}\ m^4$ (Shen, 1991). Therefore the flexural rigidity of the pipeline EI used in the computation was 7750 $kN\ m^2$. The coefficient of thermal expansion was 0.00012 $/^0C$.

The computational modelling incorporated the complete creep models which were developed is Chapter 3. The creep parameters of frozen soils at all stages are referred to Table 3.2.

6.5 Numerical Modelling of First Stage of Test

In this stage of the experimentation, the Caen silt and the SNEC sand were maintained in an initially unfrozen condition. As mentioned previously, this stage consisted of four freezing periods. The duration of the first freezing period was approximately 8.5 months from September 21, 1982 to June 8, 1983. The air temperature in the hall was maintained at -0.75^0C and pipe temperature was maintained at -2^0C. After a four month thawing period, which took place immediately after the first freezing period, the second freezing period began on October 17, 1983. In the second freezing period, the temperature of the pipe was reduced to -5^0C and maintained for a longer duration. All other operating conditions in the second period were identical to the first one. The second period lasted about 450 days. Since extensive experimental data were documented for the second freezing period (Dallimore, 1985), this period was selected for numerical modelling.

6.5.1 Temperature profiles

Before the initiation of the second freezing period, the ambient air temperature in the hall was raised to $+4^0C$ and was maintained at this temperature for 4 months. It was observed that nearly all of the annulus of frozen soil formed during the first freezing period had thawed.

The second freezing period began by lowering the air temperature to -0.75^0C and circulating gas temperature in the pipeline at -5^0C. A moving freezing front was formed by the combination of the freezing effects due to ambient air temperature and the advance of a freezing front from cooling due to the pipeline. The experimental results for the time-dependent evolutions of the frozen zone along sections of the silt and the sand are shown in Figure 6.4. These results indicate that the development of the freezing front in the sand was comparatively larger than that in the silt. This can be attributed to the higher thermal conductivity and lower heat capacity of the sand.

Figure 6.5 illustrates the temperature contours obtained from the computation modelling at section B-B (silt) for lapsed times of 21, 105 and 378 days. Figure 6.6 illustrates the computational estimation for temperature contours at section A-A (sand) for duration of 21, 105 and 378 days.

The computational results of evolution of frost bulb around the pipeline in the sand and silt, derived from Figures 6.5 and 6.6, are illustrated in Figure 6.7. The Figures 6.4 and 6.7 indicate that the contours obtained from the computational model correlate well with equivalent results obtained from the experiment. Figure 6.8 compares the frost penetration beneath the centreline of pipeline measured in the Caen pipeline test with results obtained from the computational model. There is good correlation between the experimental and computational results for both silt and

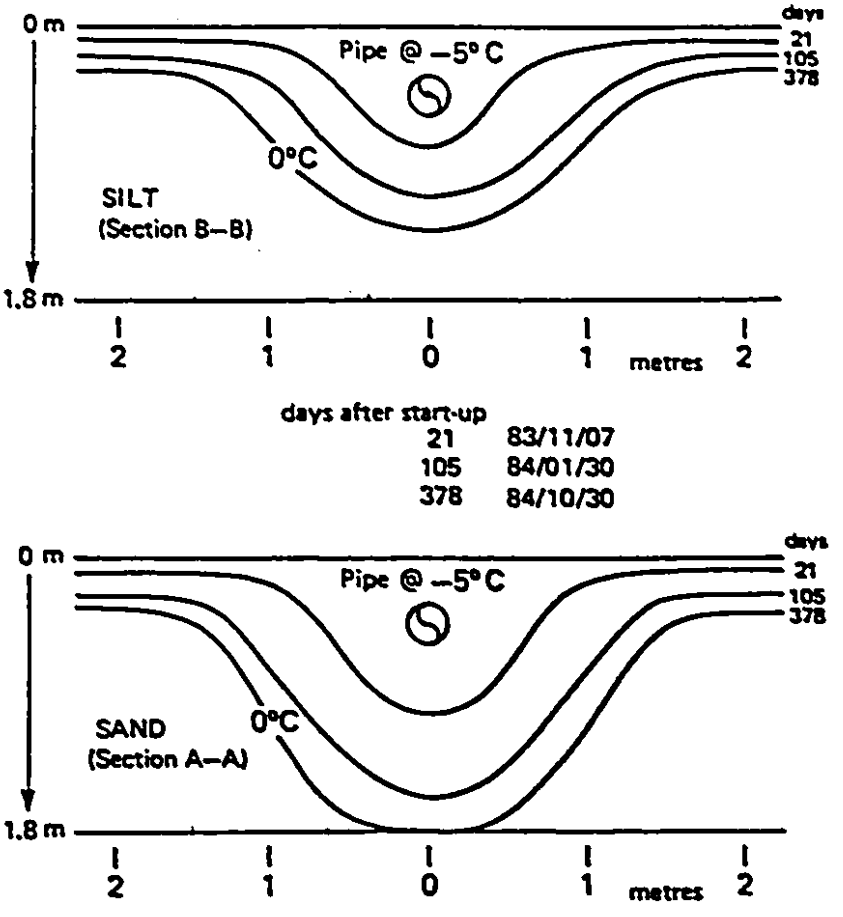

Figure 6.4: Evolution of frozen zone around pipeline in sand and silt (after Dallimore, 1985)

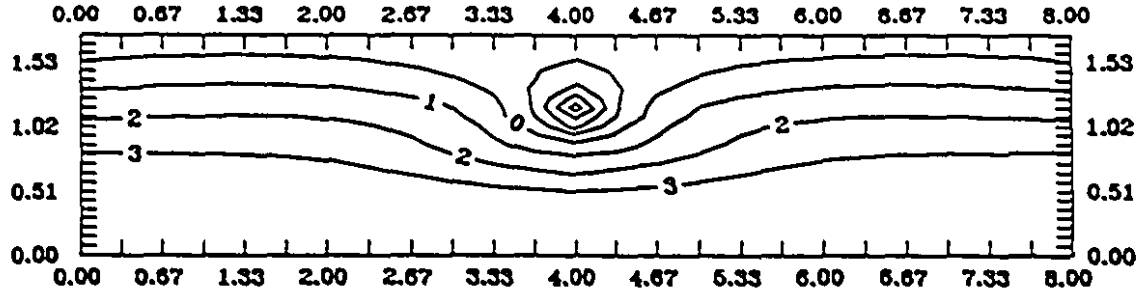

(a) At 21 days

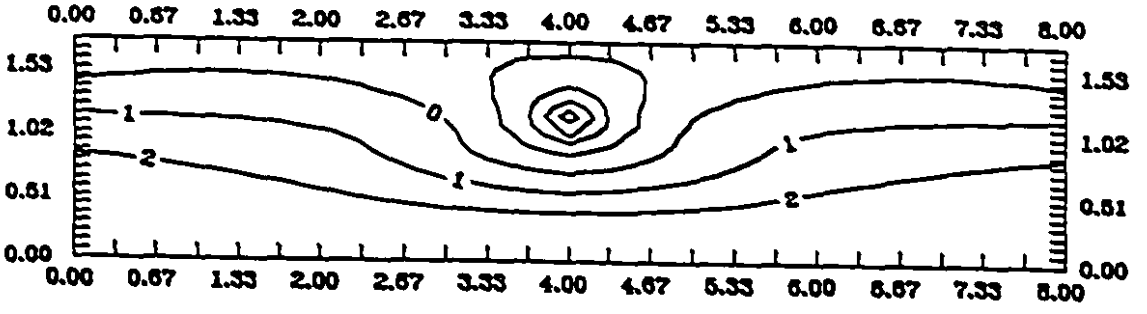

(b) at 105 days

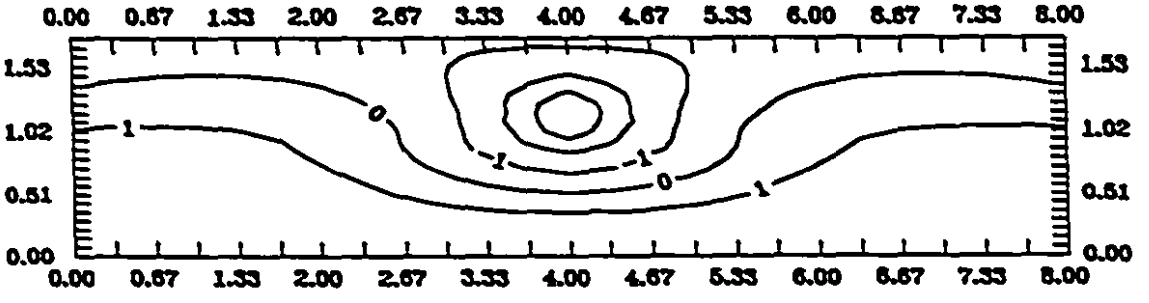

(b) at 378 days

Figure 6.5: Temperature profile (^0C) at section B-B (silt)

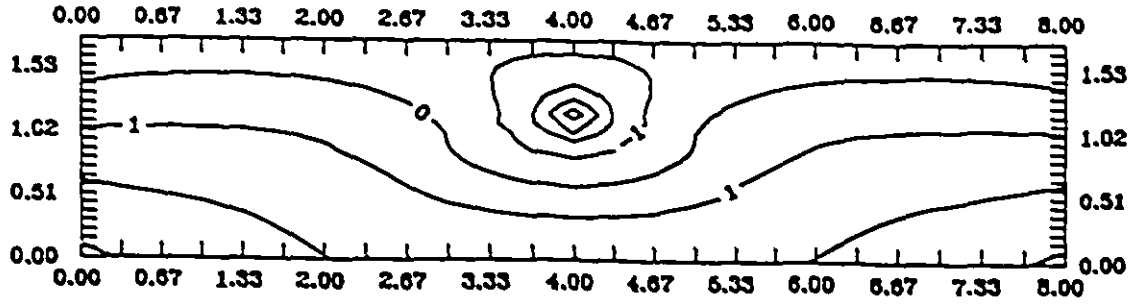

(a) At 21 days

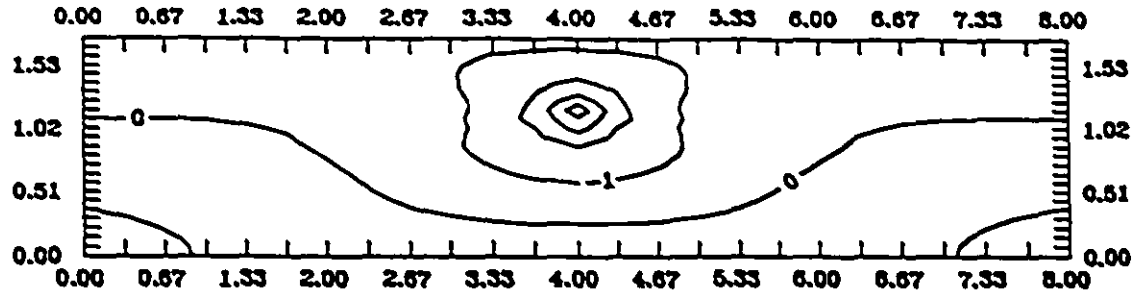

(b) at 105 days

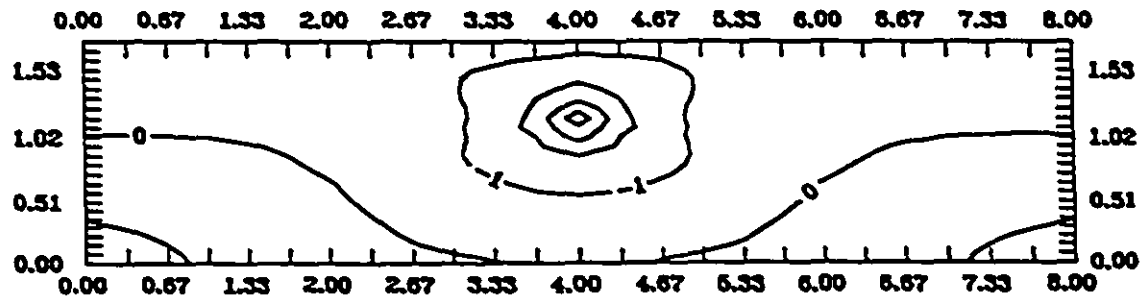

(b) at 378 days

Figure 6.6: Temperature profile (^0C) at section A-A (sand)

sand.

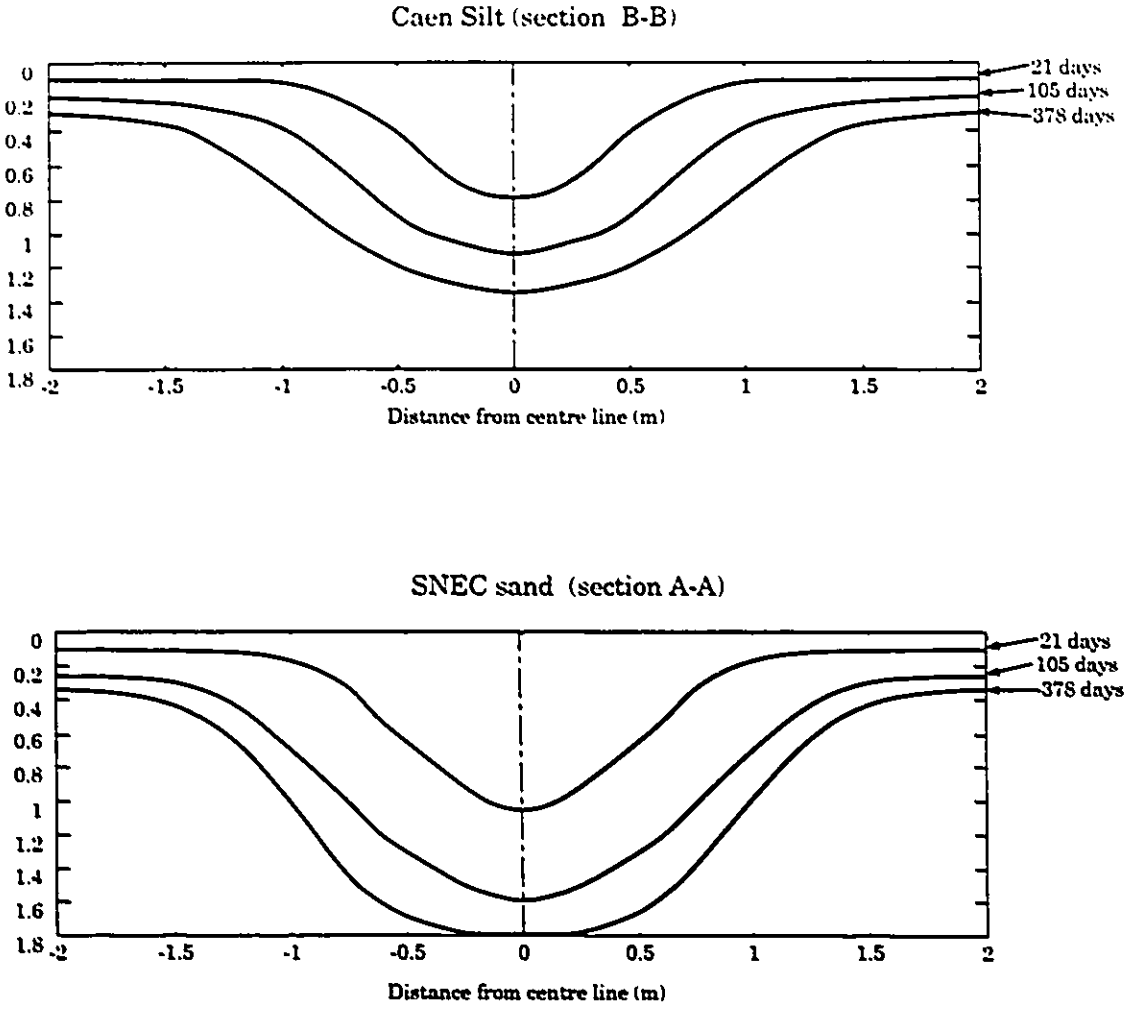

Figure 6.7: Computational modelling of evolution of frozen zone around pipeline

6.5.2 Development of frost heave

Figure 6.9 illustrates the experimental results for the surface heave of the silt and the sand after 227 days from the initiation of second freezing period. It is evident that substantial frost heave, up to 160 mm at surface occurred in the silt during this period. In contrast the SNEC sand experienced relatively small frost heave.

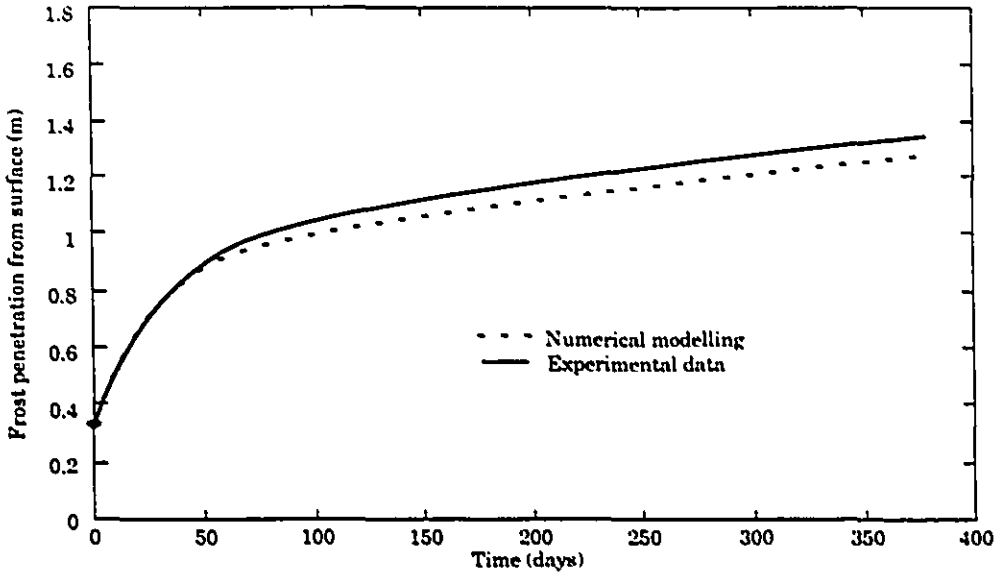

Silt (section A-A)

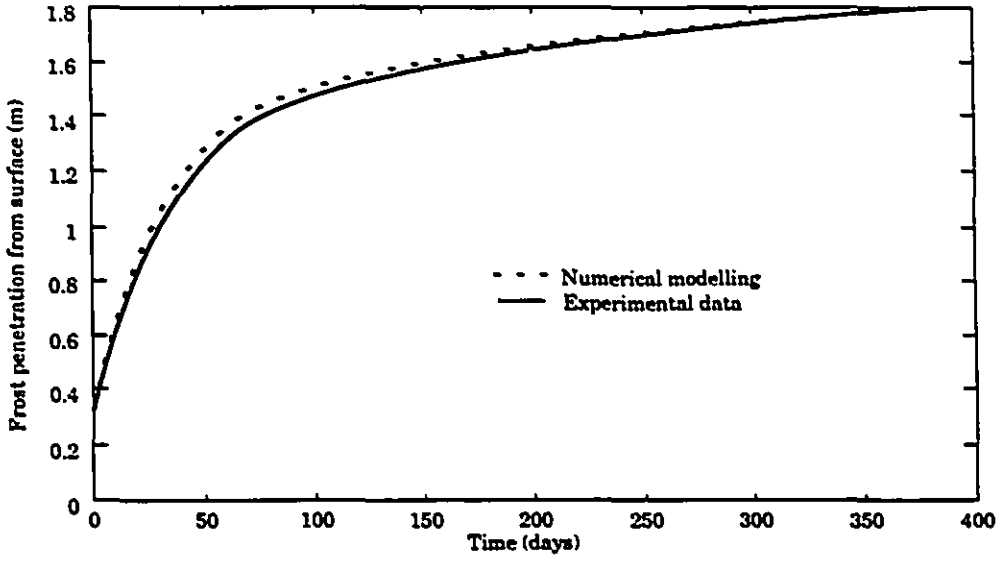

Sand (section B-B)

Figure 6.8: Frost penetration beneath the pipeline at Caen test facility

Equivalent results for the pattern of frost heave development in both soils were determined from the computational modelling are shown in Figure 6.10. It was also convenient to illustrate the results from the computational estimation in a three-dimensional fashion. Such results are shown in Figure 6.11.

Both the experimental results and computational estimates indicate that in all soils (the Caen silt and the SNEC sand) the frost heave was concentrated along the axis of the buried pipeline. Figure 6.12 compares the cumulative frost heave curves at section B-B (silt) and section A-A (sand) derived from the experiment with equivalent results obtained from the computational modelling. It is observed that a reasonable prediction was obtained for frost heave curves both in silt and in sand.

6.5.3 Displacement of pipeline

In the Caen pipeline test, the vertical displacement of the pipe was measured by direct observations of the movement of vertical rods welded to the crown of the pipeline. The distribution of longitudinal displacement shown in Figure 6.13 illustrates that the section of the pipeline buried in the highly frost susceptible Caen silt had undergone considerably larger displacements than the section of the pipeline buried in SNEC sand. The displacement of the pipeline in the transition zone was substantially reduced due to the restraint provided by the frozen sand. Figure 6.14 illustrates the corresponding displacements of the pipeline developed from the computational model. From Figure 6.13 and Figure 6.14, it is clear that the computational methodologies can predict reasonably accurately both the pattern and magnitude of the pipeline displacements.

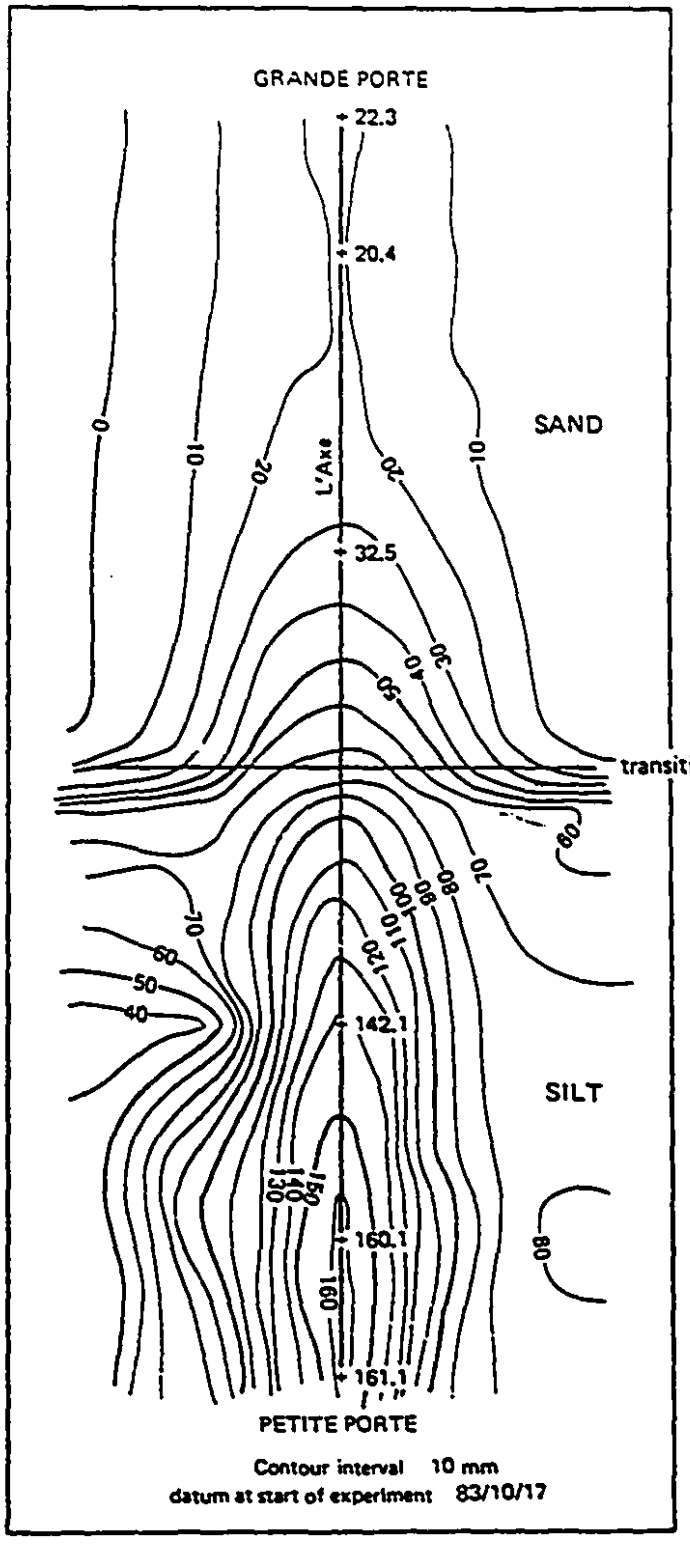

Figure 6.9: Experimental results for frost heave contours after 227 days of freezing (after Dallimore, 1985)

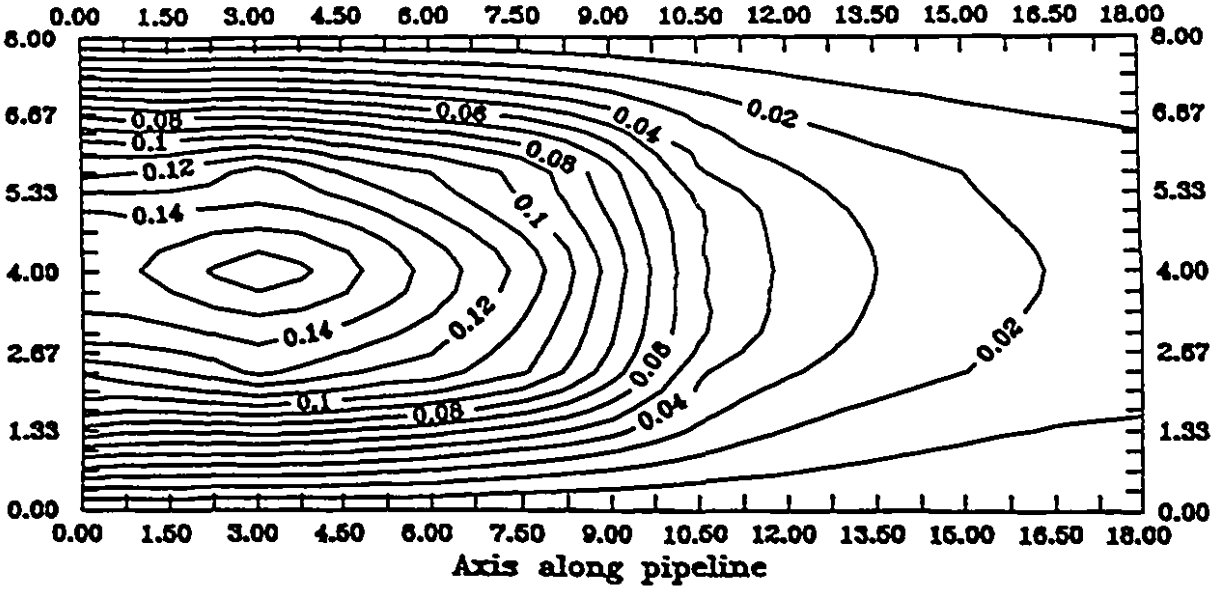

Figure 6.10: Computational estimates for frost heave development after 227 days of freezing

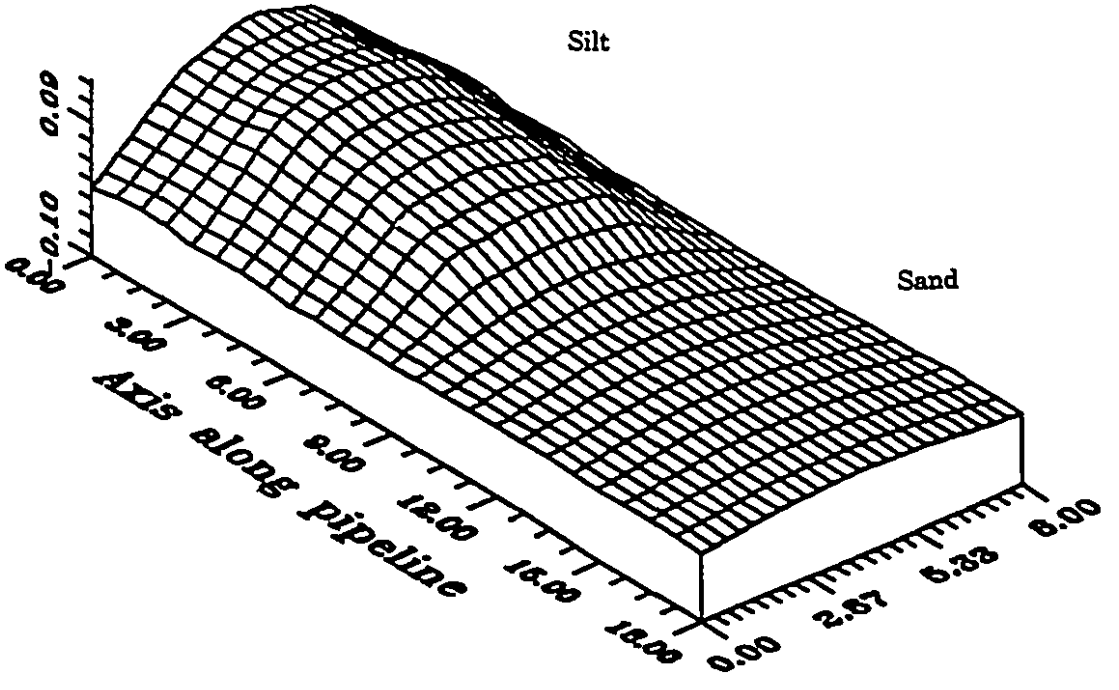

Figure 6.11: Computational estimates for frost heave development after 227 days of freezing: isometric view, maximum heave = 0.165 m

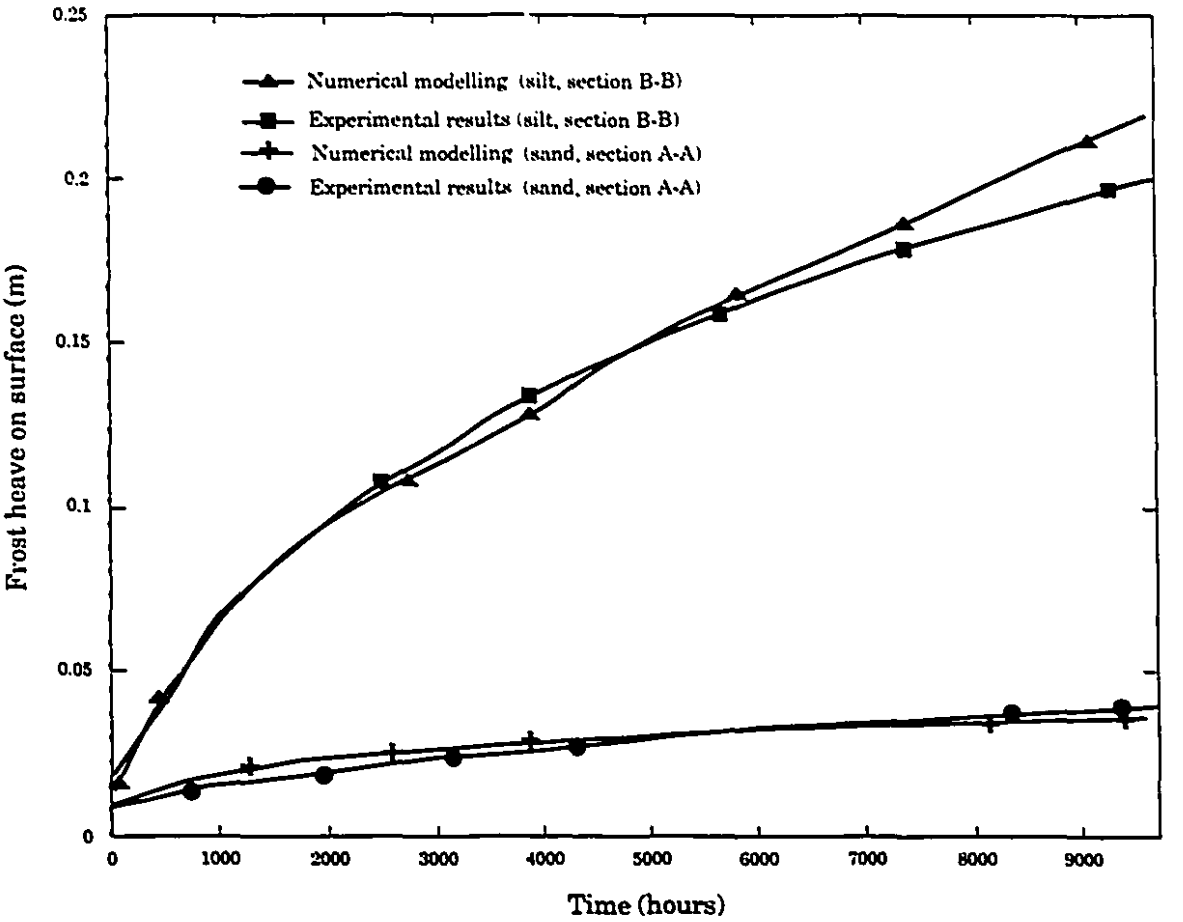

Figure 6.12: Time-dependent variation in cumulative frost heave of the soil surface

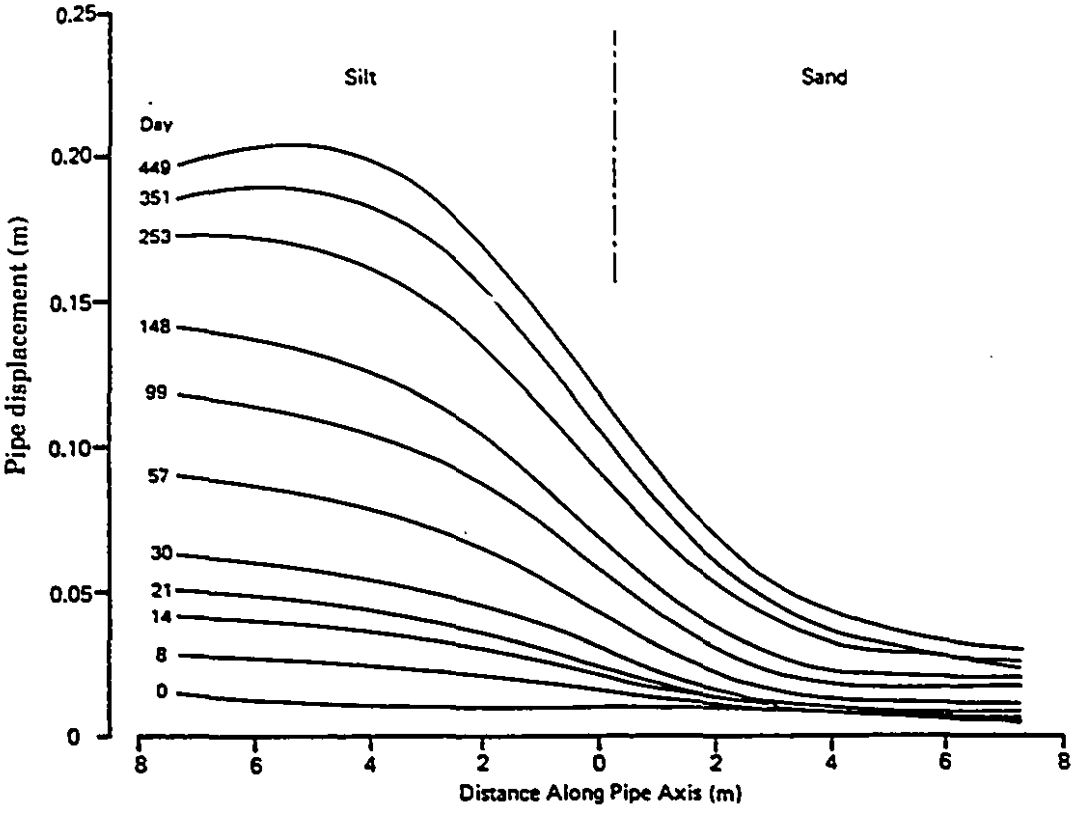

Figure 6.13: Displacement of the pipeline in the Caen experiment (after Dallimore, 1985)

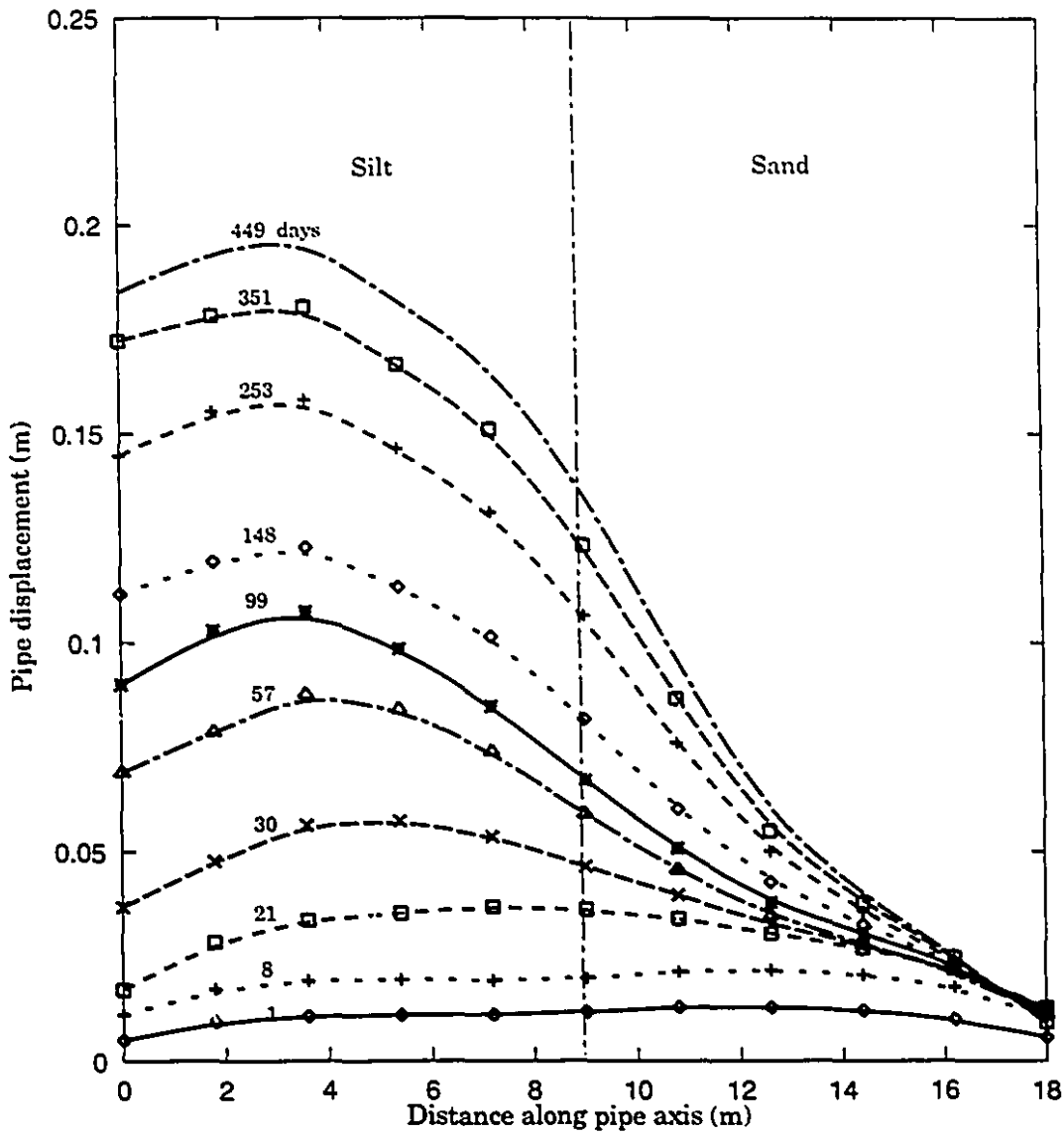

Figure 6.14: Pipeline displacement derived via the computational model: freezing induced by ambient cooling and pipeline cooling

6.5.4 Stresses in pipeline

Non-uniform displacement of a pipeline can induce large stresses in the pipeline located in the transition zone. The induced stresses were measured by strain gauges. Figure 6.15 shows the experimental results for the variation of bending stresses developed in the pipeline axis. In the numerical modelling, the pipeline was modelled by 24 beam elements which possessed flexural, axial, shear and torsional stiffness. The results for the bending stresses along the pipeline developed via the numerical modelling are shown in Figure 6.16. By comparing Figures 6.15 and 6.16, the satisfactory order of maximum bending stresses along the axis of the pipeline by computational modelling was obtained.

The computational modelling was also conducted for the two types of behaviour of the frozen soils. These included (i) no creep effects; (ii) purely primary creep. The cumulative frost heave curves from the above two models are compared with the curves obtained using the complete creep model in Figure 6.17. It is observed that the cumulative frost heave curve which incorporates the complete creep model gives the largest value of frost heave. Figures 6.18 shows time-dependent development of bending moments for the case where the frozen soil exhibits no creep effects. The stress distribution can be compared with the distribution for bending stresses derived from the Caen experiment. The comparison at salient points can be summarized as follows:

$$\left\{\frac{[M_{max}(445\ days)]_{no\ creep}}{[M_{max}(445\ days)]_{experimental}}\right\}_{initial\ frozen\ silt} = 0.901 \qquad (6.4)$$

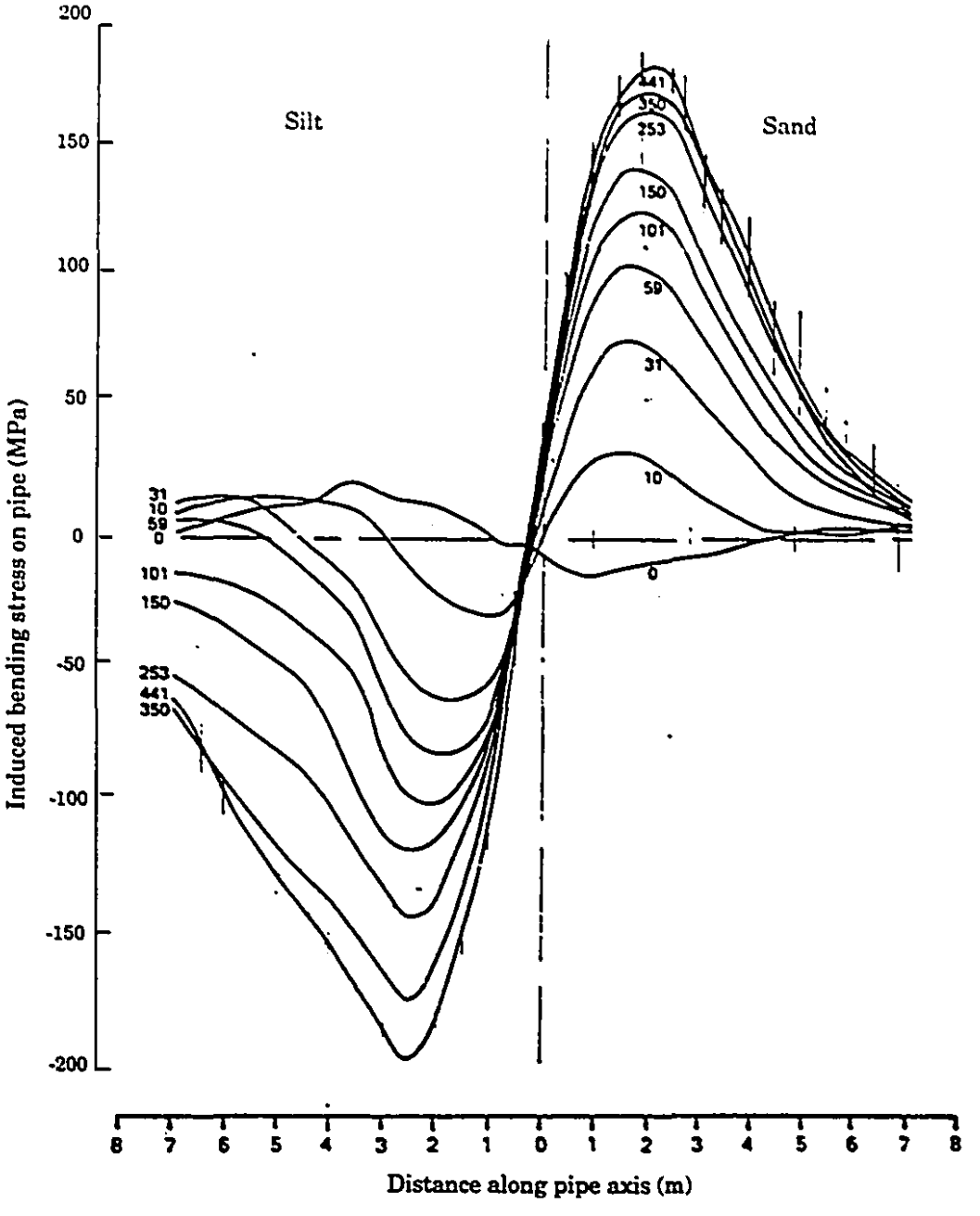

Figure 6.15: Distribution of bending stress and pipe strain (after Dallimore, 1985)

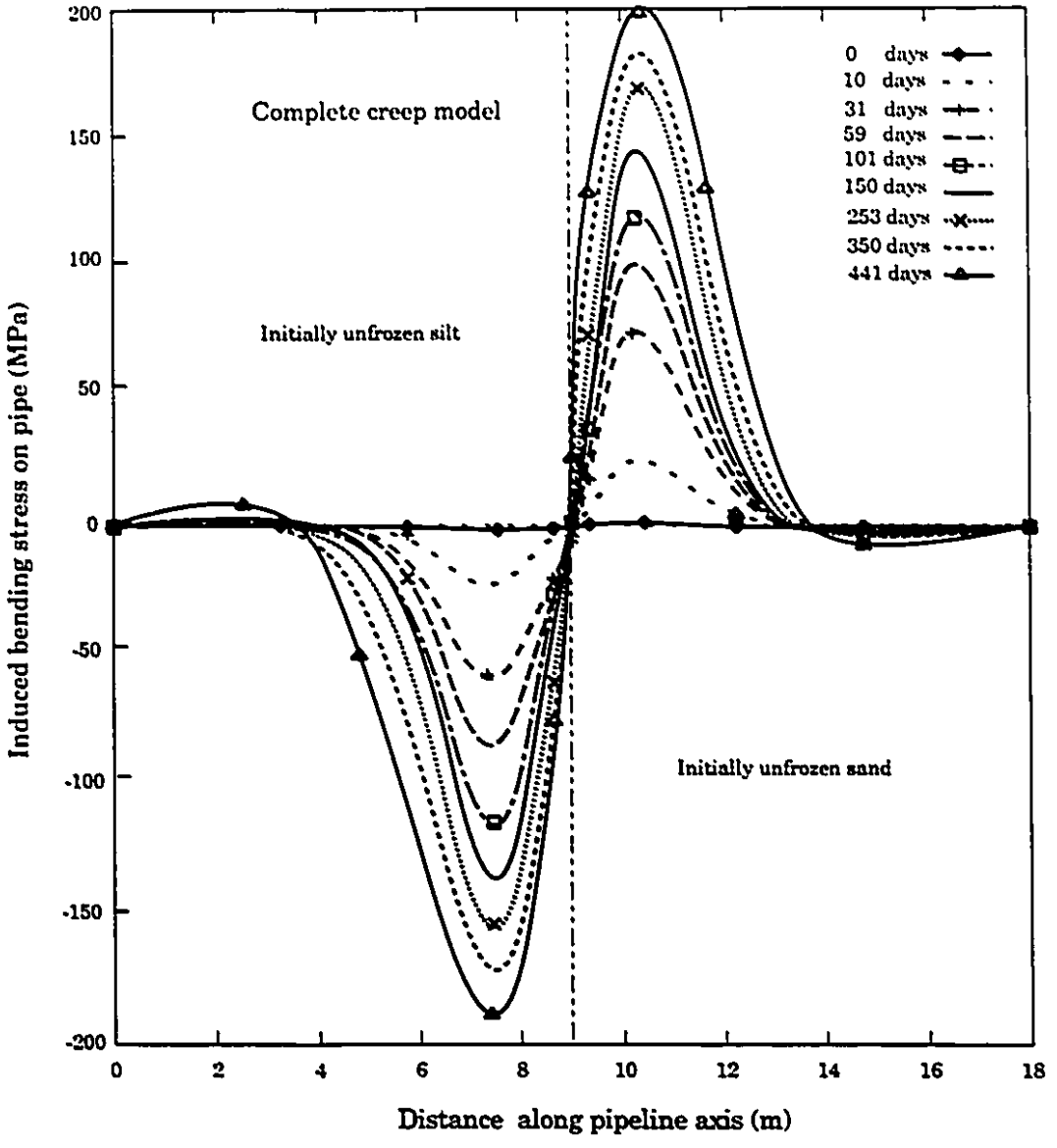

Figure 6.16: Variation of bending stresses along pipeline derived from the computational model: complete creep effects

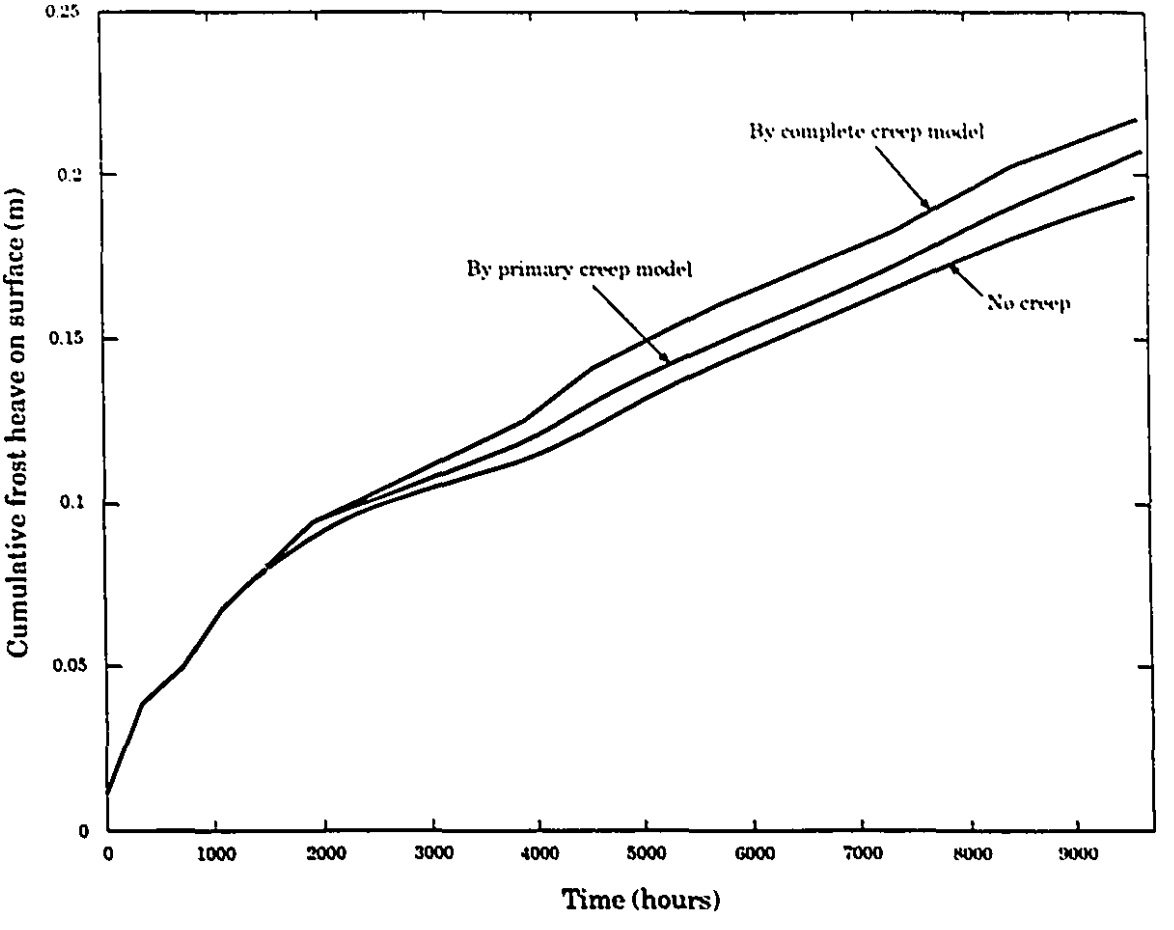

Figure 6.17: Time-dependent variation of frost heave at the surface of Caen silt

6.5.5 Range of bending stresses along pipeline

In order to examine the sensitivity of the frost heave induced soil-pipeline interaction to the soil permeability, the value of the permeability as defined by Equation (6.5) is varied by factors N (0.5 and 2.0), ie.

$$k = \begin{cases} 1.075 \times 10^{-9} e^{23.99T} \times N & -0.3^{o}C < T < T_f; \\ 8.0499 \times 10^{-13} \times N & T \leq -0.3^{0}C \end{cases} \quad m/sec \qquad (6.5)$$

Figure (6.19) shows the range of bending stress distribution obtained along the pipeline as a result of the variation in the soil permeability.

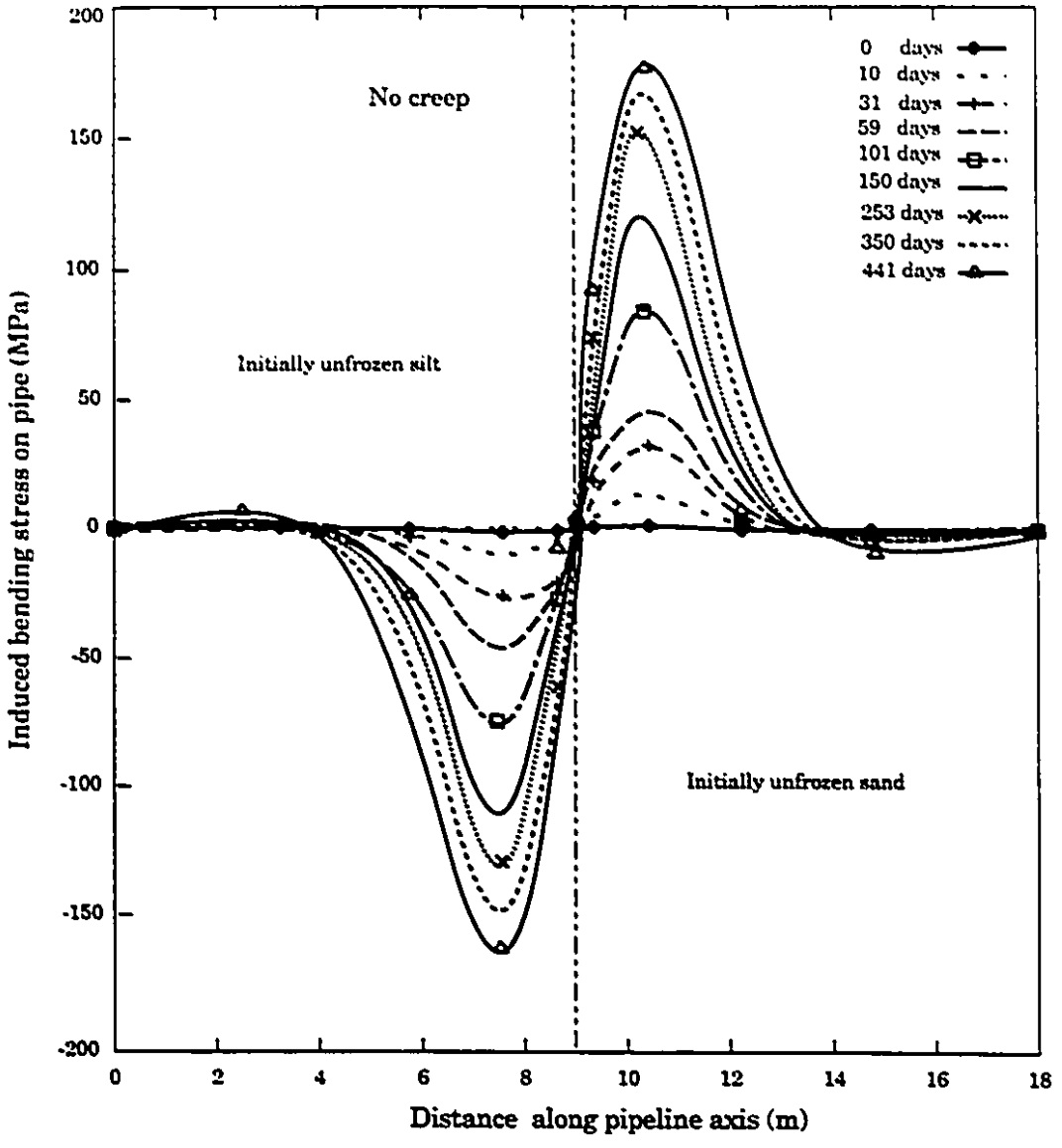

Figure 6.18: Variation of bending stresses along pipeline derived from the computational model: no creep effects

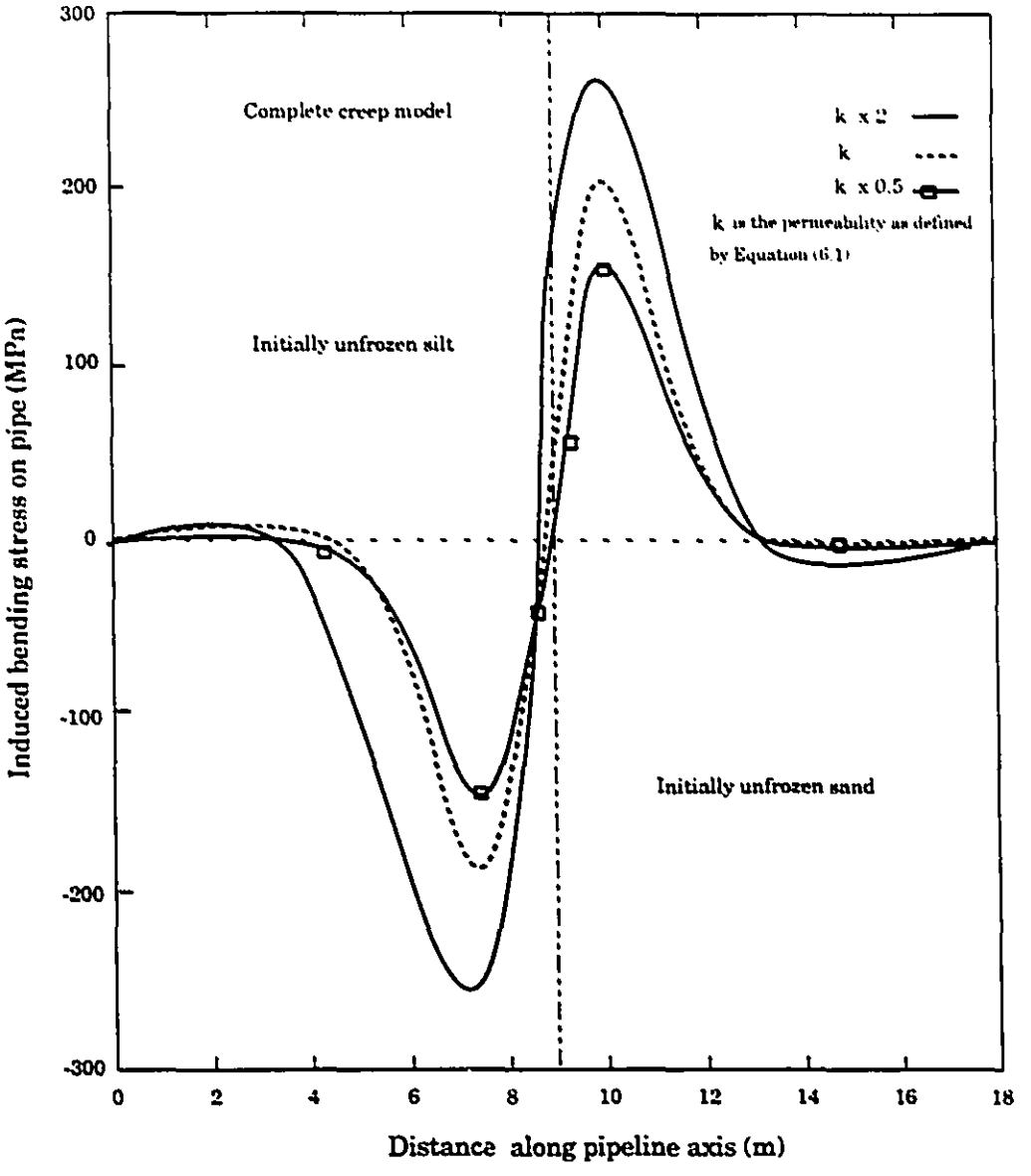

Figure 6.19: Variation of bending stresses along pipeline derived from the computational model: influence of permeabilities

6.6 Numerical Modelling of Secondary Stage of Test

The second stage of the freezing test was carried out at same site from 1990 to 1993. A pipeline was placed crossing a transition zone between the prefrozen soil and the unfrozen highly frost susceptible Caen silt. The test was designed to examine the force that would be exerted on the pipeline which was anchored by the prefrozen soil. In order to allow comparison with the previous experiment, the composition of silt, the size of pipeline, the depth of burial of the pipeline and water table remained unchanged in the second freezing stage.

An insulating thermal wall was constructed to divide the facility and soil into two sections whose temperatures could be controlled separately. Prior to the start of the experiment, the soil on one side of the wall was frozen. The first freezing period was initiated at an ambient air temperature of -0.75^0C and a pipe circulation temperature of -5^0C. This thermal condition was maintained for the first 215 days. From day 215 to day 256, the pipe temperature was lowered to about -8.5^0C. Following that, there was a thawing period and a second freezing period. The numerical computations performed took into consideration only the first freezing period from 0 to 256 days.

Due to the anchoring of the pipeline in prefrozen soil, it was to be expected that the pipeline would experience a smaller displacement and a larger bending moment in the transition zone than in the case where both the Caen silt and the SNEC sand were initially kept unfrozen. Figure 6.20 presents the variation of pipeline displacement with time for the second stage of the freezing test. At 150 days, the maximum pipeline displacement was 0.135 m in the first stage (see Figure 6.14) and 0.116 m in the second stage (Figure 6.20). It may be noted that in the situation where

the pipe was embedded in initially unfrozen soils, the vertical pipeline displacement experienced an upward movement along its entire length (see Figure 6.14). In the case of prefrozen soil test, the pipeline experienced a downward displacement at the prefrozen end (Figure 6.21). Also at 150 days, the maximum bending stress in the pipeline was 135 MPa in first stage (see Figure 6.16) and 150 MPa in the case of the initially prefrozen soil (Figure 6.22).

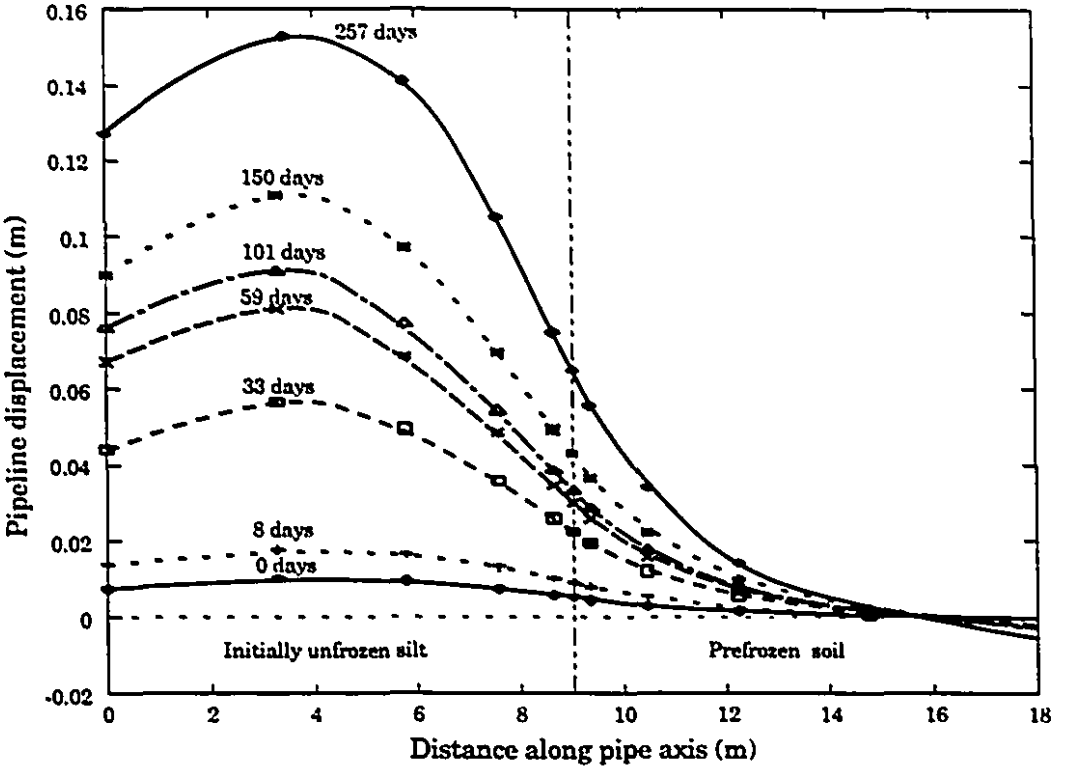

Figure 6.20: Numerical result for the displacement of the pipeline: initially prefrozen soil on one side

From the extensive measurements of surface heave made during this experiment

it was possible to determine the pattern of frost heave development with time across both the prefrozen sand and the silt. Figure 6.23 illustrates the experimental results of the frost heave pattern obtained at 246 days. Similar results can also be derived from the computational modelling. Figure 6.24 illustrates the surface heave pattern obtained from the computational modelling. The frost heave contours determined from the computational modelling are shown in Figure 6.25.

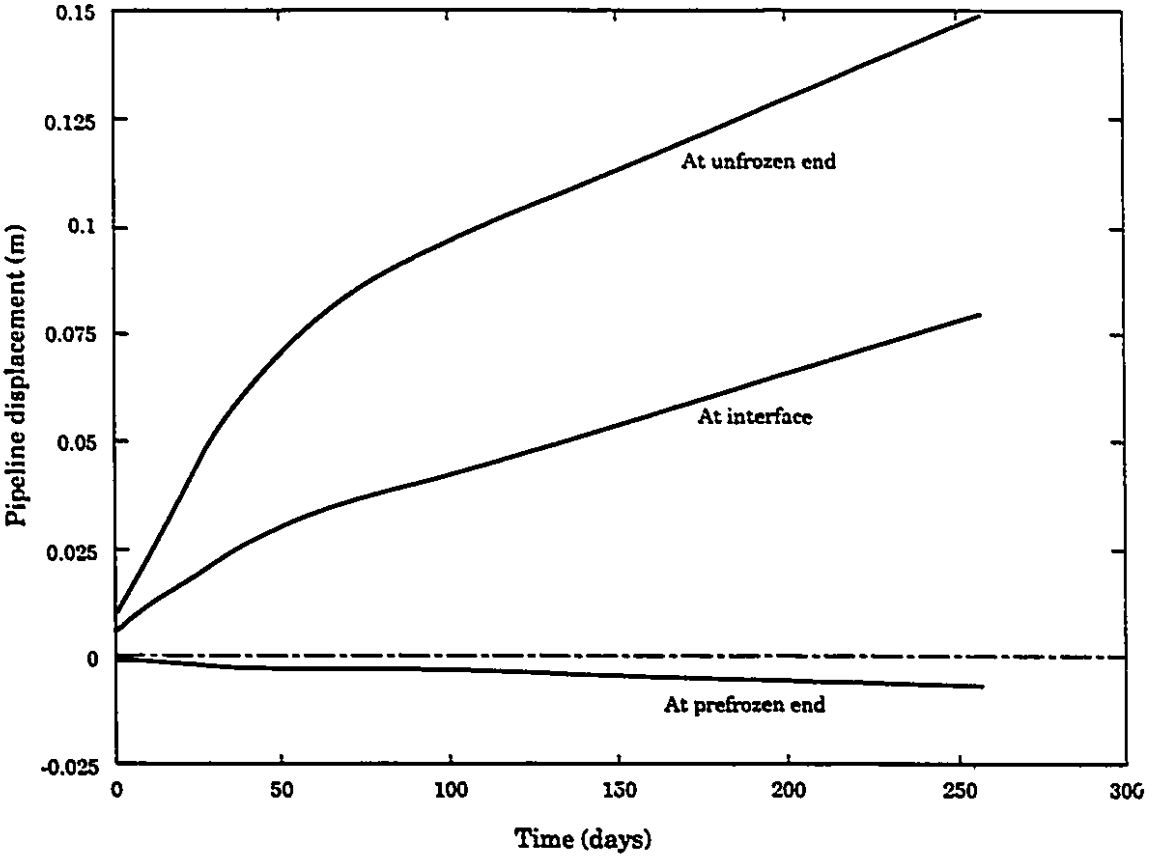

Figure 6.21: Variation of pipeline displacement with time: initially pre-frozen soil on one side

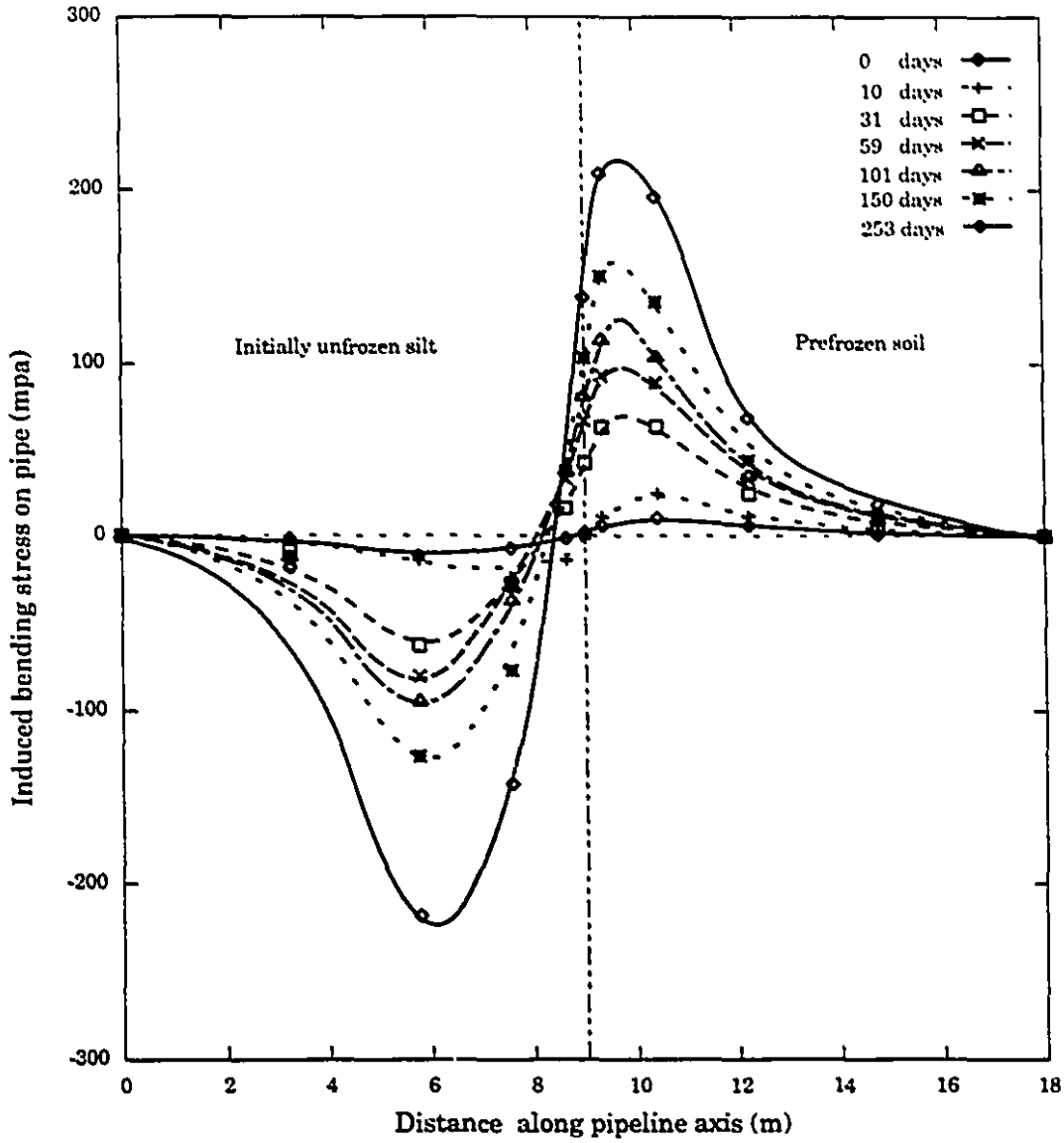

Figure 6.22: Numerical results for the variation of bending stresses along pipeline: initially prefrozen soil on one side

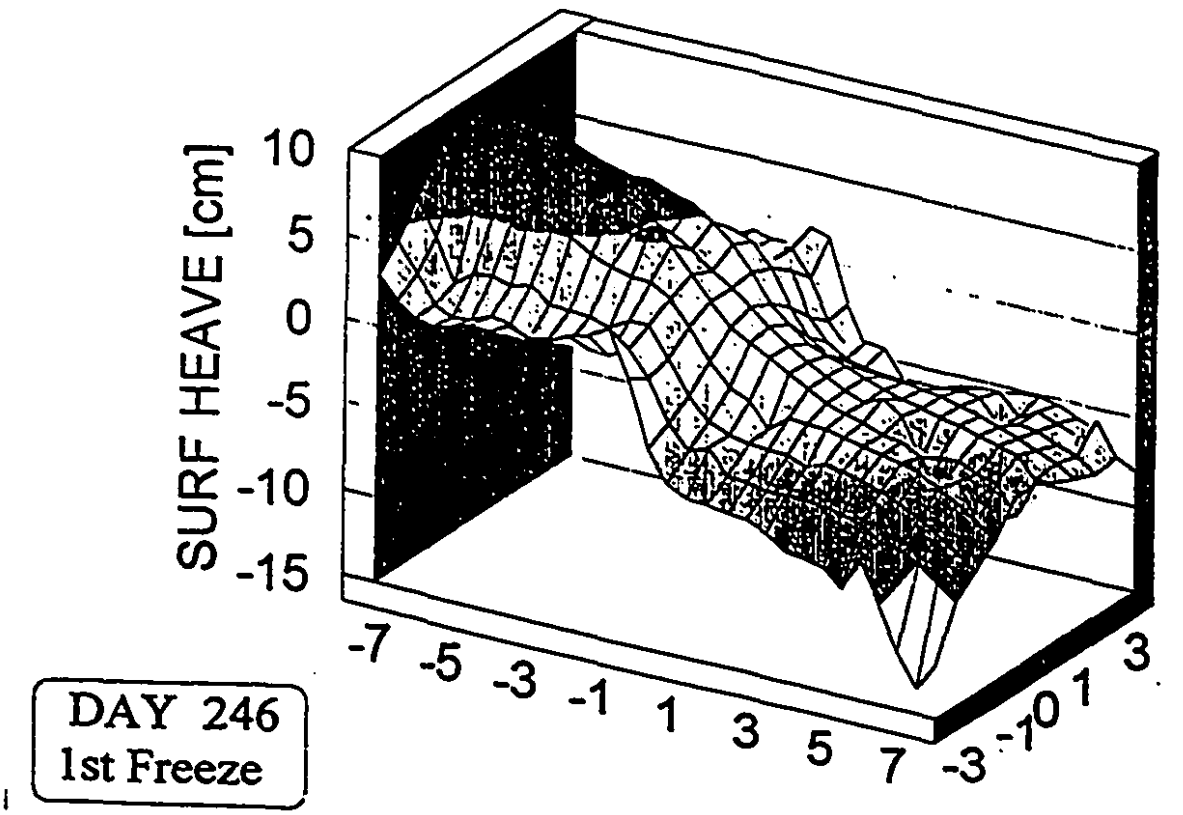

Figure 6.23: Experimental results for heave of the soil surface: initially prefrozen soil on one side (National Energy Board report, 1994)

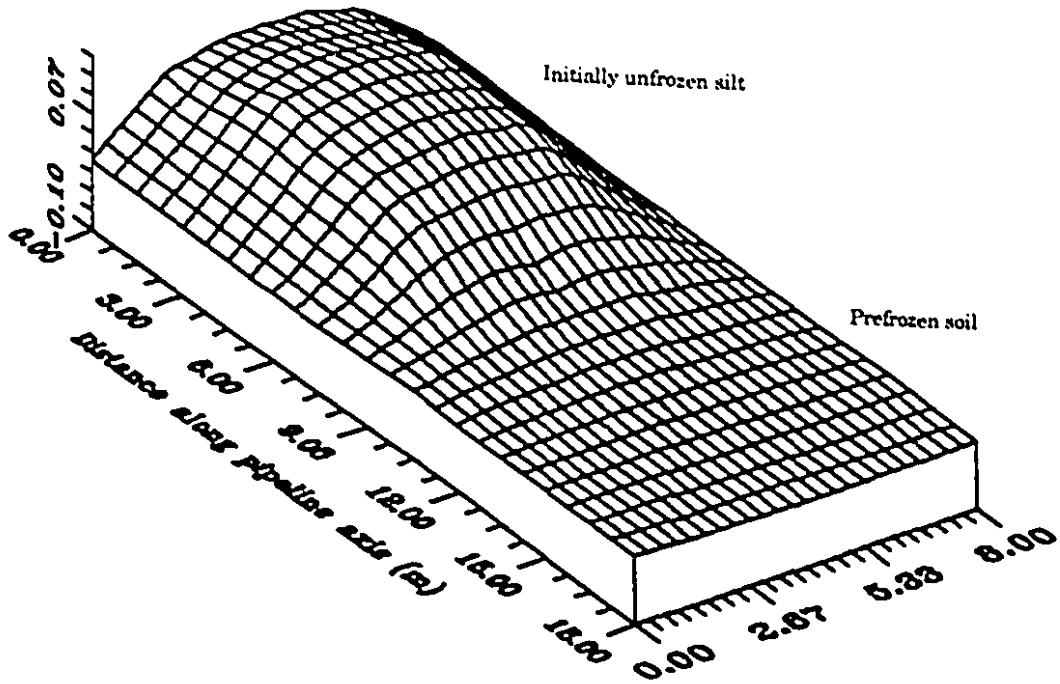

Figure 6.24: Computational results for the heave of the soil surface at 246 days: initially prefrozen soil on one side, maximum heave = 0.152 m

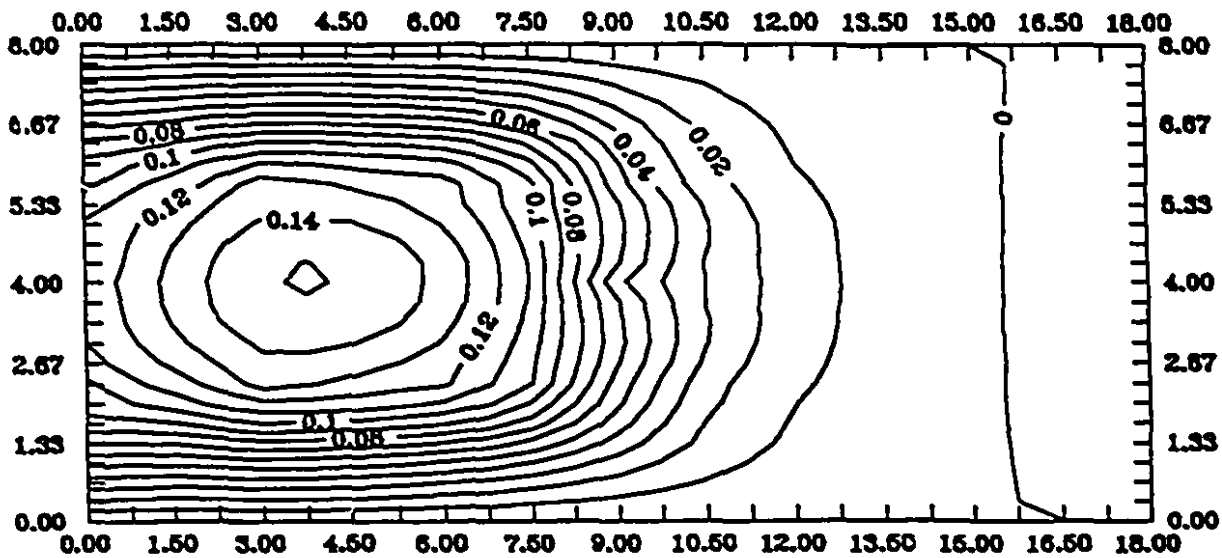

Figure 6.25: Frost heave contours at 246 days: initially prefrozen soil on one side

6.7 Modelling of Soil-Pipeline Interaction Induced by Pipeline Subjected to Cooling

We now consider a problem of the soils where the freezing is induced only by the cooling temperature -5^0C in the embedded pipeline which intersects the frost susceptible Caen silt and the SNEC sand. Both soils are initially unfrozen and air temperature is maintained at $+4\ ^0C$. This is a hypothetical problem which has not been examined in the Caen pipeline experiment.

Figures 6.26 illustrates the temperature contours in Caen silt section B-B at 21, 105 and 378 days respectively. The temperature contours in SNEC sand section A-A at 21, 105 and 378 days are illustrated in Figures 6.27. It can be observed that the freezing front advances nearly radially from the pipeline for both sand and silt, which indicates that the moving freezing fronts follow closely with the thermal boundary conditions.

The frost heave pattern obtained from the computational modelling is shown in Figures 6.28. The frost heave contours determined from the computational modelling are shown in Figure 6.29. It is evident that the magnitude of the frost heave is substantially smaller than for the cases where cooling from both soil surface and pipeline.

From the results given in Figures 6.30, it is evident that when freezing was only from the pipeline, the induced pipeline displacement was reduced to half of the maximum displacement that was associated with both ambient and pipeline cooling (see Figure 6.14). The maximum bending moment in Figure 6.31 was also reduced to about half of the values given in Figure 6.16.

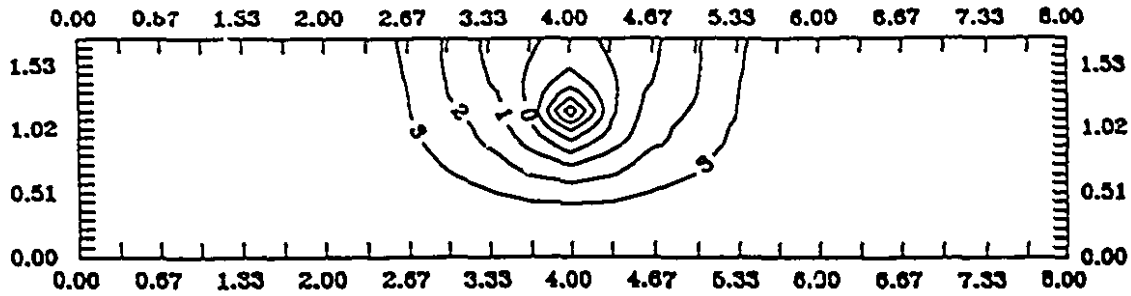

(a) At 21 days

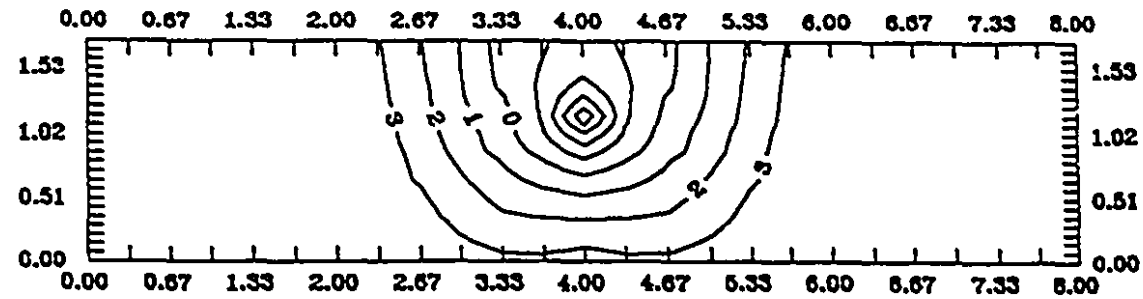

(b) at 105 days

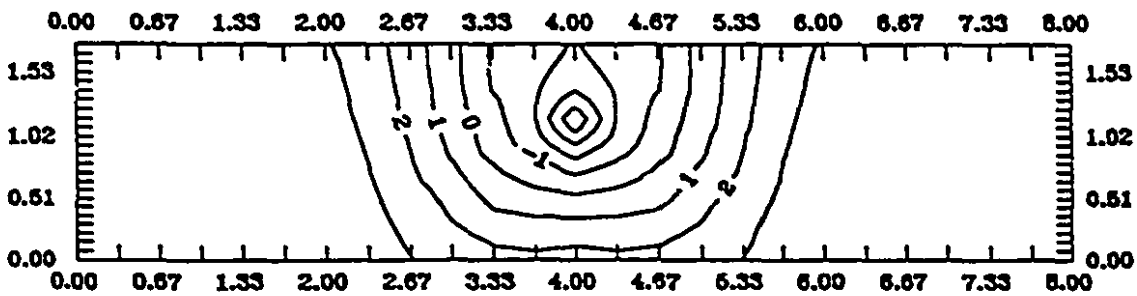

(b) at 378 days

Figure 6.26: Temperature contours (^{o}C) at section B-B (silt) for the case where cooling is induced only from pipeline

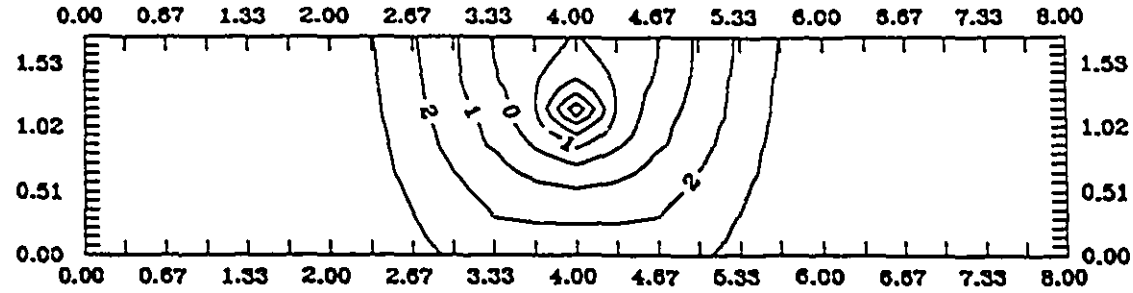

(a) At 21 days

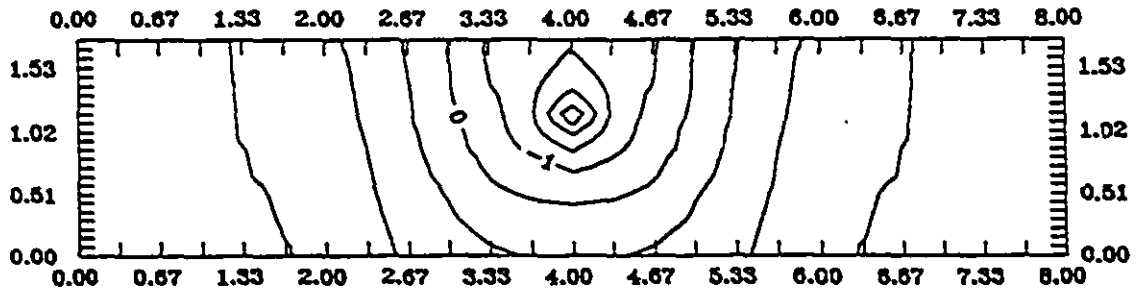

(b) at 105 days

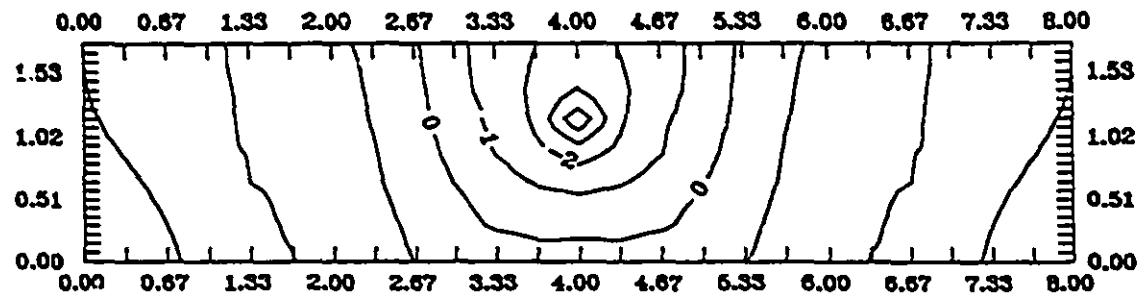

(b) at 378 days

Figure 6.27: Temperature contours (^0C) at section A-A (sand) for the case where cooling is induced only from pipeline

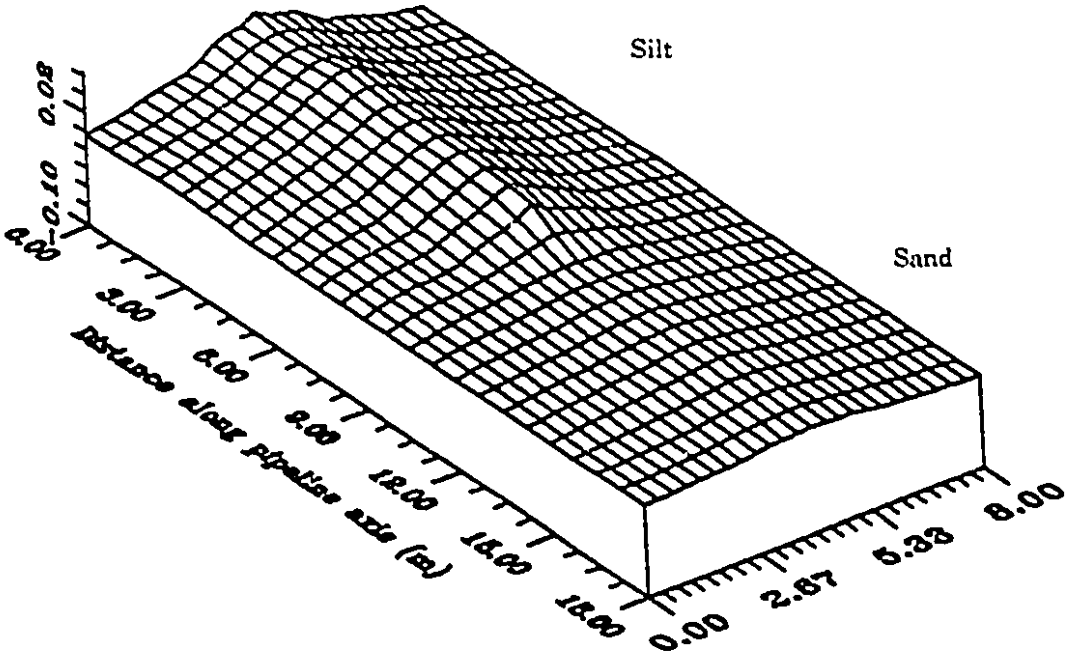

Figure 6.28: Computational results for the heave of the soil surface after 227 days of freezing: cooling is induced only from the pipeline, maximum heave = 0.075 m

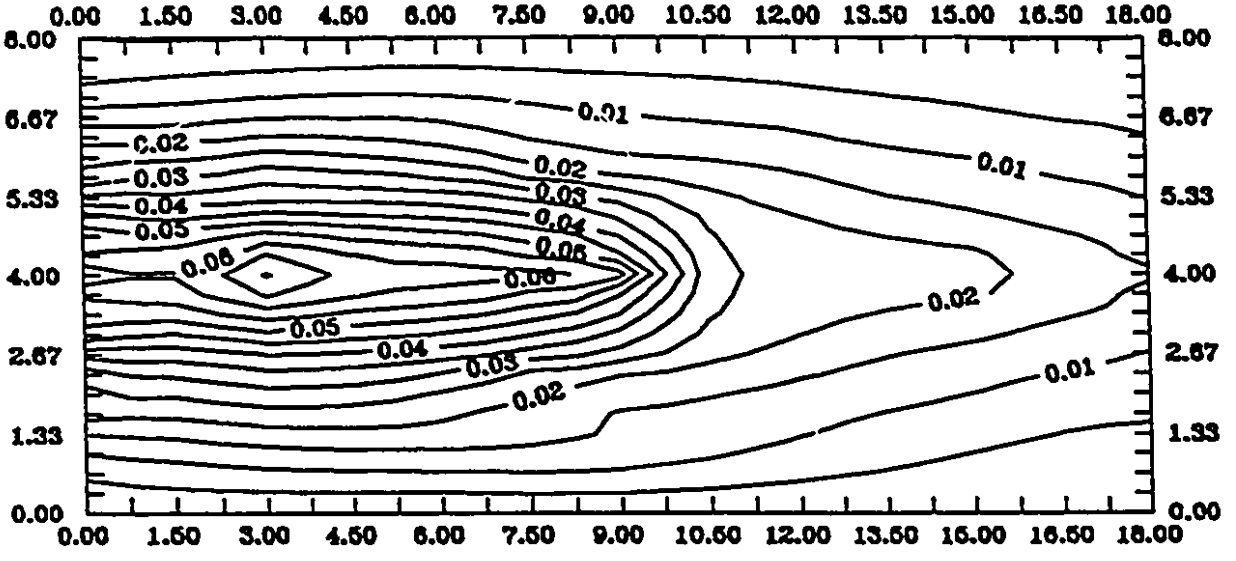

Figure 6.29: Contours of surface heave after 227 days of freezing: cooling is induced only from the pipeline

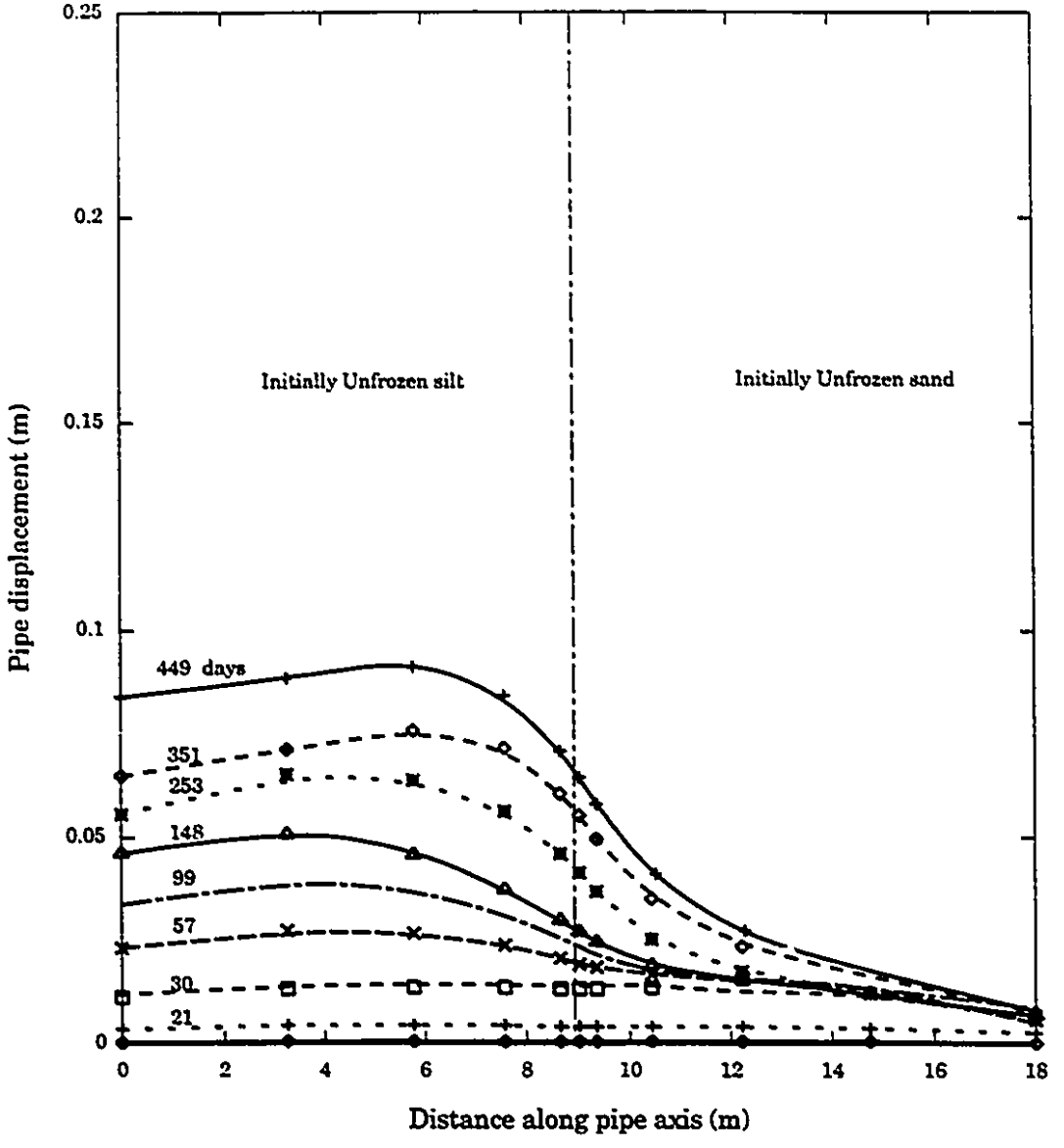

Figure 6.30: Pipeline displacements derived from the computational model: cooling is induced only from the pipeline

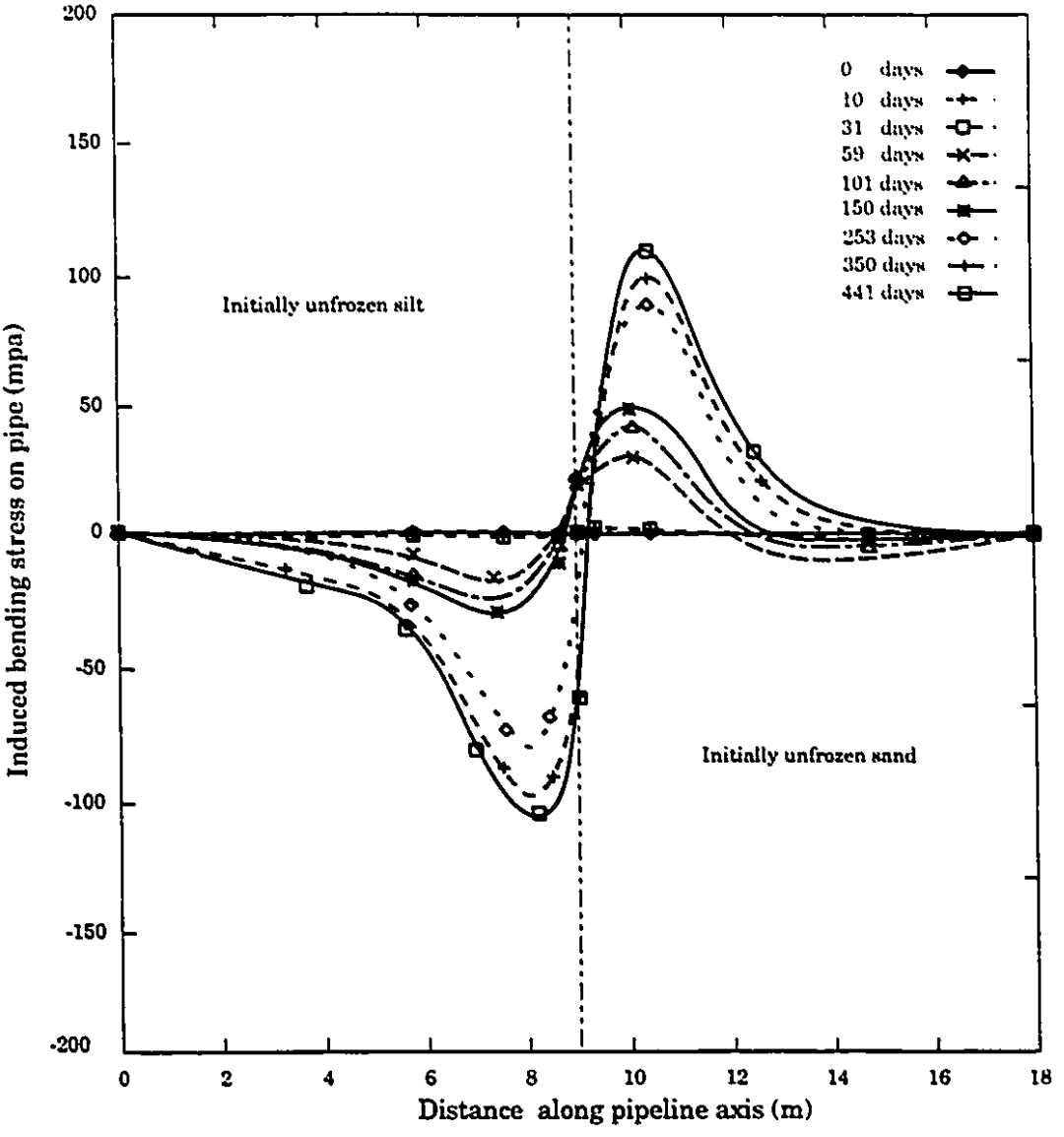

Figure 6.31: Bending moments derived from the computational model: cooling is induced only from the pipeline

6.8 Modelling of Soil-Pipeline Interaction using Shell Elements

The representation of the pipeline as a flexible beam element is an idealization which considerably reduces the computational modelling efforts. In a situation where the pipeline is subjected to a rapid change in curvature, it is necessary to take into consideration the three-dimensional configuration of the pipeline shell. In this chapter, a pipeline was modelled as a cylindrical shell . The finite element modelling of the pipeline shell element combines a plane stress element with a plate bending element. This model of the pipeline shell is used to study the flexural interaction between the soil and the pipeline. The numerical modelling assumed a complete bonded condition at the soil-pipeline interface.

As an example of the modelling, consider the second stage of the Caen pipeline freezing test, in which the SNEC sand was kept in a prefrozen condition and the Caen silt was unfrozen initially. Figure 6.32 shows the finite element discretization of the cross section through the soil-pipeline configuration. Owing to the symmetry of the problem, only half of the system needed to be discretized. There are 2256 solid elements and 144 shell elements in the finite element discretization. The boundary conditions applicable to the problem are also illustrated in Figure 6.32. The properties of the shell were as follows: $E = 200\ GPa$ and the thickness of the shell was 0.5 cm.

In the Caen pipeline test, 72 strain gauges were mounted on the pipe in two configurations:

(1) Ten radial arrays were installed at intervals of 1 m on both unfrozen and prefrozen sides, starting 0.5 m from the interface of the two soils. Each radial array consisted of six gauges which were wired for a quarter bridge measurement (Labelled 12, 2, 4, 6, 8 and 10 o'clock).

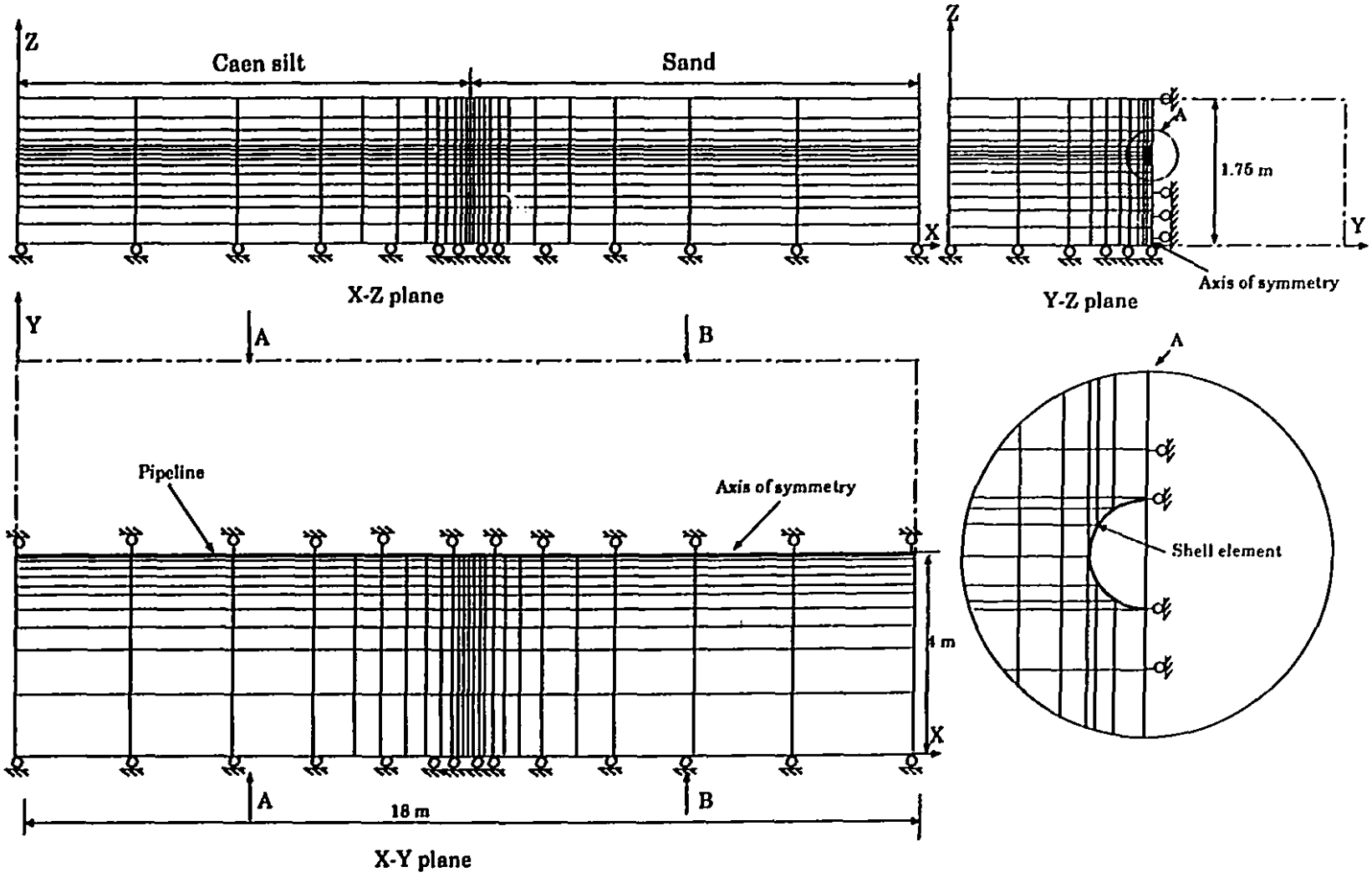

Figure 6.32: Finite element discretization of soil-pipeline system: with shell elements

(2) Six pairs of gauges were placed at 1 m intervals starting 1 m beyond the last radial array on either side of the transition. Each pair of gauges consisted of two gauges which were wired for half bridge measurement (Labelled 12, 6 o'clock).

Due to equipment malfunction, the strain gauges failed to collect the data for the first 256 days. Figure 6.33 illustrates the typical pipe strain at positions on the initially unfrozen side after the end of first freezing period (day 256). Although the period after day 256 was not simulated (following day 256, it was a relaxation period, the pipe temperature was raised to $+5\ ^0C$), strain profiles illustrate an approximately proportional relationship between strains at different locations (o'clock).

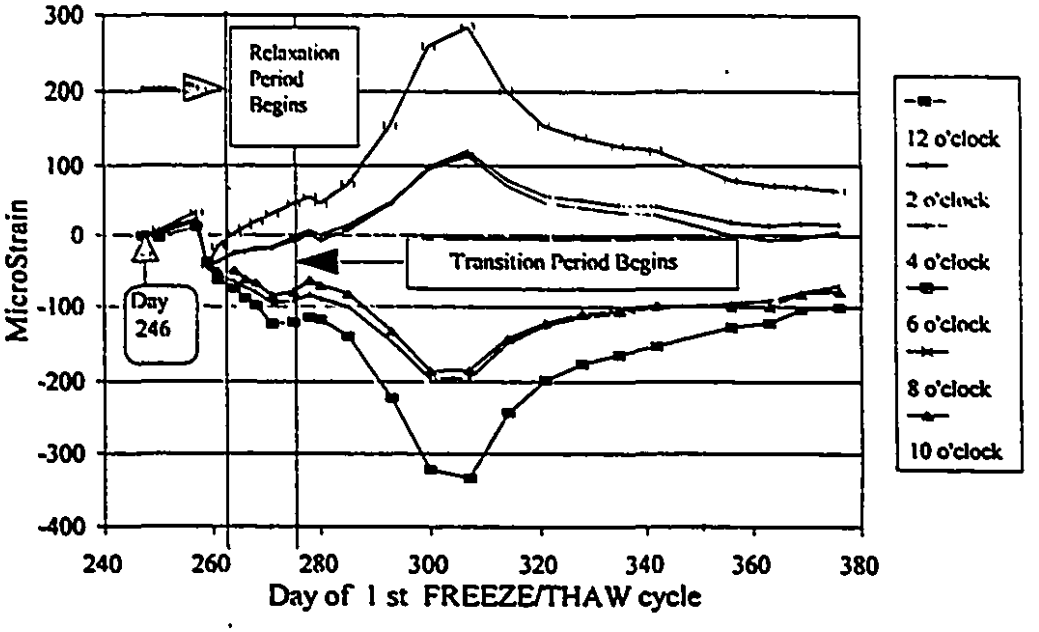

Figure 6.33: Radial strain gauge array: 0.5 m from interface, unfrozen side (National Energy Board report, 1994)

Figure 6.34 illustrates the bending stress profile at the 12, 2, 4, 6 o'clock positions for day 253 of the second stage of the test. It indicates that the maximum bending stresses took place at the 12 and 6 o'clock locations. The results also illustrated that the stresses at 2, 4 o'clock were approximately half of the stresses at 12, 6 o'clock locations, which were analogoue to Figure 6.33. The maximum bending stress predicted by the shell model was slightly greater than that predicted by the beam model. The pipe configuration after 256 days is shown in Figure 6.35.

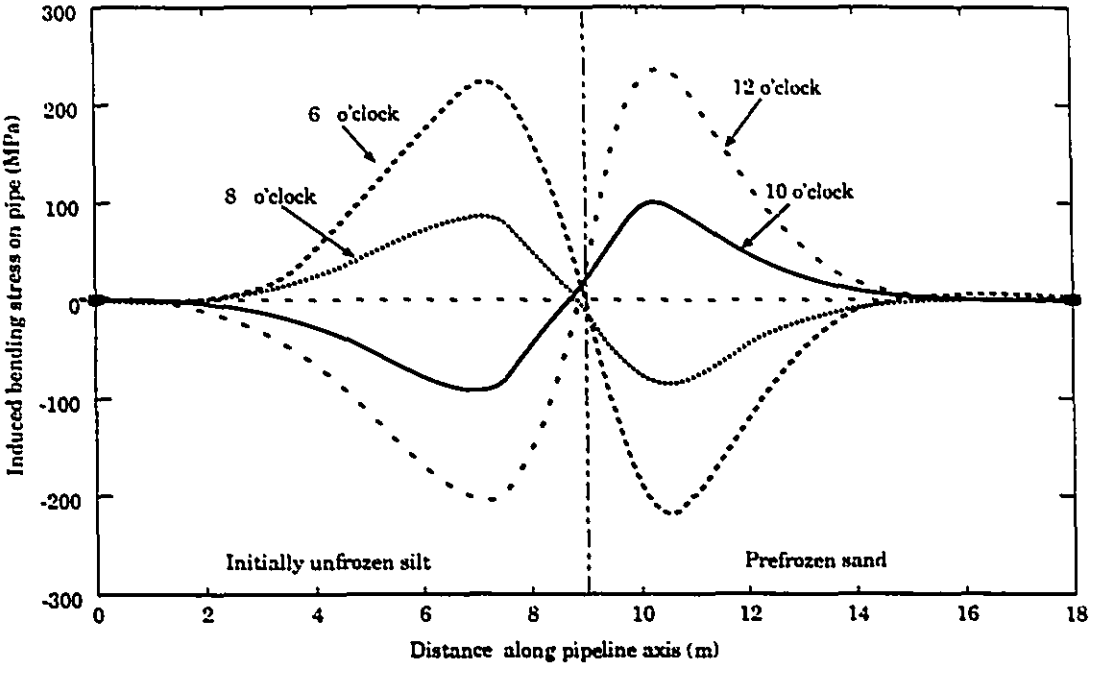

Figure 6.34: Computational results for the variation of bending stresses along the pipeline at the locations at the 12, 2, 4, 6 o'clock

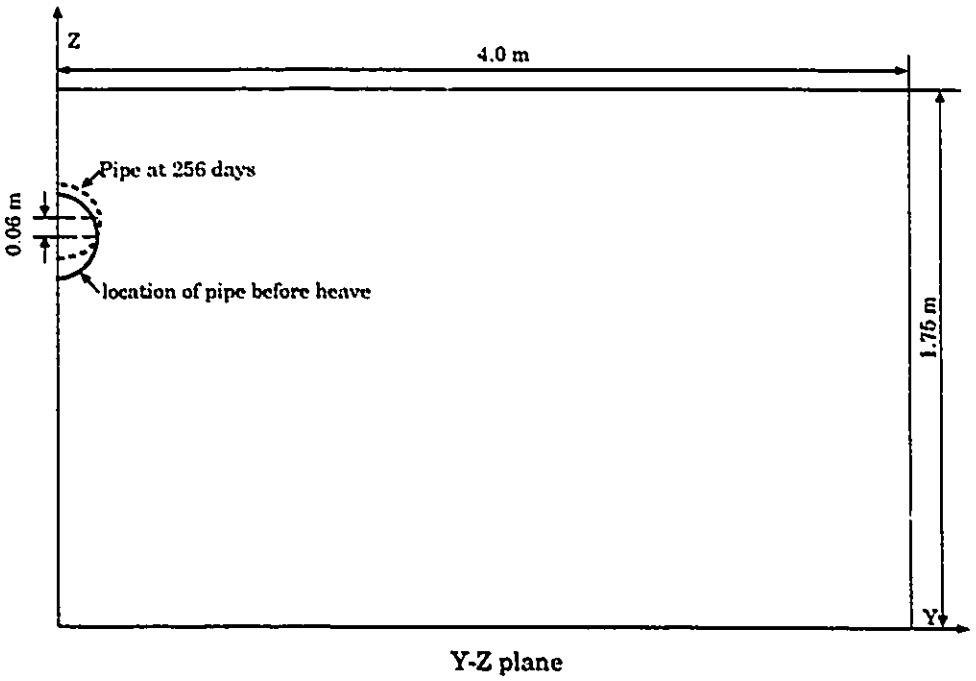

Figure 6.35: Numerical result of pipe displacement

Chapter 7

Conclusions and Recommendations

This thesis developed a computational methodology for the analysis of soil-pipeline interaction problems in which the interaction is induced by frost heave effects. As a first step towards the development of such a methodology it was necessary to identify a complete hydro-thermo-mechanical constitutive model which addresses the coupled processes of heat transfer, moisture transport, generation of freezing action and mechanical effects in frost susceptible soils. The frost action itself is governed by heat transfer, moisture transport and stress state within the soil. The development of an all encompassing model which rigorously coupled heat transfer, moisture transport and mechanical action in a freezing soil is a difficult exercise. As has been pointed out by Selvadurai and Shinde (1993), such a model involves a variety of constitutive parameters, governing both individual and coupled effects, which would be difficult to determine even under highly controlled laboratory conditions. In the context of a realistic geotechnical situation, such as that encountered along a long distance buried pipeline, the determination of these parameters for a fully coupled model is a very difficult task. For this reason a simplified model of frost heave generation was proposed in which the heat transfer and moisture transfer are weakly coupled to the mechanical variables in a frozen soil such as elasticity, plasticity, creep and failure/fracture.

The weak coupling is derived from the application of Clausius-Clapeyron relationship where the temperature field in the frozen zone is related to the pressure in the pore fluid and the pressure in the ice. The frost heave generation in the soil is achieved through the consideration of

(a) heat transfer in the soil mass

(b) moisture transport in the soil mass due to cryogenic suction and

(c) the assumption of the Clausius-Clapeyron equation which governs the relationship between temperature, water pressure and ice pressure.

The mechanical behaviour of frozen soils was modelled by continuum creep phenomena which exhibits primary, secondary and tertiary effects. In particular the tertiary effects were modelled by consideration of damage mechanics. The constitutive models governing both frost heave generation and the complete creep model which incorporated primary, secondary and tertiary creep phenomena were incorporated into axisymmetric and three-dimensional finite element computational schemes which involved spatial discretization via finite elements and temporal discretization via a finite difference scheme. The numerical procedures could examine fully three-dimensional processes of time-dependent frost heave generation and the computational methodology was applied to the examination of frost heave generation in typical frost susceptible soils. The results illustrated satisfactory trends and in particular the results of computational models correlate well with observed trends of experimental data.

The computational modelling was first applied to the study of foundations either embedded in or resting on frozen soil media. The modelling also took into account the influence of sustained loads and unloading and load reversal phenomena on the settlement behaviour. It was observed that for the particular creep damage evolution law chosen, the displacement behaviour was sensitive to the prescribed load-path. The results also demonstrated that the finite element approach, which incorporates

the proposed complete creep model, can characterize the complete creep behaviour and the modelling is viewed as a methodology for identifying time and load history dependent peak loads that can be sustained by structures located in frozen ground. The thesis also develops a method of post failure analysis which is of special interest to failure that takes place at identifiable interfaces. The finite element procedure which incorporates a complete creep model and the algorithm for post failure analysis was applied to examine the uplift behaviour of a section of pipe which is embedded in a frozen soil. The technique was applied to examine the time-dependent displacement of a section of pipe which is subjected to different magnitudes of uplift loads which remain constant with time. The time-dependent evolution of creep failure zones within the frozen soil were also examined. The numerical procedure can be applied to estimate the maximum uplift loads that can be sustained by a frozen soil in a region where an embedded pipe is subjected to uplift loads.

For the analysis of the soil-pipeline interaction, the pipeline was represented by either a flexible beam element or a shell element. Beam element used the conventional Bernoulli-Euler beam theory with a double-node configuration. The finite element modelling of a shell structure used a flat element which combined a plane stress element with a plate bending element. The finite element scheme of shell element was calibrated via known solutions of analytical results.

The computational model was applied to examine the frost heave induced interaction between a flexible near surface buried pipeline and a frost heaving zone. The thesis presented a numerical simulation of the Canada-France pipeline freezing test which was carried out at Station de Gel at the *Centre de Geomorphologie* at Caen, France. The thesis focussed on the computational modelling of the two test stages. The comparisons were conducted by the examining the temperature profiles, soil surface heave, displacements of the pipeline and stresses in the pipeline.

The results indicate that the temperature contours obtained from numerical computations compare well with results obtained from the experiment. The frost heave of the soil surface which is obtained from the numerical computation also compare well both in magnitude and pattern with results obtained from experiments. These results apply for the frost heave patterns obtained for both the silt and the sand. The computation modelling also predicts both the trend and the magnitude of pipeline displacement accurately. An accurate prediction of distribution of maximum bending stresses which are induced by non-uniform displacement of the pipeline was also given in the simulation.

Numerical modelling of the pipeline crossing a transition zone between prefrozen soil and an unfrozen soil of high frost susceptibility shows that the pipeline experiences smaller displacements, greater bending moment in the transition zone than in the case of both soil and sand initially being unfrozen in a given time. This result is identical to the experimental modelling.

Computations were also conducted to examine the idealized test problem where the freezing was induced only from the cooling temperature in the pipeline which crosses the soil with contrasting frost susceptibilities and which are maintained in an initially unfrozen condition. It is observed that the magnitude of the maximum heave is much less and such effects are more concentrated along the axis of the buried pipeline.

Finally, the Caen pipeline was modelled as a cylindrical shell which combined plane stress elements with plate bending elements. Bending stress profiles at the 12, 2, 4, 6 o'clock locations along the pipeline are presented.

The major contributions of this thesis research can be summarized as follows:
(1) development and verification of a finite element procedure for three-dimensional frost heave modelling.

(2) development and verification of the proposed complete creep model.

(3) adaptation of a creep failure model which is particularly applicable for the soil-pipeline interaction problem.

(4) incorporation of a Bernoulli-Euler beam and a cylindrical shell to represent the behaviour of pipeline.

(5) application of the developed finite element techniques to the investigation of the general creep responses of a variety of geotechnical structures.

(6) application of the computational model to the study of near large scale controlled pipeline freezing test; the results obtained from the computational model give trends which compare well with experimental observations.

(7) extension of the scope of knowledge with regarding to the soil-pipeline interaction involve interactive thermo-hydro-mechanical processes.

The following recommendations for future work are suggested:

(1) The *modified hydrodynamic model* proposed by Shen and Ladanyi (1987) is considered as a good approximation in the description of frost heave modelling. However, the phenomenon of the generation of ice lenses at *segregation temperature* is not accounted for in this model, where water freezes at all locations of the region where the temperature is below zero. The ice lenses which generate only at the freezing front in numerical modelling can better represent the frost heaving processes.

(2) Most geotechnical problems involving frost heave are primarily concerned with frost heave effects close to the ground surface. Examples of these include near surface chilled gas pipelines and highway pavements. The soils in these zones are usually unsaturated. Consequently, the assumption of a fully saturated state can be violated in these near surface frost heave effects. To account for the deficiency it is necessary to address the problem of frost heave development in unsaturated zones.

(3) The accuracy of numerical modelling of frost heave largely depends on the thermal, hydraulic and mechanical parameters of soil used in the computation. Of these parameters, a function of permeability with temperature is the most sensitive to the computational results. Accurate measurement and procedures for determining such functions will greatly enhance the modelling of the problem.

References

Andersland, O. B. and AlNouri, I. 1970. Time - dependent strength behaviour of frozen soils. *Journal of the Soil Mechanics and Foundations Division*, ASCE **96(4)**, pp. 1249-1265.

Andersland, O. B., Sayles, H. H. and Ladanyi, B. 1978. Mechanical properties of frozen ground. *Geotechnical Engineering for Cold Regions*, O. B. Andersland and D. M. Anderson (Eds.), McGraw-Hill Book Company, pp. 216-275.

Assur, A. 1963. Discussions on creep of frozen soils. *Proceedings of the 1st International Conference on Permafrost*, Purdue University, Lafayette, pp. 339-340.

Audibert, J. M. E. and Nyman, K. J. 1977. Soil restraint against horizontal motion of pipes. *Journal of the Geotechnical Engineering Division* , ASCE, Vol. **103**, pp. 1119-1142.

Berg, R. L., Guymon, G. L., Johnson, T. C. and Hromadka, T. V. 1980. Mathematical model to correlate frost heave of pavements with laboratory predictions. *CRREL Report* **80-10**, Cold Reg. Res. and Eng. Lab., Hanover, N.H., pp. 1-31.

Bergren, A-L. and Furuberg, T. 1985. A new Norwegian creep model and creep equipment. *Proceedings of the 4th International Symposium on Ground Freezing*, S. Kinoshita and M. Fukuda (Eds.), Sapporo, Japan, pp. 181-442.

Boehler, J. P. and Khan, A. S. (Eds.) 1991. *Proceedings of PLASTICITY 91: 3rd International Symposium on Plasticity and its Current Applications*, Elsevier

Applied Science, London.

Boyle, J. T. and Spence, J. 1983. *Stress Analysis for Creep*, Butterworths.

Chow, C. L. and Wang, J. 1987. An anisotropic theory of elasticity for continuum damage mechanics. *International Journal of Fracture*, **33**, pp. 3-16.

Clough, R. W. and Johnson, C. P. 1964. Analysis of thin arch dams by the finite element method. *Proceedings of Symposium on the Theory of Arch Dams*, Southampton University. (Pergamon Press, 1965).

Crank, J. and Nicholson, P. 1947. A practical method for the numerical evaluation of solutions of partial differential equations of the heat conduction type. *Proceedings of the Cambridge Philosophical Society*, **43**, pp. 50-67.

Dallimore, S. R. 1985. *Observations and Predictions of Frost Heave Around a Chilled Pipeline*, M.A. Thesis, Carleton University.

Dallimore, S. R. and William, P. J. (Eds.) 1984. *Pipelines and Frost Heave*: a seminar, Carleton University, Ottawa, Canada.

Desai, C. S. 1987. *SSTIN 3-D User's Manual, Code for Three-Dimensional Finite Element Analysis of Solids and Soil-Structure Interaction*, University of Arizona.

Desai, C. S. and Siriwardane, H. J. 1984. *Constitutive Laws for Engineering Materials (with Emphasis on Geologic Materials)*, Prentice-Hall.

Eranti, E. 1986. *Cold Region Structural Engineering*, McGraw-Hill.

Filonenko-Borodich, M. M. 1940. Some approximate theories of the elastic foundation. Uch. Zap. Mosk. Gos. Univ. Mekh., **46**, pp. 3-18 (in Russian).

Fish, A. M. 1980. Kinetic nature of the long-term strength of frozen soils. *Proceedings of the 2nd International Symposium on Ground Freezing*, P. E. Frivik (Ed.), Trondheim, Norway, pp. 95 -108.

Fish, A. M. 1983. Thermodynamic model of creep at constant stresses and constant strain rates. *U.S. Army Cold Regions Research and Engineering Laboratory*, CRREL report 83-33.

Fremond, M and Mikkola, M. 1991. Thermomechanical modelling of freezing soil. *Ground Freezing 91. Proceedings of the 6th International Symposium on Ground Freezing*, S. Yu and C. Wang (Eds.), Beijing, China, pp. 17-24.

Gardner, A. R., Jones, R. H. and Harris, J. S. 1984. A new creep equation for frozen soils and ice. *Cold Regions Science and Technology*, **9**, pp. 271-275.

Gilpin, R. R. 1979. A model for the liquid-like layer between ice and a substrate with application to wire regelation and particle migration. *Journal of Colloid and Interface Science*, **68**, 235-251.

Goodman, R. E., Taylor, R. L. and Brekke, T. L. 1968. A model for the mechanics of jointed rock. *Journal of the Soil Mechanics and Foundations Division*, ASCE, **94(SM4)**, pp. 637-659.

Greene, B. E., Strome, D. R. and Weikel, R. C. 1961. Application of the stiffness method to the analysis of shell structures. *Proceedings of Aviation Conference ASME*, Los Angeles.

Hampton, C. N., Jones, R. H. and Gardner, A. R. 1985. Modelling the creep behaviour of frozen sands. *Proceedings of the 4th International Symposium on*

Ground Freezing, S. Kinoshita and M. Fukuda (Eds.), Sapporo, Japan, pp. 27-33.

Harlan, R. L. 1973. Analysis of coupled heat-fluid transport in partially frozen soils. *Water Resources Research*, **9**, pp. 1314-1323.

Harlan, R. L. and Nixon, J. F. 1978. Ground thermal regime. *Geotechnical Engineering for Cold Regions*, O. B. Andersland and D. M. Anderson (Eds.), McGraw-Hill Book Company, pp. 103-163.

Hetenyi, M. 1946. *Beams on Elastic Foundation*, University of Michigan Press, Ann Arbor, Michgan.

Hill, R. 1950. *The Mathematical Theory of Plasticity*, Oxford, Clarendon Press.

Hoekstra, P. 1969. Water movement and freezing pressures. *Soil Science Society of America, Proceedings*, **33**, pp. 512-518.

Hopke, S. W. 1980. A model for frost heave including overburden. *Cold Regions Science and Technology*, **3**, pp. 111-127.

Hu, J. and Selvadurai, A. P. S. 1995. Influence of tertiary creep on the uplift behaviour of a pipe embedded in a frozen soil. *Proceedings of the 2nd International Conference on Advances in Underground Pipeline Engineering*, J. K. Jeyapalan and M. Jeyapalan (Eds.), ASCE, Seattle, U.S.A., pp 345-358.

Hu, J. and Selvadurai, A. P. S. 1995. Computational modelling of frost heave. *Proceedings of 5th International Symposium on Numerical Models in Geomechanics*, G. N. Pande and S. Pietruszczak (Eds.), Davos, Switzerland, A. A. Balkema, pp. 293-300.

Hult, J. A. H. 1966. *Creep in Engineering Structures*, Blaisdell Publ. Co., Waltham, Mass.

Jame, Y. W. and Norum, D. I. 1980. Heat and mass transfer in a freezing unsaturated porous medium. *Water Resources Research*, **16**, pp. 811-819.

Jeyapalan, J. K. (Ed.) 1985. *Proceedings of the International Conferences on Advances in Underground Pipeline Engineering*, ASCE, Madison, Wisc.

Kachanov, L. M. 1986. *Introduction to Continuum Damage Mechanics*, Martinus Nijhoff Publishers, Dordrecht, Holland.

Kay, B. D. and Perfect, E. 1988. State of the Art: Heat and mass transfer in freezing soils. *Proceedings of the 5th International Symposium on Ground Freezing*, R. H. Jones and J. T. Holden (Eds.), Nottingham, England, pp. 3-21.

Kay, B. D., Sheppard, M. I. and Loch, J. P. G. 1977. A preliminary comparison of simulated and observed water redistribution in soils freezing under laboratory and field conditions. *Proceedings of the International Symposium on Frost Actions in Soils*, Lulea, Sweden, pp. 92-101. pp. 29-40.

Kerr, A. D. 1964. Elastic and viscoelastic foundation models. *Journal of Applied Mechanics (Trans. A.S.M.E.)*, **31**, pp. 491-498.

Klein, J. A. H. 1979. The application of finite elements to creep problems in ground freezing. *Proceedings of the 3rd International Conference on Numerical Methods in Geomechanics*, A. A. Balkema, Rotterdam, the Netherlands, **1**, pp. 493-502.

Klein, J. A. H. and Jessberger, H. L. 1979. Creep stress analysis of frozen soils under multiaxial states of stress. *Engineering Geology*, **13**, pp. 353-365.

Konrad, J.M. and Morgenstern, N. 1980. A mechanistic theory of ice lens formation in fine-grained soils. *Canadian Geotechnical Journal*, **17**, pp.473-486.

Konrad, J. M. and Morgenstern, N. 1981. The segregation potential of a freezing soil. *Canadian Geotechnical Journal*, **18**, pp.482-491.

Konrad, J. M. and Morgenstern, N. 1982. Prediction of frost heave in the laboratory during transient freezing. *Canadian Geotechnical Journal*, **19**, pp. 250-259.

Konrad, J. M. and Morgenstern, N. 1984. Frost heave prediction of chilled pipelines buried in unfrozen soil. *Canadian Geotechnical Journal*, **21**, pp. 100-115.

Kopal, Z. 1955. *Numerical Analysis*, John Wiley & Sons Inc. New York.

Ladanyi, B. 1972. An engineering theory of creep of frozen soils. *Canadian Geotechnical Journal*, **9**, pp. 63-68.

Ladanyi, B. 1981. Mechanical behaviour of frozen soils. *Mechanics of Structured Media, International Symposium on the Mechanical Behaviour of Structured Media*, A. P. S. Selvadurai (Ed.), Ottawa, Part B, pp 205-245.

Ladanyi, B. 1985. Stress transfer mechanism in frozen soils. *Tenth Canadian Congress Applied Mechanics*, H. Rasmussen (Ed.), pp 11-23.

Ladanyi, B. and Lemaire, G. 1984. Behaviour of a buried pipeline under differential frost heave condition. *Proceedings of CSCE Cold Regions Engineering Specialty Conference*, Montreal, Quebec, pp. 161-176.

Lemaitre, J. and Chaboche, J. L. 1974. A nonlinear model of creep-fatigue damage cumulation and interaction. *Proceedings of IUTAM Symposium on Mechanics of Visco-elasticity Media and Bodies*, Gotenbourg Swedan, Springer-Verlag.

Lewis, R. W. and Sze, W. K. 1988. A finite element simulation of frost heave in soils. *Proceedings of the 5th International Symposium on Ground Freezing*, R. H. Jones and J. T. Holden (Eds.), Nottingham, England, pp. 73-80.

Loch, J. P. G., and Kay, B. D. 1978. Water redistribution in partially frozen, saturated silt under several temperature gradients and overburden loads. *Soil Science Society of America, Journal*, **43(3)**, pp. 400-406.

Miller, R. D. 1970. Ice sandwich: Functional semipermeable membrane. *Science*, **164**, 584-585.

Miller, R. D. 1978. Frost heaving in non-colloidal soils. *Proceedings of the 3rd International Conference on Permafrost*, Edmonton, Alberta, Canada, pp. 707-713.

Miller, R. D. 1980. Freezing phenomena in soils. *Applications of Soil Physics*, D.Hillel (Ed.), Academic Press, NY.

Mitchell, J. K., Campanella, G. G. and Singh, A. 1968. Soil creep as a rate process. *Journal of the Soil Mechanics and Foundations Division*, ASCE, **94(4)**, pp. 231-253.

National Energy Board, 1994. *Preliminary Database Report for the Caen Frost Heave Test Facility*, Calgary, Canada.

Nixon, J. F. 1987. Pipeline frost heave predictions using the segregation potential frost heave method. *Proceedings of the Offshore Mechanics and Arctic Engineering*, Houston, Texas, pp. 1-6.

Nixon, J. F., Morgenstern, N. R. and Reesor, S. N. 1983. Frost heave-pipeline interaction using continuum mechanics. *Canadian Geotechnical Journal*, **20**,

pp. 251-261.

Odqvist, F. K. G. 1966. *Mathematical Theory of Creep and Creep Rupture.* Clarendon Press, Oxford, England.

Odqvist, F. K. G. and Hult, J. 1962. *Kriechfestigkeit metallischer Werkstoffe.* Springer-Verlag.

Outcalt, S. I. 1980. A step function model of ice segregation. *Proceedings of the 2nd International Symposium on Ground Freezing*, P. E. Frivik (Ed.), Trondheim, Norway, pp. 514-524.

Pasternak, P. L. 1954. On a new method of analysis of an elastic foundation by means of two foundation constants. Gosudarstvennoe Izdatelstro Liberaturi po Stroitelstvui Arkhitekture, Moscow (in Russian).

Peng, L. C. 1978. Stress analysis of methods for underground pipelines. Part 2, Soil-Pipe Interaction, Vol. 47, pp. 65-74.

Penner, E. 1986. Aspects of ice lens growth in soils. *Colds Regions Science and Technology*, **13**, pp. 91-100.

Penner, E. and Ueda, T. 1977, The dependence of frost heaving on load applications. preliminary results. *Proceedings of the International Symposium on Frost Actions in Soils*, Lulea, Sweden, pp. 92-101.

Pickell, M. B. (Ed.) 1983. Pipelines in adverse environments II. *Proceedings of the ASCE Specialty Conference*, San Diego, Ca.

Puswewala, U. G. A. and Rajapakse, R. K. N. D. 1990. Numerical modelling of structure-frozen soil/ice interaction. *Journal of Cold Regions Engineering*, 4, pp.133-151.

Puswewala, U. G. A. and Rajapakse, R. K. N. D. 1993. Computational analysis of creep in ice and frozen soil based on Fish's unified model. *Canadian Journal of Civil Engineering*, **20**, pp. 120 -132.

Puswewala, U. G. A. and Rajapakse, R. K. N. D., Domaschuk, L. and Lach, R. P. 1992. Finite element modelling of pressuremeter tests and footings on frozen soils. *International Journal for Numerical and Analytical Methods in Geomechanics*, Vol 16, pp 351-375.

Reissner, E. 1958. Deflection of plates on viscoelastic foundation. *Journal of Applied Mechanics* (Trans. A.S.M.E.), **80**, pp. 144-145.

Sayles, F. H. 1973. Triaxial Constant strain rate tests and triaxial creep tests on frozen Ottawa sand. *Proceedings of 2nd International Permafrost Conference*, Yakutsk, USSR, pp. 384-391.

Sayles, F. H. 1988. State of the art: Mechanical properties of frozen soil. *Proceedings of the 5th International Symposium on Ground Freezing*, R. H. Jones and J. T. Holden (Eds.), Nottingham, England, pp. 143-165.

Selvadurai, A. P. S. 1979. *Elastic Analysis of Soil-Foundation Interaction. Developments in Geotechnical Engineering*, **17**, Elsevier, Amsterdam, The Netherlands.

Selvadurai, A. P. S. 1983. A soil-structure interaction problem for a group of connected flexible pipelines. *ASCE specialty Conference on Pipelines in Adverse*

Environments, (M.B. Pickell, Ed.), San Diego, Ca., pp. 192-211.

Selvadurai, A. P. S. 1985a. Soil-pipeline interaction during ground movement. *ARCTIC 85, Civil Engineering in the Arctic Offshore, Proceedings of ASCE Specialty Conference, San Francisco*, pp. 763-773.

Selvadurai, A. P. S. 1985b. Numerical simulation of soil-pipeline interaction in a ground subsidence zone. *Proceedings of the International Conference on Advances in Underground Pipeline Engineering, ASCE*, J.K. Jeyapalan (Ed.), pp. 311-319.

Selvadurai, A. P. S. 1985c. Elasto-static soil-structure interaction problems for embedded flexible and rigid structures. *CSCE Specialty Conference on Computer Methods in Offshore Engineering*, pp. 321-350.

Selvadurai, A. P. S. 1988. Mechanics of soil-pipeline interaction. *Proceedings of CSCE Annual Conference*, Calgary, ALTA., **3**, pp. 151-163.

Selvadurai, A. P. S. 1991. Mechanics of buried pipelines induced by random ground movements. *1991 Annual Conference of Canadian Society For Civil Engineering*, pp. 142-151.

Selvadurai, A. P. S. 1993. Uplift behaviour of strata-grid anchored pipelines embedded in granular soils. *Geotechnical Engineering*, **24**, pp. 34-55.

Selvadurai, A. P. S. 1994. Transverse loading of undirectionally reinforced composites: the role of matrix damage and matrix fracture. Proceedings of 1994 International Mechanical Engineering Congress and Exposition, ASME, D. H. Allen and J. W. Ju (Eds.), Chicago, Illinois.

Selvadurai, A. P. S. and Au, M. C. 1991. Damage and visco-plasticity effects

in the indentation of a polycrystalline solid. *Proceedings of PLASTICITY 91: 3rd International Symposium on Plasticity and Its Current Applications*, J. P. Boehler and A. S. Khan (Eds.), Elsevier Applied Science, London, pp 405-408.

Selvadurai, A. P. S., Au, M. C. and Shinde, S. B. 1990. Soil-pipeline interaction in a pipeline with prescribed displacements. *Proceedings of the First National Conference on Flexible Pipes*, Columbus, Ohio, S.M. Sargand, G.F. Mitchell and J.O. Hurd (Eds.), A. A. Balkema, Rotterdam, pp. 135-142.

Selvadurai, A. P. S. and Boulon, M. J. 1995. *Mechanics of Geomaterial Interfaces. Studies in Applied Mechanics*, **42**. Elsevier Science, Amsterdam, The Netherlands.

Selvadurai, A. P. S. and Hu, J. 1995. The axial loading of foundations embedded in frozen soils. *International Journal of Offshore and Polar Engineering and Proceedings of the 5th ISOPE Conference* , J. S. Chung, B. M. Das, B. J. Natvig and M. Olagnon (Eds.), The Hague, The Netherlands, Vol. 1, pp. 488 - 495.

Selvadurai, A. P. S. and Hu, J. 1996. Mechanics of buried chilled gas pipelines, Proceedings of International Pipeline Conference, Calgary, Alberta (Under review).

Selvadurai, A. P. S. and Lee, J. J. 1981. *Soil Resistance Models for the Stress Analysis of Buried Fuel Pipelines. Interim Report. Technical Research and Development Project. Research and Engineering*, Bechtel Group Inc., San Franciso.

Selvadurai, A. P. S. and Lee, J. J. 1982. *Soil Resistance Models for the Stress Analysis of Buried Fuel Pipelines. Final Report. Technical Research and Development Project. Research and Engineering*, Bechtel Group Inc., San Franciso.

Selvadurai, A. P. S., Lee, J. J., Todeschini, R. A. A. and Somes, N. F. 1983.

Lateral soil resistance in soil-pipeline interaction. *Pipelines in Adverse Environments II. Proceedings of ASCE Specialty Conference*, (M.B. Pickell, Ed.), San Diego, Ca., pp. 259-278.

Selvadurai, A. P. S. and Pang, S. 1988. Non-linear effects in soil- pipeline interaction in a ground subsidence zone. *Proceedings of the 6th International Conference of Numerical Methods in Geomechanics*, Innsbruck, Austria, G. Swoboda (Ed.), **2**, pp. 1085-1094.

Selvadurai, A. P. S. and Shinde, S. B. 1993. Frost heave induced mechanics of buried pipelines. *Journal of Geotechnical Engineering, Proc. ASCE*, **119**, pp. 1929-1951.

Shen, M. 1991 *Mathematical Modelling and Application of Coupled Processes in Freezing Soil*, Ph.D Thesis, Ecole Polytechnique, University of Montreal.

Shen, M. and Ladanyi, B. 1987. Modelling of coupled heat, moisture and stress field in freezing soil. *Cold Regions Science and Technology*, **14**, pp. 237-246.

Shen, M. and Ladanyi, B. 1991. Soil-pipe interaction during frost heaving around a buried chilled pipeline. *Cold Regions Engineering, ASCE, Sixth International Specialty Conference*, pp. 11-21.

Sheppard, M. I., Kay, B. D. and Loch, J. P. G. 1978. Development and testing of a computer model for heat and mass flow in freezing soils. *Proceedings of the 3rd International Conference on Permafrost*, Edmonton, Alberta, Canada, pp. 76-81.

Slusarchuk, W. A., Clark, J. I., Nixon, J. F., Morgenstern, N. R. and Gaskin, P. N. 1978. Field test results of a chilled pipeline buried in unfrozen

ground. *Proceedings of the 3rd International Conference on Permafrost*, Edmonton, Alberta, Canada, pp. 877-883.

Smith, M. W., Dallimore, S. R. and Kettle, R. J. 1985. Observations and prediction of frost heave of an experimental pipeline. *Proceedings of the 4th International Symposium on ground freezing*, S. Kinoshita and M. Fukuda (Eds.), Sapporo, Japan, pp. 297-304.

Soldatos, K. P. and Selvadurai, A. P. S. 1985. Flexure of beams resting on hyperbolic elastic foundations. *International Journal of Solids and Structures*, **21(4)**, pp. 373-388.

Soo, S., Wen, R. K. and Andersland, B. 1987. Finite element method for analysis of frozen earth structures. *Cold Regions Science and Technology*, **13**, pp. 121-129.

Taylor, G. S. and Luthin, J. N. 1978. A model for coupled heat and moisture transfer during soil freezing. *Canadian Geotechnical Journal*, **15**, pp. 548-555.

Timoshenko, S. and Woinowsky-Krieger, S. 1959. *Theory of Plates and Shells*. McGraw-Hill Book Company.

Ting, J. M. 1983. Tertiary creep model for frozen sand. *Journal of Geotechnical Engineering*, ASCE, **109(7)**, pp. 932-945.

Ting, J. M. and Martin, R. T. 1979. Application of the Andrade equation to creep data for ice and frozen soil. *Cold Regions Science and Technology*, **1**, pp. 29-36.

Trautmann, C. H. and O'Rourke, T. D. and Kulhawy, F. H. 1985. Uplift force-displacement Response on buried pipe. *Journal of Geotechnical Engineering*.

ASCE, Vol. 111, No. 9, pp. 1061-1076.

Vlazov, V. Z. and Leontiev, U. N. 1966. *Beams, Plates and Shells on Elastic Foundations*. Israel Program for Scientific Translations, Jerusalem (translated from Russian).

Vyalov, S. S. 1963. Rheology of frozen soils. *Proceedings of 1st International Conference on Permafrost*. Nat. Academy of Sciences, pp 332-339.

Vyalov, S. S., Gmoshinskii, V. G., Zaretskii, Yu. K., Pekarskaia, N. K. and Shusherina, E. P. 1963. The strength and creep of frozen soils and calculations for ice-soil retaining structures. *U.S. Army Cold Regions Research and Engineering Laboratory*. Translation 76.

Williams, P. J. 1986. *Pipelines and Permafrost*. Carleton University Press, Ottawa, Canada.

Winkler, E. 1867. Die Lehre Von der Elastizitat und Festigkeit. Dominicus, Prague.

Wolbert, G. Jr. 1979. *U.S. Oil Pipe Lines*. American Petroleum Institute, Washington.

Wood, J. A. And Williams, P. J. 1985. Internal stresses in frozen ground. *Proceedings of the 4th International Symposium on Ground Freezing*, S. Kinoshita and M. Fukuda (Eds.), Sapporo, Japan. pp. 165-171.

Zienkiewicz, O. C. 1977. *The Finite Element Method*. 3rd Ed. McGraw-Hill Co., London, United Kingdom.

Zienkiewicz, O. C. and Cheung, Y. K. 1964. Finite element method of analysis

for arch dam shells and comparison with finite difference procedures. *Proceedings of Symposium on the Theory of Arch Dams*. Southampton University.